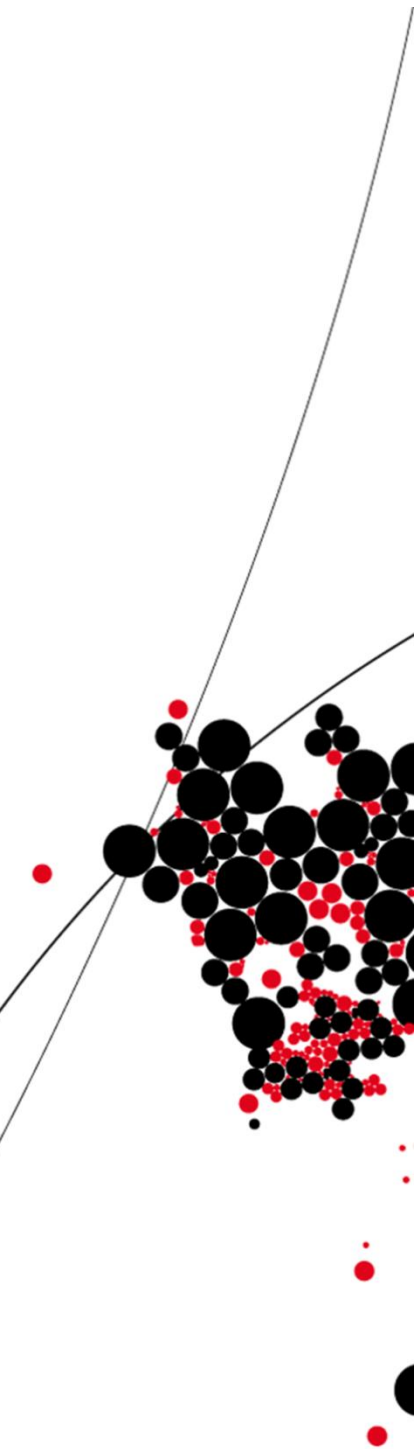




# UNIVERSITY OF TWENTE.

Faculty of Engineering Technology



## **SUPERCritical WATER GASIFICATION OF BIOMASS: MODELING OF CHAR FORMATION AND A SOCIO-ECONOMIC STUDY**

Christian Andrés Polanco Pacheco  
M.Sc. Thesis  
August 2017

---

Exam committee:  
prof. dr. ir. G. Brem  
M.Sc. R. Yukananto  
Dr. ir. A. Pozarlik  
Ir. E. Bramer  
Dr. ir. M. Arentsen

Thermal Engineering Group  
Faculty of Engineering Technology  
University of Twente  
P.O. Box 217  
7500 AE Enschede

---



*Para mis padres.  
Porque todo lo que fui, soy y seré.  
Es gracias a ustedes...*

*For my parents.  
Because everything that I was, I am and I will be.  
It is thanks to you...*

## SUMMARY

Supercritical water gasification is an exciting technology and a more convenient choice against anaerobic digestion for the recycling of wet streams of organic biomass. This technology does not need drying as pre-treatment and also takes considerably less residence time, minutes or even seconds depending on the conditions.

In this process, highly pressurized water is in contact with organic biomass which is instantly decomposed into gaseous products but also into unwanted side-products known as char. This char is a cracking product, which decreases the gasification efficiency, causing plugging in the heat exchanger or deposits on the reactor walls which leads to fouling.

This study investigates the char formation problem in supercritical gasification through a Computational Fluid Dynamics (CFD) numerical model using commercial software ANSYS Fluent with glucose as biomass model compound. The model includes complete thermo-physical properties at supercritical conditions for all species involved, chemical reactions and kinetic data from lab-scale experimental results for the formation of char and gaseous products.

The numerical simulations were carried in laminar and turbulent flow. The results were replicated and show good agreement with experimental data. Therefore, the developed numerical model is considered as successful. It can mimic the char formation behavior under the influence of changing temperature and give valuable insights for future reactor and process optimization.

In the last part of the thesis, a socio-economic assessment of the technology under a Dutch context is presented. Results showed that a supercritical water gasification process design could be economically feasible and that has fascinating perspectives as a tailor-made waste management solution for specific niches, where it can further mature and consolidate.

# CONTENTS

SUMMARY.....	4
CONTENTS.....	5
LIST OF FIGURES AND TABLES.....	7
1. INTRODUCTION .....	9
1.1. BACKGROUND.....	9
1.2. SUPERCRITICAL WATER GASIFICATION (SCWG) .....	11
1.3. TECHNOLOGICAL CHALLENGES: CHAR FORMATION PROBLEM.....	12
1.4. RESEARCH OBJECTIVE .....	12
1.5. OUTLINE .....	13
2. LITERATURE STUDY .....	15
2.1. INTRODUCTION.....	15
2.2. PROPERTIES OF WATER AT SUPERCRITICAL CONDITIONS.....	15
2.3. SUPERCRITICAL WATER GASIFICATION (SCWG) OF GLUCOSE.....	17
2.4. MODELING APPROACHES .....	19
2.4.1. KINETIC MODELING .....	19
2.4.2. COMPUTATIONAL FLUID DYNAMICS (CFD) MODELING.....	19
2.4.3. OTHER MODELING TECHNIQUES.....	20
2.5. DISCUSSION.....	23
3. SCWG MODEL WITH CHAR FORMATION.....	24
3.1. INTRODUCTION.....	24
3.2. THERMO-PHYSICAL PROPERTIES .....	24
3.3. CHEMICAL REACTIONS AND KINETIC MODEL .....	25
4. CFD OF THE EXPERIMENT #1.....	30
4.1. INTRODUCTION.....	30
4.2. EXPERIMENT .....	30
4.3. NUMERICAL MODEL .....	31
4.4. RESULTS .....	32
4.5. DISCUSSION.....	38
5. CFD OF THE EXPERIMENT #2.....	40
5.1. INTRODUCTION.....	40

5.2. EXPERIMENT .....	40
5.3. NUMERICAL MODEL .....	43
5.4. MESH INDEPENDENCE STUDY.....	43
5.5. RESULTS .....	45
5.6. DISCUSSION .....	53
6. IMPACT OF SCWG UTILIZATION FOR AGRICULTURAL LIFE.....	54
6.1. INTRODUCTION.....	54
6.2. ENERGY SITUATION IN THE NETHERLANDS.....	55
6.3. ESTIMATION OF POTENTIAL.....	57
6.4. TECHNO-ECONOMIC ASSESSMENT OF SCWG .....	58
6.4.1. ESTIMATION OF THE TOTAL CAPITAL INVESTMENT (TCI).....	60
6.4.2. DIRECT AND INDIRECT COSTS .....	61
6.4.3. OPERATING COSTS.....	62
6.4.4. COST LEVELIZATION.....	62
6.4.5. RESULTS.....	63
6.4.6. DISCUSSION .....	64
7. CONCLUSIONS AND RECOMMENDATIONS .....	66
7.1. CONCLUSIONS .....	66
7.2. RECOMMENDATIONS.....	67
BIBLIOGRAPHY .....	68
APPENDIX 1 .....	72
APPENDIX 2 .....	74
APPENDIX 3 .....	76
APPENDIX 4 .....	77
APPENDIX 5 .....	78
APPENDIX 6 .....	81

# LIST OF FIGURES AND TABLES

Figure 1: Parameter settings and operating conditions for laminar flow simulations [2] .....	10
Figure 2: Scheme of Biomass Conversion Routes [4] .....	11
Figure 3: Phase diagram of water [9] .....	16
Figure 4: Density vs. Temperature [10] .....	16
Figure 5: Dynamic viscosity vs. Temperature [10] .....	16
Figure 6: Dielectric constant of water [10] .....	15
Figure 7: Ternary diagrams for char formation [33] .....	21
Figure 8: Effect of biomass composition [34] .....	22
Figure 9: Glucose char particles formation pathways [14] .....	25
Figure 10: Char formation Arrhenius plot .....	27
Figure 11: Output gas composition experimental results from [13] .....	28
Figure 12: SCWG with Char formation model schematic .....	29
Figure 13: Laminar flow experimental setup [13] .....	29
Figure 14: Laminar flow domain scheme .....	32
Figure 15: Output gas composition comparison .....	34
Figure 16: Char content comparison .....	34
Figure 17: GCE comparison .....	34
Figure 18: Char mass fraction contours .....	35
Figure 19: Glucose mass fraction contour .....	35
Figure 20: Water mass fraction contours .....	36
Figure 21: Hydrogen mass fraction contours .....	36
Figure 22: Carbon monoxide mass fraction contours .....	36
Figure 23: Carbon dioxide mass fraction contours .....	37
Figure 24: Methane mass fraction contours .....	37
Figure 25: Char velocity vectors .....	37
Figure 26: Temperature contours .....	38
Figure 27: Mixture velocity vectors .....	38
Figure 28: Turbulent flow experimental setup [20] .....	41
Figure 29: Product distribution of hydrothermal decomposition of glucose [14] .....	41
Figure 30: Turbulent flow domain scheme .....	41
Figure 31: Velocity profiles comparison .....	41
Figure 32: Glucose decomposition results .....	46
Figure 33: Char formation results .....	46
Figure 34: Output gas formation results .....	47
Figure 35: Char mass fraction transient contours .....	48
Figure 36: Hydrogen mass fraction transient contours .....	49
Figure 37: Carbon monoxide mass fraction transient contours .....	50
Figure 38: Carbon dioxide mass fraction transient contours .....	51
Figure 39: Methane mass fraction transient contours .....	52
Figure 40: Dutch energy matrix [51] .....	55
Figure 41: Schematic overview general integrated biorefinery process [54] .....	56
Figure 42: Flowchart of SCWG process: .....	59
Figure 43: Volume expansivity vs. Temperature [10] .....	72
Figure 44: Kinematic viscosity vs. Temperature [10] .....	72
Figure 45: Specific heat vs. Temperature [10] .....	72

Figure 46: Thermal conductivity vs. Temperature [10].....	72
Figure 47: Specific enthalpy vs. Temperature [10] .....	73
Figure 48: Prandtl number vs. Temperature [10] .....	73
Figure 49: Laminar flow domain definition.....	78
Figure 50: Velocity profiles comparison .....	79
Figure 51: Temperature profile comparison.....	80
Figure 52: Velocity and turbulence intensity contours .....	81
Figure 53: Bulk fluid temperature profiles.....	82
Figure 54: Char kinetic profiles at different operating temperatures.....	83
Figure 55: Kinetic rates at 623 K .....	83
Table 1: Overview of lab-scale tubular reactor experiments.....	18
Table 2: Classification of glucose SCWG reactions [14] .....	26
Table 3: Parameter settings and operating conditions for laminar flow simulations .....	31
Table 4: Experimental results for numerical model validation [13] .....	33
Table 5: Numerical model results for laminar flow.....	33
Table 6: Parameter settings and operating conditions for turbulent flow simulations .....	45
Table 7: Biomass-based waste for SCWG [57] .....	57
Table 8: Total waste available [58] .....	58
Table 9: Total waste available [58] .....	58
Table 10: Total waste available [58] .....	58
Table 11 Total waste available [58] .....	58
Table 12: Product and by-products output .....	64
Table 13: Domain parameters .....	78

# 1. INTRODUCTION

## 1.1. BACKGROUND

Nowadays, it is widely known that climate change represents a grave threat to the human population, wildlife, and environment. Its consequences can be felt already with impacts such as melting icecaps, stronger hurricanes, accelerated sea level rise, severe heat waves, drought, floods, dangerous forest fires, etc. According to the latest Intergovernmental Panel on Climate Change (IPCC) report [1], the “global carbon budget” which is the amount of carbon dioxide emissions that can be emitted, while still having a chance of limiting the global temperature rise to 2 °C (above pre-industrial levels) will be exceeded in about 30 years with the current rate of emissions.

The latest humankind's effort to face the climate change battle is the Paris Agreement, which was signed by 195 parties to the United Nations Framework Convention on Climate Change (UNFCCC) and entered into force in November 2016. The agreement comprises of greenhouse gas emissions (GHG) mitigation, adaptation, and finance starting in the year 2020. In general terms, each country voluntarily determines plans and reports its contribution to fight the climate change problem through pledges.

The current contributions is only sufficient to slow the projected rise in global energy-related CO<sub>2</sub> emissions, which will result in not less than a 2 °C warming. In retrospect, if we consider the data for the period from 1850 to 2011 for cumulative CO<sub>2</sub> emissions (see Figure 1), the five top emitters (USA, EU, China, Russia and Japan) together contributed approximately with two-thirds of the world's historic emissions, which means 37% of the global carbon budget was used already.

Despite the seriousness of this problem, not everyone is fully involved in the climate change battle. On 1 June 2017, the current president of the United States announced its withdrawal from the agreement. This forces other countries to become even more involved with this battle. The 2 °C pathway is very tough indeed and brings with it many challenges. Efforts in all areas must be carried out; special attention must be done into policy making. Policies can accelerate further low carbon technologies and energy efficiency in every sector. To make our global economy carbon neutral it would be necessary for example to exceed the number of electric cars by 700 million and displace approximately 6 million barrels a day of oil by the year 2040. This is highly ambitious, and the current deploy of renewables is more focused on the electricity production only.

It is necessary to expand the use of renewables into other sectors and applications. Biomass can be used not only to produce traditional fuels, but also to produce useful compounds for the industry sector. There is a large opportunity for its utilization. Therefore it can play an important role towards the transition to a more sustainable worlds. This is where biomass-based energy has its opportunity; the potential to replace chemicals (currently made from fossil fuel based sources)

and traditional fuels is enormous for example and will help the transition towards a more sustainable world.

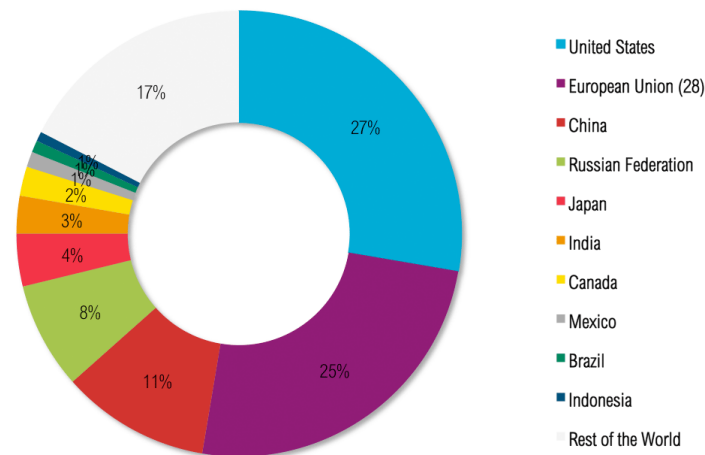


Figure 1: Parameter settings and operating conditions for laminar flow simulations [2]

Nowadays bioenergy accounts for approximately 10% (50 Exajoule or EJ) of the world total primary energy supply, most of it in the fuel form for cooking and heating in developing countries. A more refined used of bioenergy in the form of heat for industries and buildings sector is rather small (around 13 EJ), but is increasing. Furthermore, 370 TWh of biomass-based electricity were produced in 2012 (1.5% world electricity generation) using conventional combustion or the more novel gasification power plants [3].

However, a more interesting use of the biomass energy is in the synthesis of fuels, chemicals, and materials. Within this field, the first efforts were made using "food" crops like corn, sugarcane and vegetable oils (the so-called first generation) to produce ethanol or biodiesel. However, this road led to a discussion about food competition and security of supply. From this learning process, it was concluded that it was necessary to use crops that are not used for human or animal consumption or are waste from the first generation crops. And it was envisioned that the third generation or the so-called "advanced biofuels" which includes biofuel from lignocellulosic biomass (such as cellulosic ethanol, BtL-diesel or syngas) or even more novel technologies such as algae-based biofuels with technology that is mainly in research and development (R&D) or pilot phase scale still.

Conversion of biomass to energy is done typically using two primary process technologies: thermochemical and biochemical/biological. Depending on where the feedstock comes from (agriculture, forest or wastes) and its properties, the selection of the conversion route is taken. In the thermo-chemical conversion, four options are available: combustion, pyrolysis, gasification, and liquefaction. And in the biochemical conversion, only two choices are available: digestion (for the production of biogas) and fermentation (production of ethanol). These routes with their standard final products are shown in Figure 2:

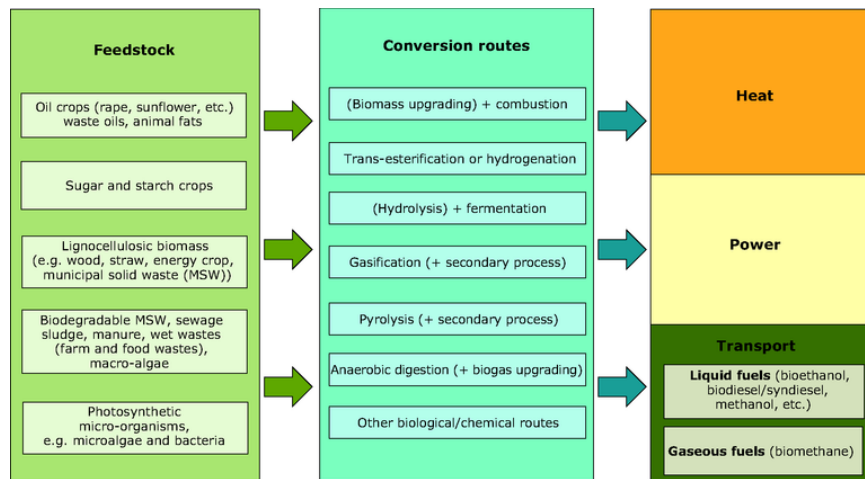


Figure 2: Scheme of Biomass Conversion Routes [4]

Due to its high moisture content, wet biomass such as lignocellulosic biomass, sludge and manure is the most difficult biomass to deal with. This high content of moisture or water, impacts negatively on the overall energy efficiency of the process (because of the wasted portion of energy in drying).

Supercritical water gasification (SCWG) is the ideal solution for this problem. Differs with the digestion process, it does not need big storage volume and long residence times. It does not require a drying pre-treatment step like conventional gasification, and instead uses water as its gasification medium. In the next section, the concept of the supercritical water gasification is thoroughly explained.

## 1.2. SUPERCRITICAL WATER GASIFICATION (SCWG)

Supercritical water gasification technology, in general, is considered the most promising and straightforward way of processing aqueous biomass, for the simple reason that the contained water is the same as the solvent used in the reaction itself. Its research goes back as far at the 1970s by the NASA where the objective was to determine the process feasibility to decompose cellulosic waste materials in long-term space missions [5]. Since that the interest from the scientific community in this technology has not decreased.

This technology has several advantages, such as: the output gas is already at high pressure (typically 22-25 MPa) and free of impurities, is not diluted with nitrogen (as in normal gasification, where extra separation steps are needed) and depending its operating conditions high content of  $H_2$  or  $CH_4$  can be found. The latter is interesting because depending on the fine tuning of operating conditions the production can be oriented towards hydrogen, synthesis gas (minimum amounts of  $CH_4$ ) or synthetic natural gas (minimum amounts of CO and maximization of  $CH_4$ )

In SCWG biomass-based model compounds, such as glycerol and glucose are used to simplify the problem, and therefore mimic and understand the particularities of the physical phenomenon. Real biomass is used to obtain the desired output gas, and up today the feedstock used so far

goes from paper sludge, sawdust, manure, wastewater, food and agricultural waste, sludge, algae slurry, etc.

For industrial applications, some technological challenges must be addressed, such as pumpability of the biomass, corrosion in the reactor due harsh operating conditions, plugging due char and coke formation, salts precipitation, need to increase thermal efficiency, etc. In order for this technology to enter and compete in the market, this challenges must be overcome.

### **1.3. TECHNOLOGICAL CHALLENGES: CHAR FORMATION PROBLEM**

Pyrolysis, liquefaction, and gasification are the thermochemical conversion routes available to process biomass in order to obtain biofuels or chemicals. It is known that one common problem that these technologies share is the formation of solids like char/coke. However it was noted for the first time by Modell [5], that char and coke formation is reduced using hydrothermal gasification, which led to numerous research and publications describing this process.

The hydrothermal process behavior, chemistry, and kinetics of the reactions involved (using biomass model compounds) have been studied for years already. Also, experiments with real biomass have been carried away showing great potential. Identifying the biomass heating-up step as the key to understand how the char/coke formation occurs and how it influences the overall process.

One of the current disadvantages found in SCWG technology, is the char/coke formation. Because it decreases gasification efficiency for the simple reason that a portion of the available biomass is being converted into an “undesired” product instead of gas. Also, these particles inside the reactor move freely with the other fluids, depositing on the walls (producing hot spots which lead to fouling) or even worst case scenario, plugging the reactor itself or downstream equipment causing a situation that jeopardizes the safe operation and integrity of the facility.

Further describing char [6], two kinds can be recognized: primary char which is produced from hard plant tissue (in lignocellulosic biomass such as leaves, pine cones, wood or coconut shell). The solid biomass goes through a partial liquefaction and turns mostly into carbon (the char morphology is similar to the original biomass one). The second type of char (sometimes also called coke) is the result of the structural decomposition of water-soluble biomass components, which condenses into a solid residue. This char is richer in oxygen and hydrogen, and its structure is different than the original biomass. Although by definition there are two types of char, these are mixed and considered as a whole into this lumped by-product of the supercritical gasification process.

### **1.4. RESEARCH OBJECTIVE**

The objective of this work is to contribute to the solution of SCWG technological challenges. Specifically, the need of understanding the char formation problem in the SCWG process and find out if this technology can be feasible to implement in a socio-economic context.

From this objective, is expected to answer the following research questions:

1. Develop and validate a kinetic model for biomass conversion in supercritical water gasification including the char formation process.
2. What are the key parameters controlling the char formation in supercritical water gasification?
3. Compare the model results with applicable experimental data.
4. Is supercritical water gasification a socio-economic feasible technology for handling wet biomass in comparison with other competing techniques?

In order to answer the research questions, the following method was applied:

For the char formation process, a numerical model was developed using Computational Fluid Dynamics (CFD), with glucose as biomass model compound. The model is expected to replicate the results of a real lab experiment. The tasks in this step are:

- Set up a model using commercial software, ANSYS Fluent, that solves numerically the equations involved in the supercritical water gasification.
- Verification of the model, through the replication of real lab experiments and comparison of the results.

The feasibility of the SCWG technology is investigated, through a techno-economic assessment enclosed in the Dutch context. Taking into account biomass availability and its impact in the agricultural life.

This work is within the framework of the project "Scarlet plus" supported by AgentschapNL (RVO) TKI.

## 1.5. OUTLINE

The work presented in this thesis is divided into four chapters.

Chapter 2 is devoted to literature review. First, supercritical water gasification concepts are introduced. Then, results from previous works and current state of supercritical water gasification using glucose with focus in the char formation process is shown. Finally, this theoretical background is complemented by a review of the different SCWG modeling efforts available.

In Chapter 3, the collected information and insights from the literature review allow the development of a numerical model of the SCWG. Careful selection and calculation of the thermo-physical properties of the species involved is shown. Kinetic data from experimental results is analyzed and used for the implementation of the right kinetics parameters for the chemical reactions component of the model.

Chapter 4 and 5 are dedicated to the CFD modeling of the SCWG. First, a laminar flow model results are presented in Chapter 4. The investigation is then extended, to a turbulent flow model in order to further understand the char formation problem in Chapter 5. The results of the numerical simulations are compared against experimental data for the amount of produced char and characteristics of the output gas.

In Chapter 6, how supercritical gasification can impact the agricultural life in the Netherlands is shown. An estimation of the biomass resource potential is calculated, this is the base for the socio-economic assessment of the technology. Then, discussion and arguments of why this technology should be pushed forward and implemented are shown.

In the last chapter, conclusions and recommendations for further research are presented.

## 2. LITERATURE STUDY

### 2.1. INTRODUCTION

This chapter presents the necessary concepts to understand supercritical water gasification and why the scientific community interest in its benefits. A literature review is done with the goal of understand what have been done so far in previous works and what is the current state of the char formation modeling specifically. This knowledge is necessary to give the necessary framework for the model development presented in the next chapter.

### 2.2. PROPERTIES OF WATER AT SUPERCRITICAL CONDITIONS

The use of supercritical fluids (SCFs) is not new, it has been utilized in the food industry for many years establishing it as a well-known process [7], examples of some applications are: decaffeination of coffee using CO<sub>2</sub>, extraction of lipids, production of natural colorants and aromas, elimination of pesticides, sterilization of milk and juices, deodorization of fish oil, encapsulation of oils, deodorization of corks, etc.

Nowadays supercritical fluids are used too in the following industries: cosmetic, pharmaceutical, polymer and plastics, chemical, material, wood, textile, power production, waste treatment, etc. What make supercritical fluids so interesting, are their properties. Because in this state, the fluid has the advantageous properties of liquids and gas at the same time, for example: it has a sufficiently low density to have considerable dissolving power, high diffusivity of solutes and low viscosity facilitating mass transport making it a excellent solvent [8].

A substance is in the supercritical region when its temperature and pressure are above its critical point. In the context of this work, the SCF of interest is water. In the Figure 3 the phase diagram of water is shown. Water is considered in the supercritical region above its critical point 374 °C (647 K, 705 °F) and 22.064 MPa (3,200 psia or 218 atm).

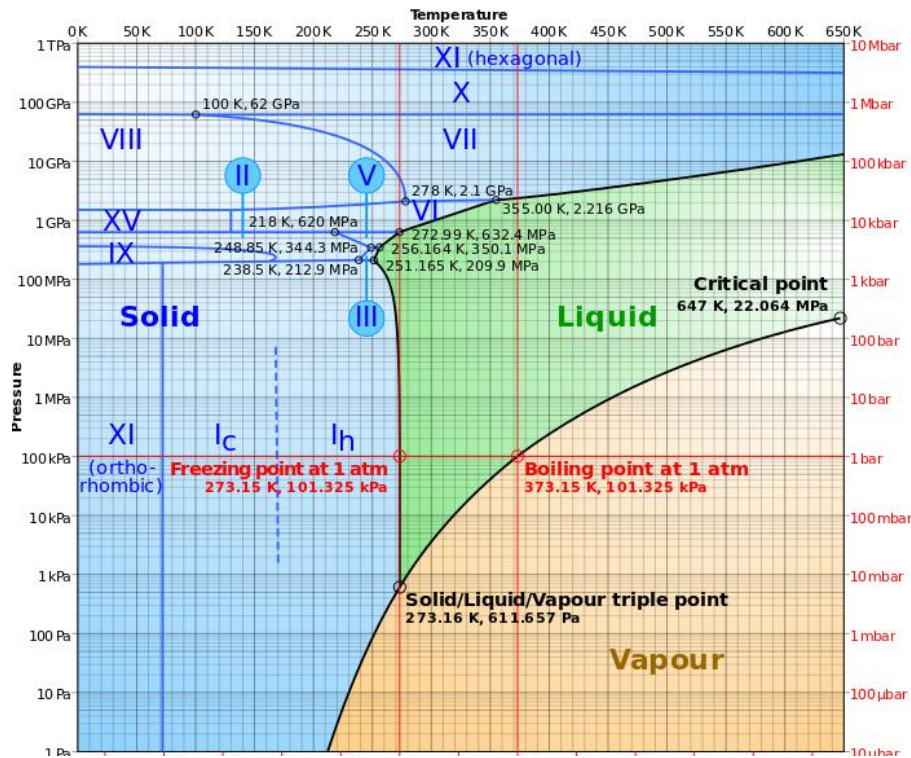


Figure 3: Phase diagram of water [9]

To be more precise, as the critical point is approached properties as: density and viscosity suddenly drop and near this point, the drop is vertical for a very small range in temperature (approximately in a 50 °C delta), density decreases about 70% and viscosity about 50% then stabilizes with increasing temperature as can be seen in Figure 4 and Figure 5 respectively.

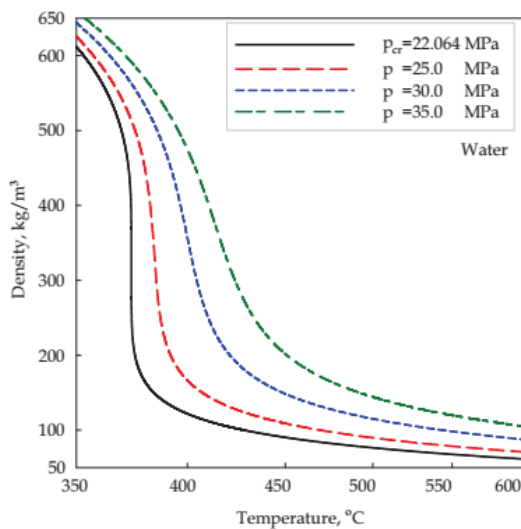


Figure 4: Density vs. Temperature [10]

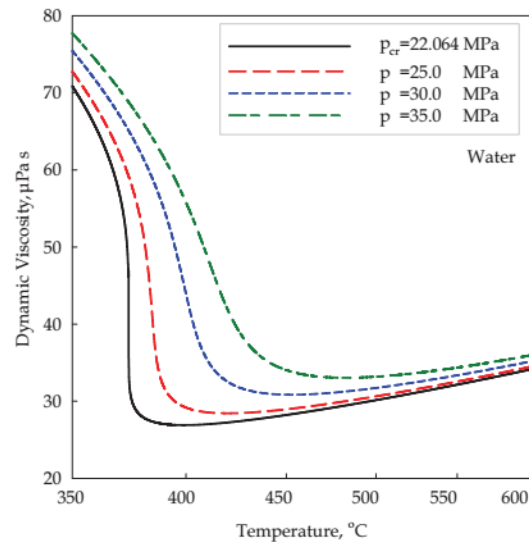


Figure 5: Dynamic viscosity vs. Temperature [10]

Also volume expansivity, specific heat, thermal conductivity and Prandtl number experience sudden increase near the critical point (See Figure 43, Figure 45, Figure 46 and Figure 48 respectively in Appendix1), at the same time kinematic viscosity and specific enthalpy go through a peak rise (see Figure 44 and Figure 47 respectively in Appendix1).

However with increasing pressure, these top values tend to decrease rapidly too and then “stabilize”, this stabilization behavior towards a minimum value can be seen also for the dynamic viscosity, kinematic viscosity and thermal conductivity after the critical and pseudo critical points (see Figure 5, Figure 44 and Figure 46 respectively in Appendix1).

The changes above in properties also affect another one, such as dissolving power, degrees of hydrogen bonding, polarity, dielectric strength, molecular diffusivity and viscosity (all these variations at the molecular level) [11]. Is worth noticing; for the understanding of how properties changes influence the water behavior in the typical gasification chemical reactions, the dielectric constant.

In the supercritical region, dielectric constant decrease (see Figure 6) and water behave like an organic, non-polar solvent. With poor solubility for inorganics, but with excellent miscibility with gases and hydrocarbons. This almost complete miscibility is a very good setting for homogenous reactions of water with biomass compounds [12].

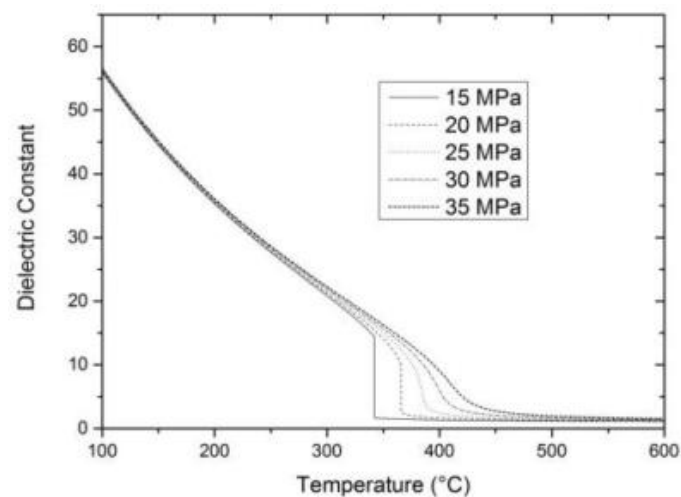


Figure 6: Dielectric constant of water [10]

### 2.3. SUPERCRITICAL WATER GASIFICATION (SCWG) OF GLUCOSE

Understanding the chemical reactions involved real biomass gasification is a challenging and highly complex task. Instead, performing lab experiments of biomass model compounds (such as glycerol, methanol, glucose, etc.) teach valuable lessons to understand further and predict how real biomass can behave in the same operating conditions.

Being glucose the dominant compound in biomass, it can adequately reproduce the reactions and interactions that occur during the SCWG process, therefore is selected as a model compound for this work. Also, the amount of published literature about hydrothermal reactions with glucose is extensive, providing enough experimental data to validate the numerical model.

The earliest research with glucose goes back as 1975 by Amin et al. [5]. Yakaboylu et al. [12] collected and shows historical information about it from the last 25 years at least. These studies independently concluded that an increasing temperature and residence time under supercritical pressure increases glucose conversion into output gas with a focus on hydrogen production.

For the interest of this work, an emphasis was put into the publications where char was obtained and the used reactor is tubular (which means a continuous process), aiming to achieve results that could be useful for the future development of a pilot plant. In the Table 1 below can be seen in details the publications found.

Table 1: Overview of lab-scale tubular reactor experiments

wt %	Temp. (°C)	Pres. (MPa)	Res. time (s)	GCE (%)	H <sub>2</sub>	CO	CO <sub>2</sub>	CH <sub>4</sub>	Char cont. (%)	Ref.
5-20	550	25	NA	12.4	10-15	10-50	20-30	10-20	Max yield 8.7	[13]
1.5	573-733	25	0-60	NA	NA	NA	NA	NA	Max yield 0.12	[14]
5	400	25	10-240	10	12	41.4	43	3.2	NA	[15]
1.8-15	600-767	25	15-60	91	68 (mol%)	0.9 (mol%)	29.4 (mol%)	1.7 (mol%)	NA	[16]
10-15	750-800	22	4-6.5	47.4-117.5	0.26-0.4 (mol/mol)	0.01-0.48 (mol/mol)	0.09-0.32 (mol/mol)	0.12-0.26 (mol/mol)	NA	[17]
5	600	24	28,800	75.2	8.7	55.1	18.3	11.5	2.1	[18]
1.5-3	300-400	25	70	NA	NA	NA	NA	NA	NA	[19]
0.02-0.15M	350-450	25	80-3,000	NA	NA	NA	NA	NA	NA	[20]
0.1-0.8M	600-650	34.5	24-318	29.2-133.7	26-38	26.7-7	45.3-39.8	1.4-11.3	NA	[21]
0.6M	480-750	28	10-50	16.5-99.7	0.08-4.78 (mol/mol)	0.47-1.3 (mol/mol)	0.4-3.52 (mol/mol)	0.03-1.26 (mol/mol)	NA	[22]
NA: Not reported or not available data										

After a careful inspection of the literature review shown above, can be identified two groups of experiments: the ones that produced and reported char formation and the ones that did not produce (or not reported) it. Our interest is focused in the first group, which are the work done by: Molino et al. (2016), Promdej and Matsumura (2011) and Zhang et al. (2016).

## 2.4. MODELING APPROACHES

The overall goal of this master thesis is to develop a "model" that can mimic the SCWG process. This means that the model must be able to reproduce the physics and chemical reactions of the species involved. A working model can allow the simulation of different operating conditions, scenarios, parametric studies, etc. Tools that ultimately serve the purpose of improving the SCWG technology.

In this effort, several methodologies have been applied to describe the SCWG process such as kinetic modeling, computational fluid dynamics modeling, thermodynamic equilibrium modeling, and process modeling. Each method has different objectives and results, in the following paragraphs the most relevant for this work are explained.

### 2.4.1. KINETIC MODELING

As introduced in Section 1.3 (Chapter 1), char formation is a problem in the SCWG technology. It can lead to fouling and heat exchanger/reactor plugging. Therefore much interest by the scientific community was put into this topic. For example Muller and Vogel (2012), performed experiments at several operating conditions (300-430 °C, residence times of 5-120 minutes, feed concentration up to 30 wt% at pressures around 30 MPa) with glycerol and glucose to quantify the char produced. Their results led to the conclusion that the highest formation rates are present near the supercritical temperature, along residence times between 15-60 minutes and with high concentrations of the feedstock [6].

This type of experiments with biomass model compounds stimulated curiosity towards more realistic operating conditions and use of raw material, for example, Karayildirim et al. (2008) performed experiments using real biomass (artichoke stalk, pinecone, and sawdust) at several operating conditions (400-600 °C during one hour at 20-34 MPa). From this investigation, it was concluded that can be identified two chemical pathways for the formation of char: direct conversion from the feedstock and polymerization of intermediates reaction products. And is suggested that the biomass should be heated up as fast as possible as a countermeasure to slow down the formation of char [23].

This explanation of the biomass decomposition pathways towards the products and char has been widely studied by several authors for years such as: Lee et al. (2002) [22], Williams and Onwudili (2005) [24] and Matsumura's group (publications from period 2006-2011) [14, 19, 20, 25, 26]. From the literature review of these papers, the kinetics for the numerical model was chosen.

### 2.4.2. COMPUTATIONAL FLUID DYNAMICS (CFD) MODELING

With the help of a numerical analysis tool such as a CFD model, is possible to simulate endless configurations of different operating conditions and scenarios. This versatility is desirable for the design process of the reactor in the SCWG technology. Optimization can be achieved in a

CFD model before actually performing real lab or pilot experiments, which optimizes economic resources and time. Several CFD models have been developed over the years, Yakaboylu et al. (2015) in his publication shows a historical review of this particulate topic [12], however to the best of my knowledge, a CFD model that also includes char formation for the SCWG of glucose has not been developed to date.

Little related literature can be found about this topic specifically. Jin et al. (2016) [27] develop a 3D model of the SCWG of glycerol (which is known for not producing char), where the chemical species, full flow, and temperature field were calculated with the goal to calculate the optimum length of the reactor to ensure complete gasification. Using glucose as feedstock, Su et al. (2015) developed a 3D model involving heat transfer and chemical reactions with kinetics (but only for output gas production) in a fluidized bed in a temperature range between 823-923 K at 25 MPa [28].

Caputo et al. (2015) [29] performed lab-scale experiments in glucose gasification at 25 MPa, and 650 °C, output gas composition and gasification efficiency parameters are reported however char is not produced because of the high temperature of the experiment. Also, a 3D model was developed too, which was used to investigate the fluid dynamics itself by changing the injection angle of the feedstock to optimize the reactor design.

Aligned with the same goal, Matsumura and Yoshida (2009) [30] went deeper and developed three 3D models to describe the pyrolysis individually, catalytic and oxidation "parts" of the SCWG reactor. Char was included in these simulations but the chemical reactions did not create it, it was "introduced" assuming its thermo-physical properties in order only to study its dynamic behavior inside the reactor. This study concluded that the char particles with a larger diameter than 20  $\mu\text{m}$  would likely precipitate to the bottom of the reactor, while the particles with a smaller diameter than 10  $\mu\text{m}$  will probably try to "escape" from the top.

### 2.4.3. OTHER MODELING TECHNIQUES

Another effort to model SCWG different than the previous ones is the thermodynamic approach (also called stoichiometric model). The objective of this model is to estimate the equilibrium composition in chemical and phase of the species involved in the gasification process. Tang and Kitagawa (2005) [31] developed an algorithm based on Peng-Robinson Eos formulations with direct Gibbs free energy minimization for several feedstock (methanol, glucose, cellulose and real biomass).

Applying the same method, Lu et al. (2007) [32] went deeper and using wood sawdust as feedstock modeled the entire process design for the maximum production of  $\text{H}_2$ . Also, a parametric study was done to determine the influence of temperature, feedstock concentration, oxygen addition, pressure and recycling water. This study (like kinetic models) concluded that increasing temperature and pressure favor the production of output gas.

Regarding char formation, Castello and Fiori (2011) [33] using glycerol and microalgae *Spirulina* as feedstock proofed that at equilibrium char it is formed under certain conditions. It was found that at high temperatures (800 °C at 25 MPa); char is not expected up to 72% feed concentration. But when the temperature reduces, char is formed a lower feedstock concentration. The interesting contribution of this work is the development of ternary diagrams (shown in the Figure

7 below) for generic biomass, which mapped the char formation "zones" under different temperatures and pressures. This information can be particularly useful for the selection of the appropriate feedstock.

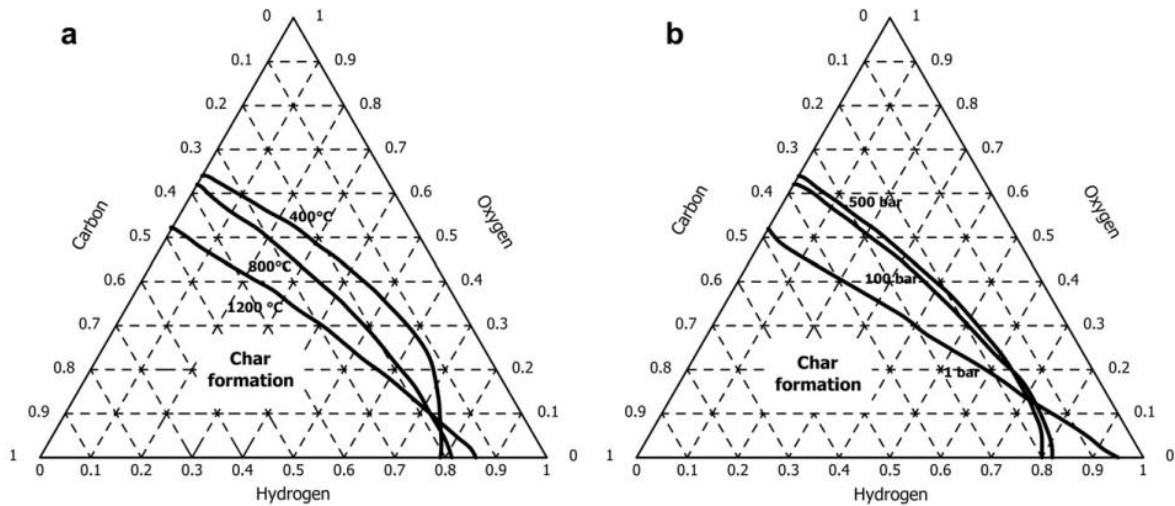


Figure 7: Ternary diagrams for char formation [33] (a) Char formation at varying temperature ( $P=25$  MPa); (b) at varying pressure ( $T=800$  °C)

Similar work was done by Louw et al. (2014) [34], with an emphasis on the development in performance indicators contours for gas yields, cold gas efficiency, the calorific value of product gas and heat reaction. These results complement the previous one because also include the applicable thermodynamic limitations at various operating conditions. A relevant example of these results is shown in the Figure 8 below:

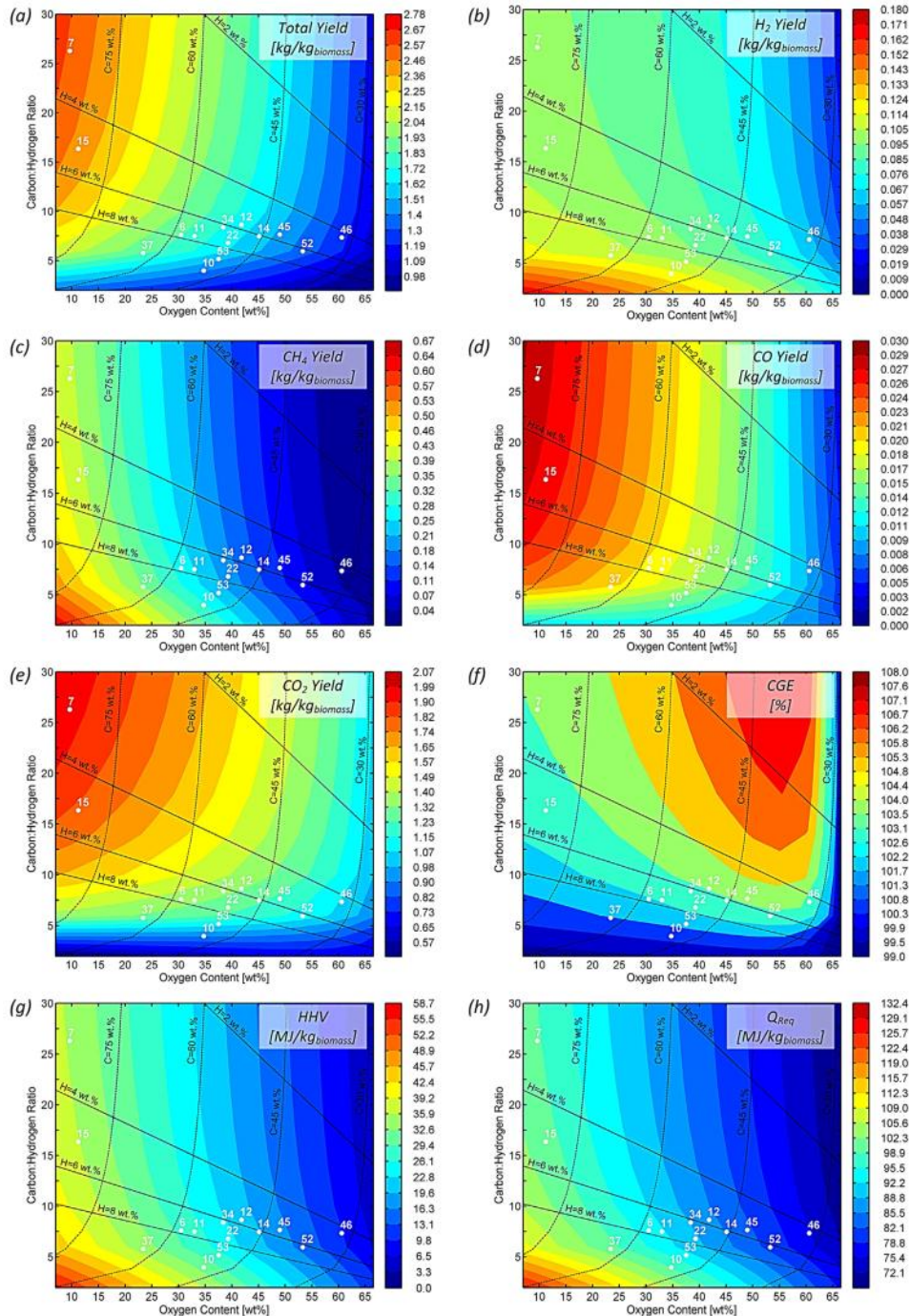


Figure 8: Effect of biomass composition [34] (a) total mass yield; (b)  $H_2$ ; (c)  $CH_4$ ; (d)  $CO$ ; (e)  $CO_2$ ; (f) CGE; (g) HHV of product gas (b) Heat for isothermal operation

In 2015, Castello and Fiori published an update of their work [35] expanding it to different types of biomass as feedstock (glucose, phenol, glycerol, paper residue, sludge, microalgae Spirulina, oak wood, pinewood and grape marc). The novelty relies on the development of a graphical approach to the values of the reaction extent of water-gas shift (WGS) and CO methanation at equilibrium. They concluded that high temperature is needed to suppress methanation and increase the yield of  $H_2$ .

## 2.5. DISCUSSION

From the literature review about previous experiments with glucose as feedstock, it was found that only three publications reported char formation during the supercritical water gasification process and therefore are of the interest of this work. However, certain observations can be made to each of them.

From this three publications, Molino et al. (2016) results do not specify the residence time applied and only report the output gas composition while the flow rate or yield is missing. Promdej and Matsumura (2011) results show in detail the residence time influence, however is not reported the output gas composition and only the yield is shown. And finally, Zhang et al. (2016) results shows output gas composition and some yield of individual gases but the residence time up to 28,800 seconds can be an obstacle regarding simulation time and computation resources.

Therefore, for the validation of the numerical model to be developed in the following chapters of this master thesis. For the kinetics of chemical reactions of glucose decomposition and char production, the data of Promdej and Matsumura (2011) is used. And for the composition and quantity of the final products a combination of Molino et al. (2016) and Promdej and Matsumura (2011) are considered.

## 3. SCWG MODEL WITH CHAR FORMATION

### 3.1. INTRODUCTION

This chapter presents the necessary parts to assemble the numerical model for the supercritical water gasification process including char formation. First, the calculation and implementation of the thermo-physical properties of the involved substances (water, glucose, char and output gas) is shown. Then, the necessary chemical reactions are defined with their respective kinetic parameters. Special emphasis is put in the derivation of the right kinetics for the char formation process. These different elements working together allow the simulation of the SCWG process, in order to replicate experimental lab results in the next chapters.

### 3.2. THERMO-PHYSICAL PROPERTIES

The region of interest of the substances involved in the SCWG process, is the supercritical region. It was mentioned before than the properties in this particulate region, have mixed behavior between liquid and gas properties. The properties of interest for this work are: density, specific heat capacity, enthalpy, standard enthalpy of formation, standard molar entropy, dynamic viscosity and thermal conductivity. The values of these properties in the supercritical region is not easy to find in tables or charts, therefore they had to be calculated through specific formulas and correlations. The following paragraphs explain how all properties were obtained and then implemented into the numerical model.

Regarding the numerical model itself, ANSYS Fluent has material databases which collect all type of thermo-physical properties and information for its use in the simulations. ANSYS Fluent also allows the creation of new materials and the input of its properties. This properties can be defined in several ways such as temperature-dependent functions or using specific correlations or formulas.

In general, the majority of the properties have been computed using temperature-dependent functions at a given pressure, which in their most basic form looks like the Equation I shown below, where  $\varphi$  is the property of interest. Then, these coefficients were tabulated and inserted in ANYS Fluent through user-defined functions (UDF). A UDF is a C program or a C function (programming script) which is loaded in ANSYS Fluent to enhance its capabilities.

$$\varphi(T) = A_1 + A_2 * T + A_3 * T^2 + \dots$$

*Equation I: Temperature-dependent properties*

All the water properties were defined using the IAPWS-IF97 formulation [36, 37] which is the international industrial standard for thermodynamic properties of water and steam, this formulation is valid from 273.15 K to 1,073.15 K at pressures to 100 MPa. These coefficients were tabulated and implemented using a dedicated UDF for this purpose.

For the rest of the species involved: the densities were calculated using the Peng-Robinson equation of state (EoS) with the corresponding acentric factors and critical properties (pressure and temperature) [38]. The specific heats and enthalpies were calculated using the thermodynamic functions from NASA Lewis coefficients [39], the applicable coefficients can be found in the Appendix 2.

The calculation of viscosities and thermal conductivities were done using the expressions given by Chung et al. [40], the prediction for diffusivities of sub- and supercritical water are recommended with the Tracer Liu-Silva-Macedo (TLSM) equation [41]. In the same way than the water properties, this data was tabulated and implemented in ANSYS Fluent through the use of several UDFs.

### 3.3. CHEMICAL REACTIONS AND KINETIC MODEL

Glucose gasification is a complex process where several side products can be found during the hydrothermal reaction. Matsumura's group [14, 19, 20, 25, 26] have elucidated a complete pathway and measured the kinetic parameters for the temperature range where char formation takes place. This pathway is shown in Figure 9 below:

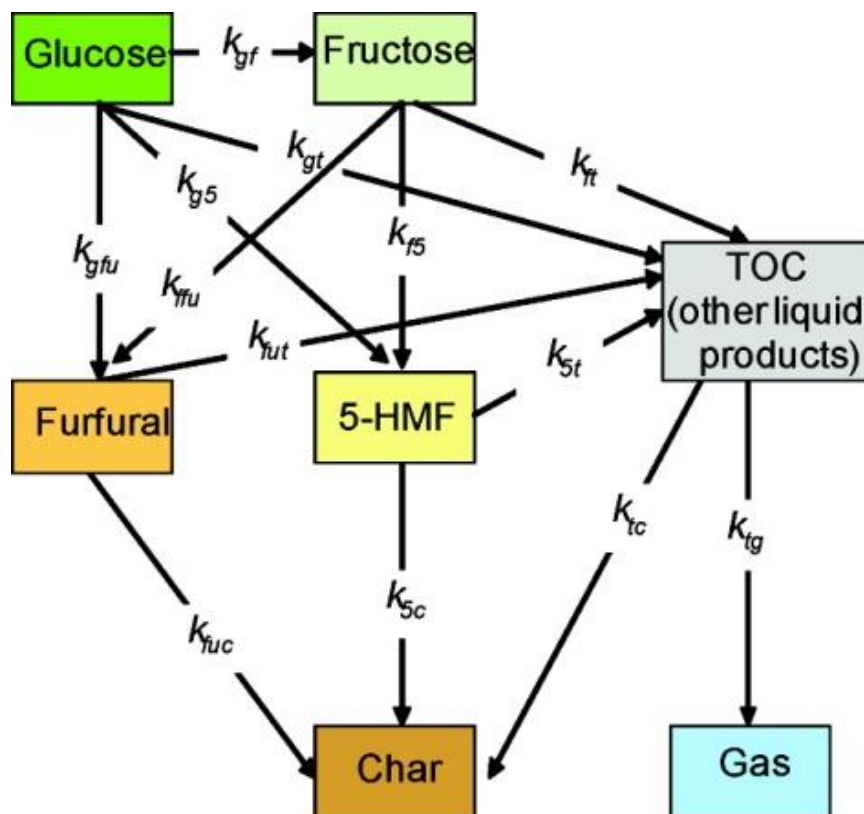


Figure 9: Glucose char particles formation pathways [14]

At first sight, it can be noted that in between the glucose (input), char (by-product) and the gas (output) there are several intermediate substances such as: fructose, furfural, hydroxymethylfurfuraldehyde (hereafter called only as 5-HMF) and other liquid products (hereafter called TOC, which means "total organic content"). All the elements in this pathway have a relationship with each other, moreover a chemical reaction with a particular kinetic parameter.

Glucose is decomposed first in fructose, furfural and 5-HMF. This intermediate components can individually contribute to char. This contributions can be grouped in two: furfural and 5-HMF are different to the ones from the water-soluble products (TOC). Glucose and these intermediate components also decompose towards liquid products (TOC), which is then gasified to obtain the final output gas or be polymerized to form char too [19].

According to Matsumura et al. [14] findings, two types of chemical reactions were identified: ionic and radical. This two reaction pathways provide an explanation of why char formation rate is decreased when the temperature is increased. Buhler et al. [42] elucidated that ionic reactions prefer high pressures and/or lower temperatures, while according to Kruse and Gawlick [43] in the supercritical region free-radical reactions and indispensable for the production of output gas.

Given the fact that char production is confined to the subcritical region (increasing yield with temperature) and strongly prohibited in the supercritical one. Matsumura, inferred that " the low dielectric constant inhibited char production, which is ionic" [14]. Is in fact by the change in the dielectric constant (or ion product) when moving from sub- to the supercritical region, in the case of a radical chemical reaction Arrhenius behavior will be followed. But in the case of ionic chemical reactions, the ion stability will be affected. Therefore it will now follow an Arrhenius behavior. In Table 2 below an overview of the chemical reactions involved in the pathways shown in Figure 9.

Table 2: Classification of glucose SCWG reactions [14]

Ionic reaction		Radical reaction	
Non-Arrhenius		Arrhenius	
gf	isomerization	gt	decomposition
gfu	dehydration	5t	decomposition
g5	dehydration	fut	decomposition
f5	dehydration	tg	gasification
ffu	dehydration		
ft	decomposition		
5c	polymerization		
fuc	polymerization		
tc	polymerization		

From all the chemical reactions involved in this complex pathway, for the interest of this work the following kinetic parameters are thoroughly inspected: fuc, 5c, tc (for the polymerization towards char formation) and tg (for the gas production). The complete kinetic parameters for the temperature range between 573-733 K for all the chemical reactions can be found in Appendix 4.

For the overall decomposition rate of glucose ( $k_1$ ), Promdej and Matsumura [14] reported a pre-exponential factor (A) of  $6.9 \times 10^7 \text{ s}^{-1}$  and an activation energy ( $E_a$ ) of  $9.554 \times 10^7 \text{ J/kg mol}$ , which is

in good agreement with other published results. For the char formation process, the derivation of the kinetic parameters is obtained with the following procedure:

- 1) In a x-y plot, the natural logarithm of the kinetic data ( $k_r$ ,  $t_{5c}$  and  $t_c$ ) are placed with the inverse of their corresponding temperature.
- 2) Following the form of the Arrhenius equation (shown in Equation II), the best exponential fitting possible is calculated in order to obtain the kinetic parameters of interest: the pre-exponential factor ( $A$ ) and the activation energy ( $E_a$ ), which are given by the slope of the line and the factor that accompanies the temperature variable respectively.

$$k_r = A \exp \frac{E_a}{RT}$$

*Equation II: Arrhenius equation*

The Arrhenius plot for the char formation mechanism ( $k_2$ ) is shown in Figure 10, this graph gives a pre-exponential factor ( $A$ ) of  $3.527 \times 10^{-6} \text{ s}^{-1}$  and activation energy ( $E_a$ ) of  $-3.363 \times 10^7 \text{ J/kg mol}$ .

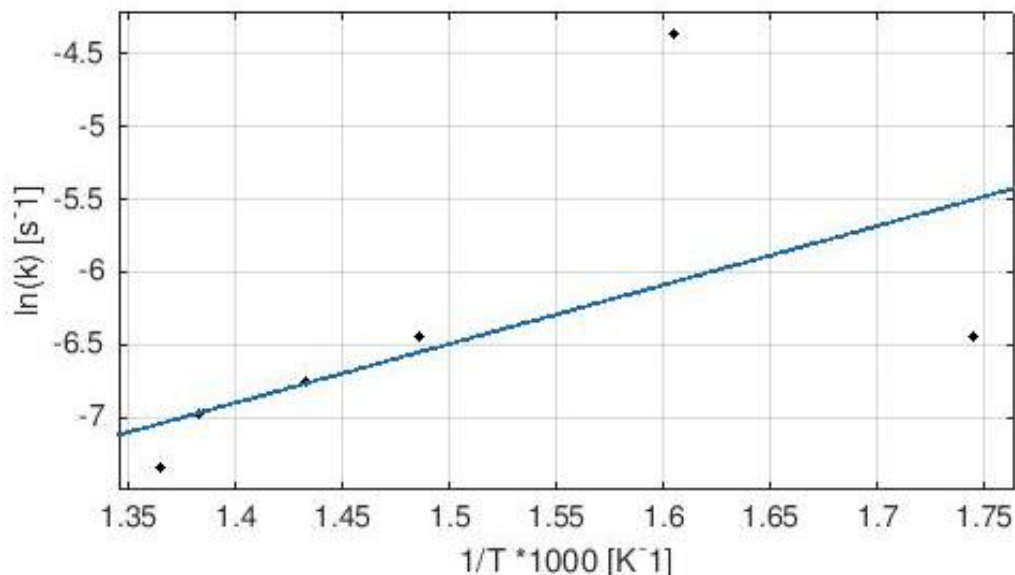
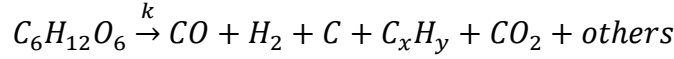


*Figure 10: Char formation Arrhenius plot*

Regarding the chemical reactions itself; first the substances involved in the glucose gasification were identified, which are: water, glucose, hydrogen, carbon monoxide, carbon dioxide, methane and carbon (as char). Then, the appropriate chemical reactions were selected. Two different chemical reactions were used: one for the glucose decomposition towards gaseous products and another one for the char formation from glucose. The glucose decomposition reaction involves water and glucose as reactants that are transformed into hydrogen, methane, carbon monoxide and carbon dioxide.

The char formation reaction involves glucose transforming into char and as "by-product" some gaseous species which are hydrogen, carbon monoxide, carbon dioxide, traces of other hydrocarbons and "other" products. Only the recognizable species are considered. This reaction is known as the glucose pyrolysis and was taken from the work of Susanti et al. [16] and is shown in the Equation III below:



Equation III: Glucose pyrolysis reaction from Susanti et al.

The numerical model investigation, began using the balanced reaction for the glucose decomposition and then, this stoichiometry was adjusted into a "empirical" one using the experimental gas composition (chosen in the literature review section) according to the real lab-scale results from Molino et al. [13], applying mass balance and the output gas composition shown in the Figure 11.

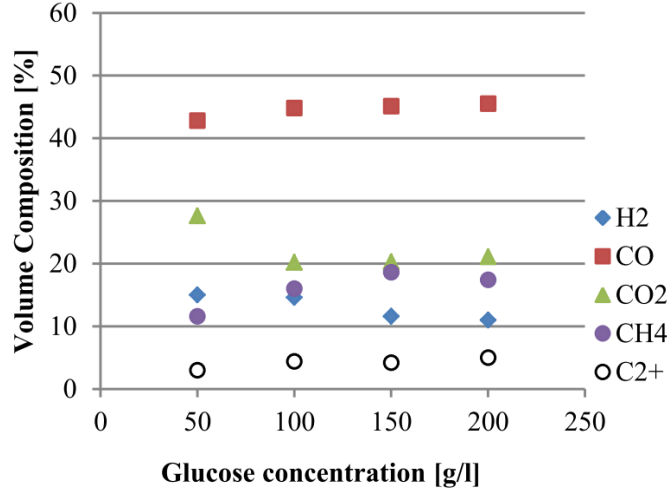
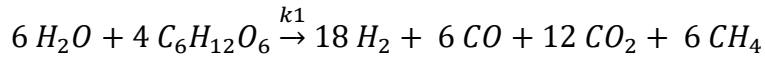


Figure 11: Output gas composition experimental results from [13]

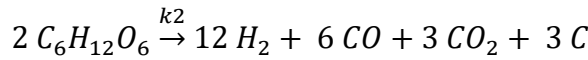
The balanced reaction is shown in the Equation IV, while the empirical one is shown in the Equation V. For the char formation, a balanced equation was used and is shown in Equation VI below: The chemical reactions formulas shown below combined with the selected kinetic parameters allow the formation of the output gas and char in the numerical model.



Equation IV: Glucose decomposition balanced reaction



Equation V: Glucose decomposition empirical reaction



Equation VI: Char formation chemical reaction

The thermo-physical properties, chemical reactions and kinetic parameters are the building blocks for the CFD numerical model, afterward the model is complemented with the appropriate selection of the physics (according to the experiment to be simulated). Finally, the obtained results are then validated or replicated with experimental data. A schematic of the model is shown in the Figure 12 below:

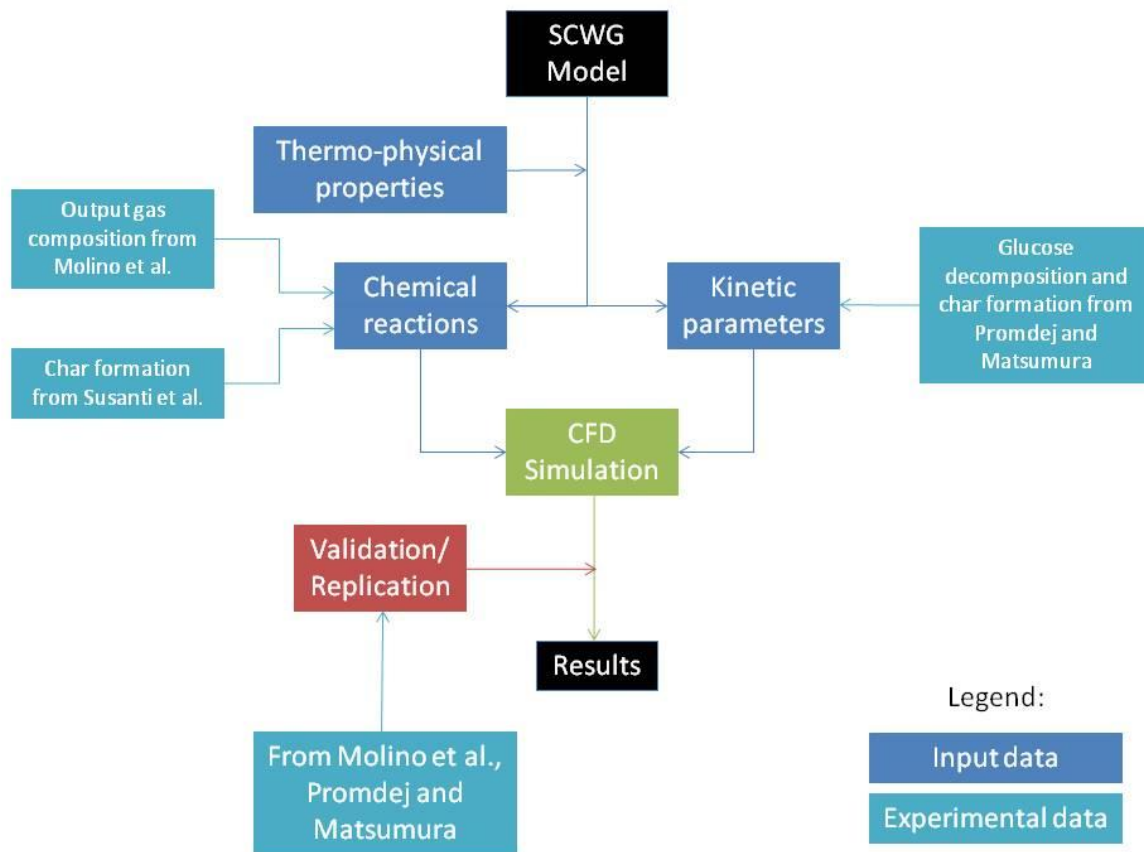


Figure 12: SCWG with Char formation model schematic

## 4. CFD OF THE EXPERIMENT #1

### 4.1. INTRODUCTION

The result presented in this and next chapter were obtained using a Computational Fluid Dynamics numerical model implemented in ANSYS Fluent. For the flow, in this numerical model conservation equations for mass, momentum, energy, and species conservation are solved. The properties of the flow, the discretization of the domain and the correct boundary conditions allow the solution of the equations mentioned above. The equations are solved numerically using a finite-volume formulation; these equations expressed in the strong conservative form are shown in the Appendix 2.

### 4.2. EXPERIMENT

The study of the SCWG process was done through a numerical simulation of the work of Molino et al. [13]. The reactor has a tubular configuration, with an internal diameter of 25 mm, external diameter of 48 mm and with a length of 1,120 mm (including a 900 mm heated length). The reactor material is stainless steel T316 type, and it has two inlets: one for the water and another one for the glucose flow. The experimental setup is shown in the figure below:



*Figure 13: Laminar flow experimental setup [13]*

According to the experimental procedure by Molino et al. [13], an aqueous solution of glucose at different concentrations and flows was tested. Water is fed into the reactor at a pressure of 25 MPa and a temperature of 550 °C, and then the glucose solution is fed into the reactor. In the experiments, the influence of two main parameters was investigated: flow rate and glucose concentration at fixed pressure and temperature. However, from the reported experimental results only the set of operating conditions which produced char is of the interest of the numerical simulations. The simulated condition is at 200 grams of glucose per liter in a 5 milliliters per minute flow.

Taking into account the operating conditions of the experiment, the Reynolds number is calculated (considering only water) to select the appropriate viscous physical model using the Equation VII. This calculation is shown below:

$$Re = \frac{\rho V_{axial} D_H}{\mu} = \frac{78.54 \text{ kg/m}^3 * 0.00017 \text{ m/s} * 0.0025 \text{ m}}{3.25 * 10^{-5} \text{ Pa/s}} \cong 1.03$$

*Equation VII: Reynolds number calculation for the laminar flow case*

Where  $\rho$  and  $\mu$  are the density and viscosity at the operating pressure and temperature respectively,  $V_{axial}$  is the mean velocity of the fluid and  $D_H$  the hydraulic diameter which in this case is the reactor diameter. From this calculation it was obtained a Reynolds number below 2,100 which means that the regime flow is laminar. Therefore the laminar viscous physical model was used in the simulations.

The numerical model validation is achieved by comparing three main parameters: output gas composition, the amount of produced char (in %wt) and global gasification efficiency (GCE). These definitions are shown in the Equation VIII and Equation IX respectively.

$$char \% = \frac{\dot{m}_{carbon}}{\dot{m}_{glucose\ inlet}}$$

*Equation VIII: Char production respect to the glucose fed*

$$GCE = \frac{\dot{m}_{syngas}}{\dot{m}_{glucose\ inlet}}$$

*Equation IX: Global gasification efficiency (GCE)*

### 4.3. NUMERICAL MODEL

The CFD numerical simulation includes the model developed in Chapter 3. Meaning that includes the thermo-physical properties, chemical reactions and kinetic parameters in order to recreate the SCWG process. To decrease the needed simulation time and computational power, it was decided to perform simulations in a 2D domain. This domain was made using another tool from ANSYS called ICEM CFD, which allows CAD design and application of meshing tools in the same environment. Given the 2D representation of the domain, the glucose inlet location had

to be slightly modified to represent the real life reactor. In the Figure 14 below, a scheme of the meshed domain is shown.

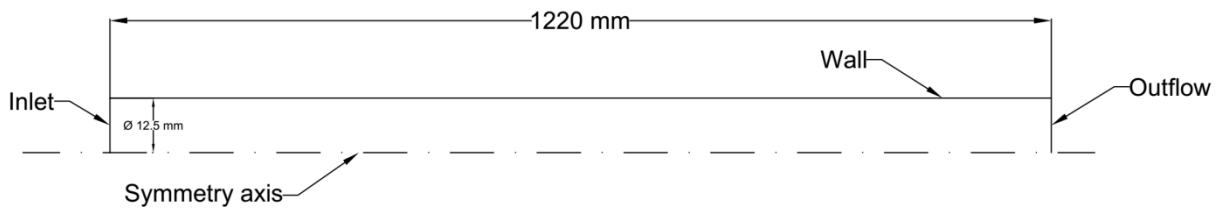


Figure 14: Laminar flow domain scheme

A total of 23,600 equally distributed rectangular elements were used for the simulation. The mesh is finer in the radial direction than the axial one. In the axial direction, spacing increases progressively using the geometric meshing law. A mesh independence study for this experiment simulation was done and is shown in Appendix 4.

Steady-state simulations were conducted, the applied solution method considers pressure-velocity coupling (with an absolute velocity formulation) and a second order upwind scheme for the solution of all the equations. The convergence criteria of the simulations aim for residuals in the  $10^{-3}$  order for continuity, velocity, and species except for the energy residual which aims for  $10^{-6}$ . Also, the mass and energy net imbalance was monitored and is preferred to keep it below 0.5% and 5% respectively. The selected step size is 0.1 s during the necessary number of iterations until the convergence criteria are reached.

The simulation was run in "pseudo-transient" mode and to obtain good convergence the equations were solved in a ladder: first the flow and energy, then the glucose inlet and finally the remaining species. The simulation strategy to terminate the simulations and obtain satisfactory results is based on the following criteria:

- a) Accurate balance between entering and exiting flow rates,
- b) Acceptable trade-off between sufficient reduction of the residuals against computation time and,
- c) Small oscillations in the variable values.

#### 4.4. RESULTS

The learning curve of this experiment involved solving numerical simulations of progressively complexity. In the beginning of the experimentation, only balanced chemical reactions (with and without kinetic parameters) was considered. After learning more about how to handle the model and ANSYS Fluent particularities. Numerical simulations using the empirical chemical reactions with complete kinetic parameters were carried out. A summary of the numerical simulation settings and applied operating conditions is shown in the table below:

Table 3: Parameter settings and operating conditions for laminar flow simulations

Parameters	Value
<b>Geometry</b>	
Diameter (m)	0.0025
Length (m)	1.22
Grid size (mm)	2.8 axial, 0.2-0.3 radial
<b>Boundary conditions</b>	
<b>Inlet</b>	
Feed mass flow rate (kg/s)	$1.67 \times 10^{-5}$
Feed inlet pressure (MPa)	0
Water mass flow rate (kg/s)	$7.25 \times 10^{-5}$
Water inlet pressure (MPa)	25
Feed and water inlet temperature (K)	823
<b>Wall</b>	
Wall temperature (K)	823
Characteristics	Stationary, no slip, material: steel
<b>Outlet</b>	
Average pressure specification (MPa)	25
Average temperature specification (K)	823
<b>Methods</b>	
Scheme	Second order upwind
Algorithm	Coupled
Time step	0.1
Relaxation factors	0.25-0.75
Convergence criteria	0.001-0.000001

The validation of the numerical simulations results is obtained by comparing them against the experimental results reported by Molino et al. [13], which are shown in the Table 4 below for easier review.

Table 4: Experimental results for numerical model validation [13]

Output	H <sub>2</sub>	CO	CO <sub>2</sub>	CH <sub>4</sub>	Total	Char % wt	GCE %
Volume composition %	10.9	45.6	20.8	17.2	94.6	8.6	12

After several rounds of numerical simulations, sufficient know-how was gathered to produce the results shown in the following graphs and tables. In order to present clearly the results, only the volume composition of the gaseous products is considered (meaning that the water content is not taken into account). In the Table 5 below the numerical simulation results and the experimental data for their validation is shown:

Table 5: Numerical model results for laminar flow

Experiment/ Simulation	Output gas, vol. composition %				Char content, wt%	GCE, %
	H <sub>2</sub>	CO	CO <sub>2</sub>	CH <sub>4</sub>		
Molino et al. [13]	10.9	45.6	20.9	17.3	8.6	12
Empirical stoichiometry	56	29.6	14.4	0	10.0	90

For better understanding and comparison, the results shown in Table 5 can be also seen in a graphical way in the figures below: output gas composition, char content and global conversion efficiency comparison are shown in the Figure 15, Figure 16, and Figure 17 respectively.

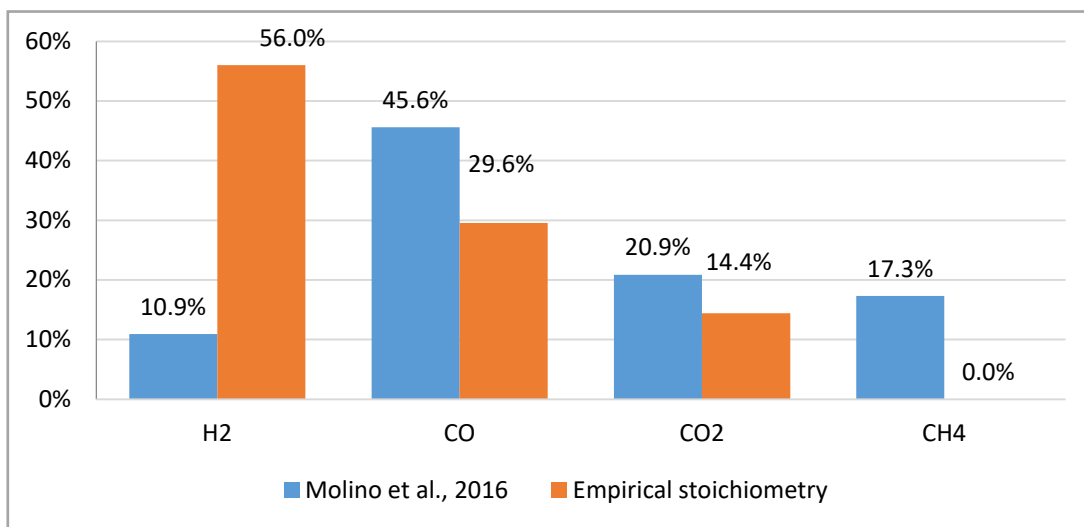


Figure 15: Output gas composition comparison

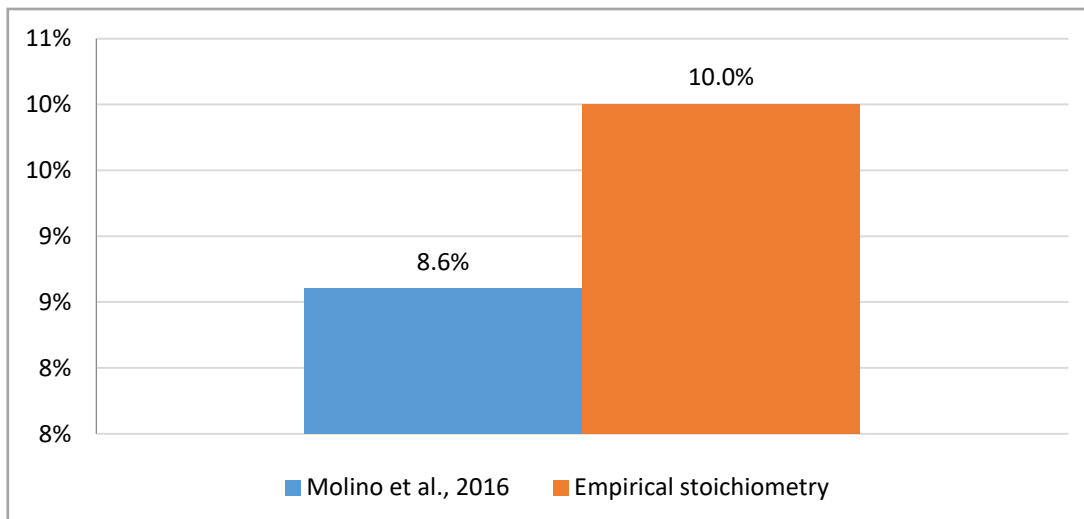


Figure 16: Char content comparison

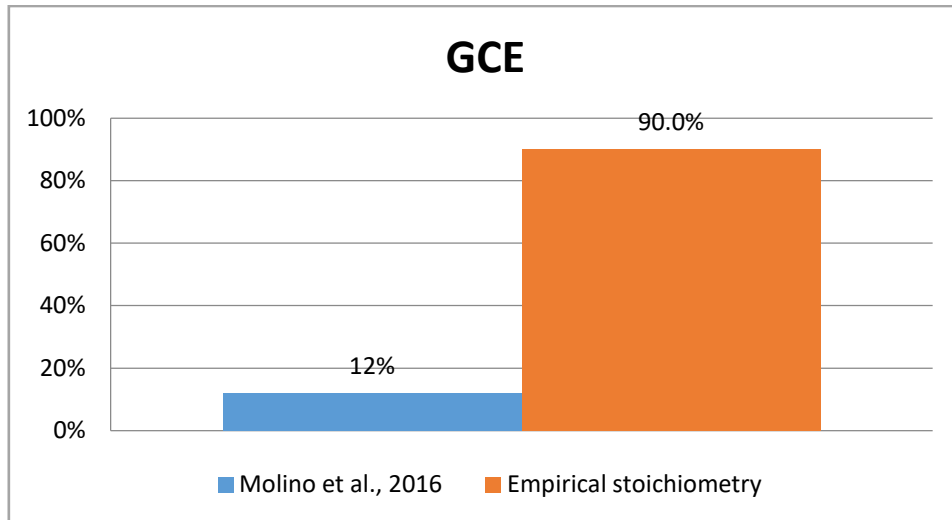


Figure 17: GCE comparison

Expanding the results, now in the following figures a visual review of the different species mass fractions contours along the reactor at steady-state condition are shown. In the Figure 18 the char mass fraction contours are shown. When compared to the (expanded view of the inlet zone) glucose mass fraction contours it can be noted how the glucose is rapidly consumed and converted into species products and char which dissipate along the reactor.

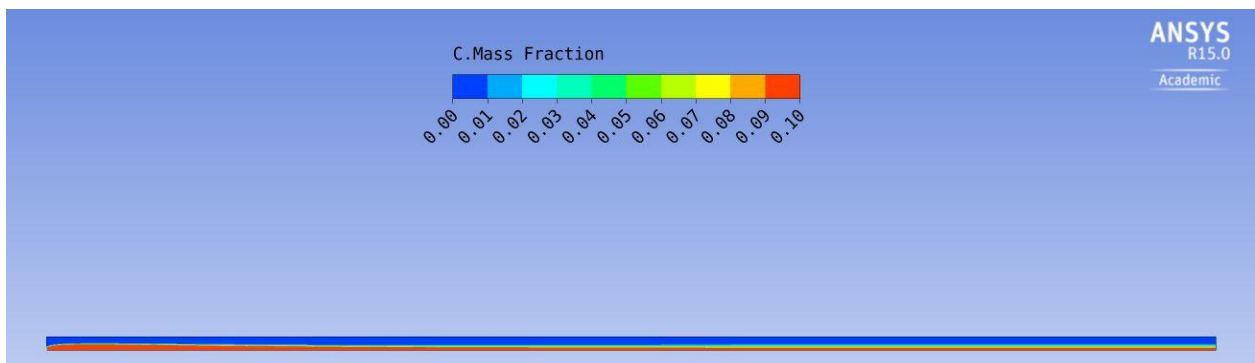


Figure 18: Char mass fraction contours

After this the glucose is basically entirely consumed and the mass fraction is zero along the reactor, which is in agreement with the expected behavior of the kinetic and chemical reactions established in the model.

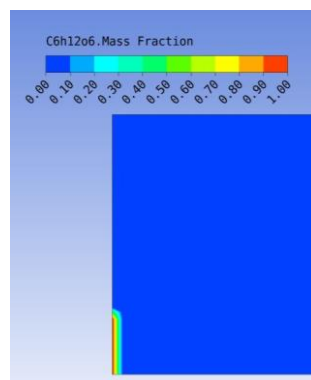


Figure 19: Glucose mass fraction contour

The latter is also supported by the Figure 19 which shows the water mass fraction contours. Inside the glucose inlet zone the water mass fraction is zero, while outside this zone the mass fraction is maximum 0.9 given the fact that this zone is shared also with the produced gaseous species of the gasification.

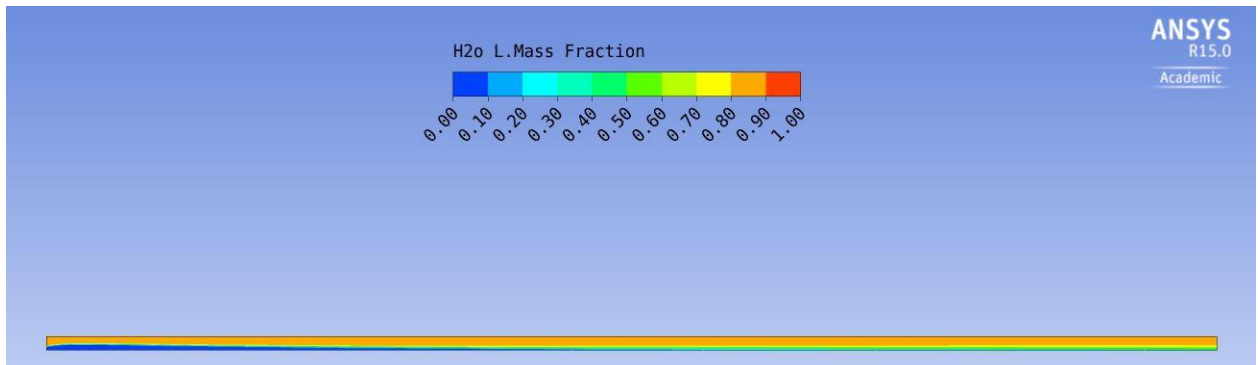


Figure 20: Water mass fraction contours

Additionally in the Figure 21, Figure 22, Figure 23 and Figure 24 the mass fractions contours for the hydrogen, carbon monoxide, carbon dioxide and methane are shown respectively. The first three show a similar "formation" behavior along the reactor, while the methane is formed towards the middle section in a very low quantity in comparison with the other gaseous species.

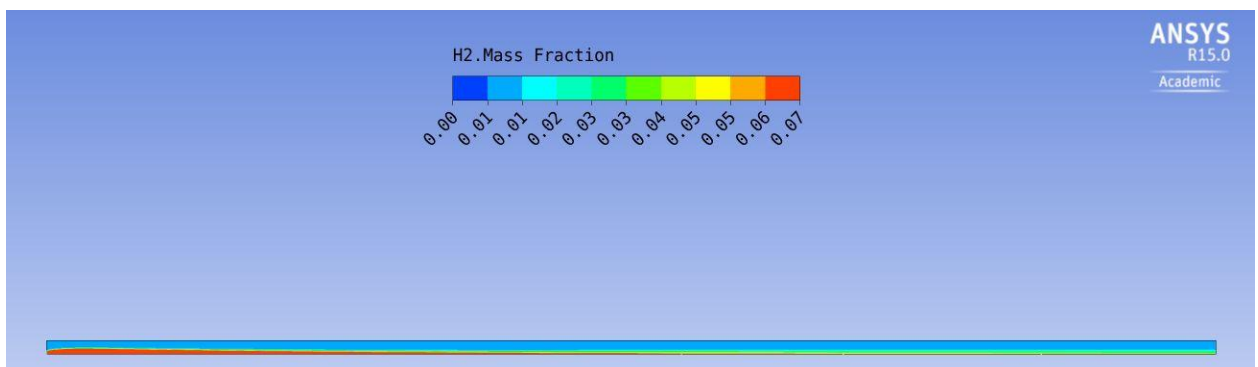


Figure 21: Hydrogen mass fraction contours

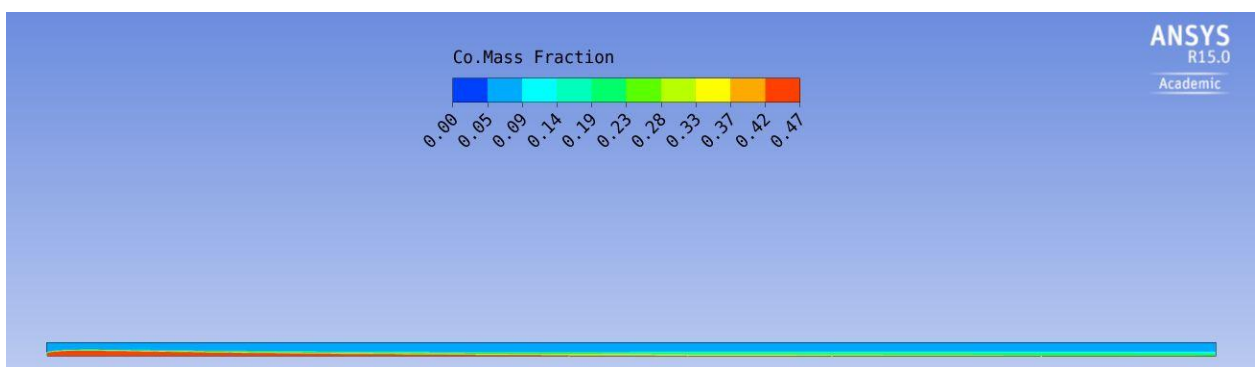


Figure 22: Carbon monoxide mass fraction contours

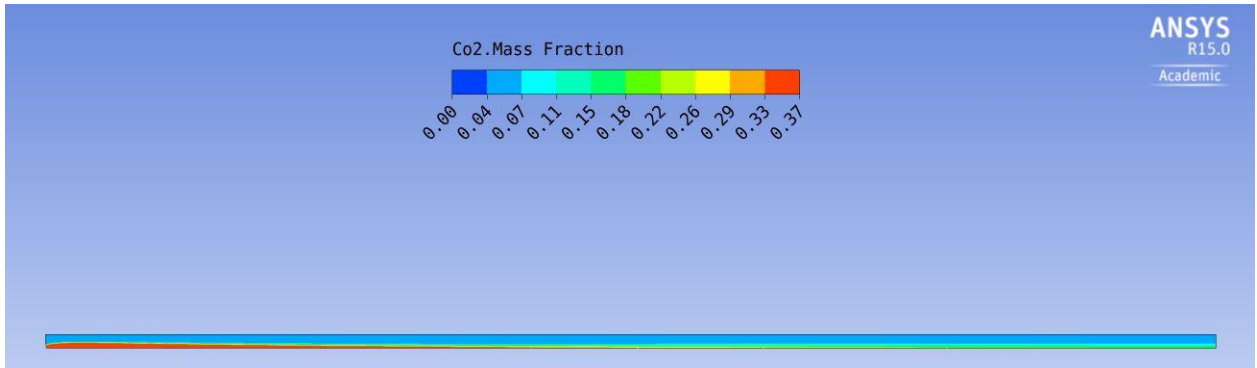


Figure 23: Carbon dioxide mass fraction contours

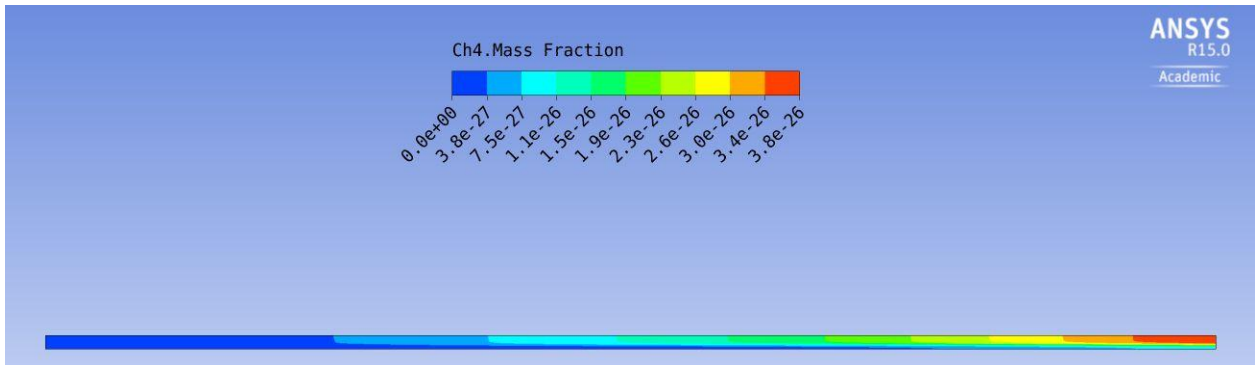


Figure 24: Methane mass fraction contours

Furthermore on the char formation, the Figure 25 shows its velocity vectors (colored in grayscale by the mass fraction) against the temperature profile in the reactor. First it can be noted the temperature difference between the wall (at 823 K) and the glucose inlet zone (300 K), which rapidly decays due to the energy taken by the char formation reaction (bluish zone). It can be seen also how the velocity vectors progressively change from white to black along the reactor.

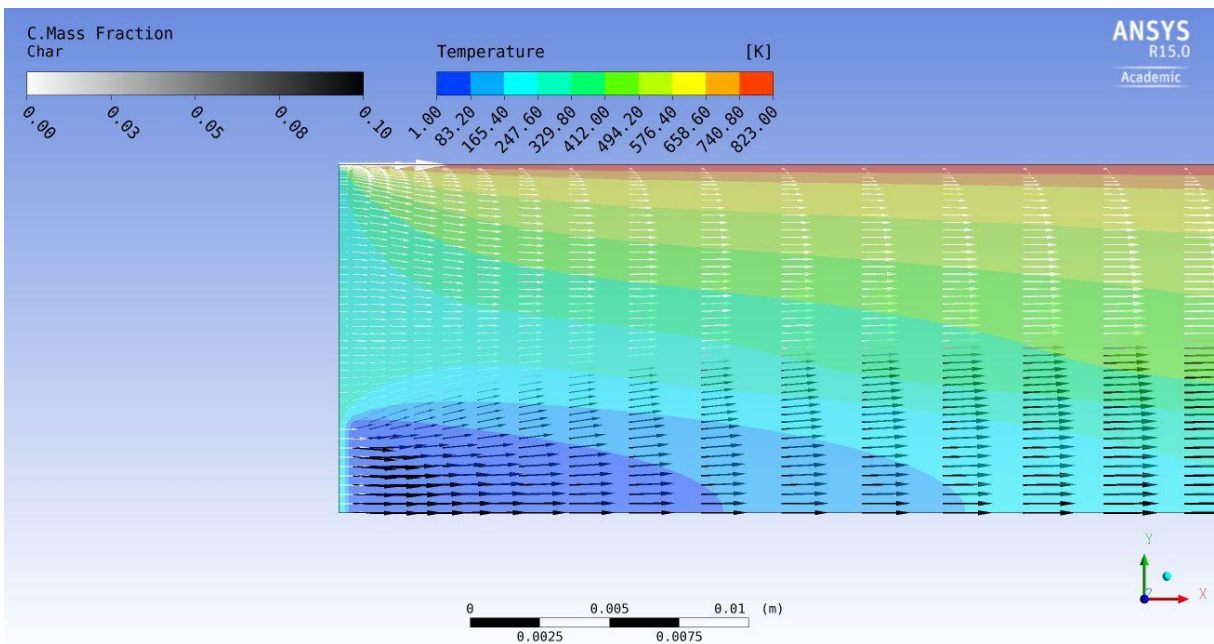


Figure 25: Char velocity vectors

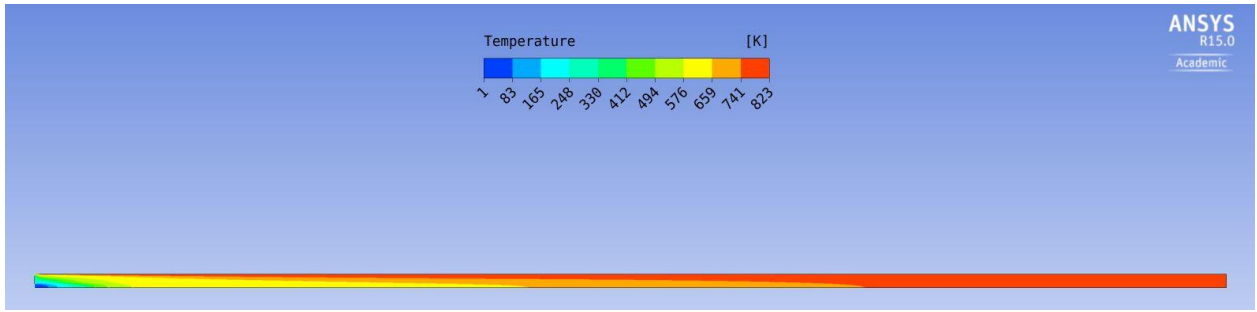


Figure 26: Temperature contours

Finally the velocity vectors of the whole mixture are shown in the Figure 27 below (expanded view of the inlet and outlet). As can be seen the velocity in general is low and increases progressively to a maximum value of 0.0048 m/s at the end. This low velocity influences greatly in the global conversion efficiency (GCE) as will be explained in the following discussion section.

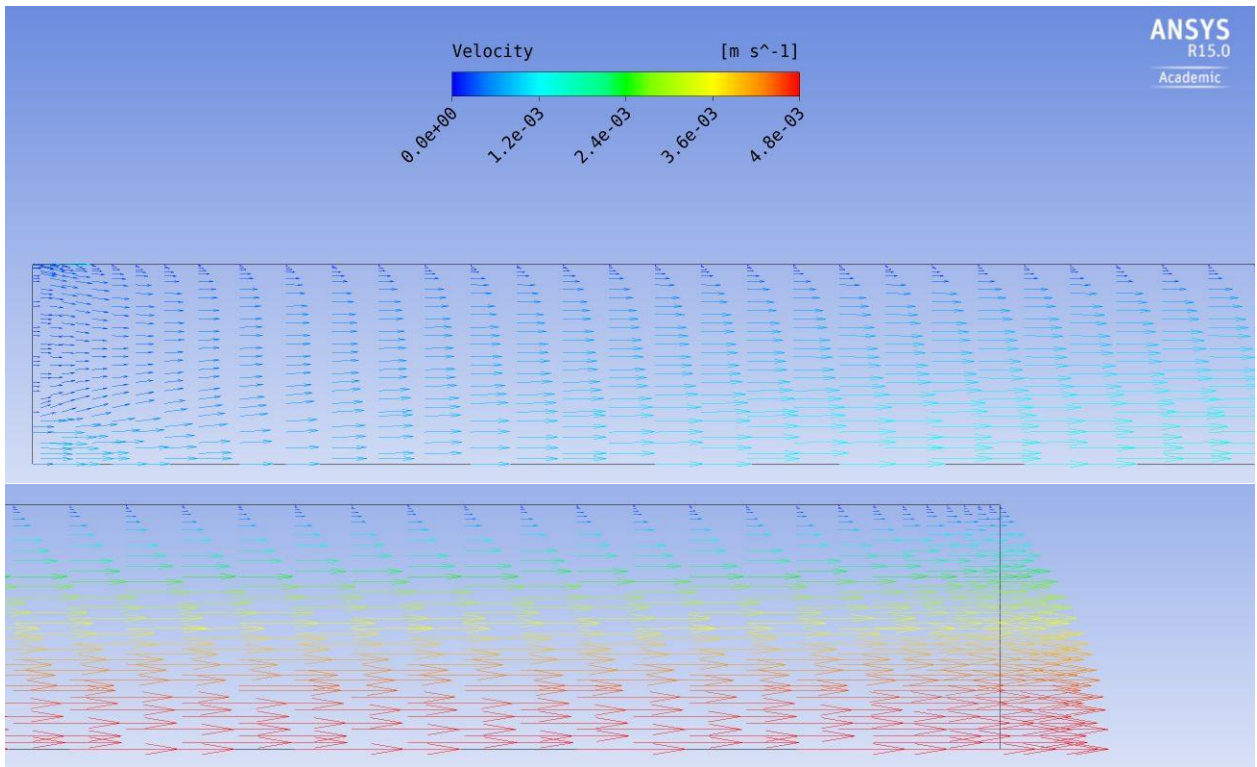


Figure 27: Mixture velocity vectors

#### 4.5. DISCUSSION

From the numerical simulation results shown above, it can be noted right away that they do not agree with the experimental data. Regarding char formation, the numerical result (10%) is quite close to the experimental data one (8.6%). A significant conclusion can be inferred from the gasification conversion efficiency (GCE) parameter, the numerical simulations result show a very

high value (90%) while the experimental data (12%) is quite low. Which means that overall kinetics is not in agreement with the data of the experiment.

The over production of char and the high value for the GCE, can be explained by considering the axial velocity of the fluid (0.0023 m/s) and the residence time in the reactor. This velocity means that the fluid takes approximately 9 minutes to reach the end of the reactor, this is considered too much time residence time. This slow velocity is allowing almost entire conversion of the glucose into gaseous products (which translate into high global gasification efficiency value) and is allowing glucose to have a longer residence time in a low temperature region, which gives room to produce more char.

About this difference between the experimental and simulations results, communications with the authors was established in order to confirm the operating conditions, applied boundary conditions and obtain comments about the results. The input data was confirmed but no comments were received about the results itself. Which leads to the conclusion that the reported experimental results may not be reliable.

As an additional note, simulation with the gravity influence is very difficult to obtain. Certain residual levels oscillates between high and low values (energy and continuity), and the results may depend on when the simulation is stopped. The combination of slow velocity, sudden heat transfer between the hot wall and cold fluid with concurring endothermic species formation (which needs energy) makes particularly difficult this simulation. The required computation time sometimes extended up to three days with a sixteen core computer.

Although good results were obtained for char formation prediction, there is disparity for the GCE result against experimental data (which perhaps is not reliable). This led to the conclusion that the results cannot be validated. Given this situation, an alternative plan was conceived and executed. Simulation of a different operating condition and flow regime in a new reactor, which is described and explained in Chapter 4.

## 5. CFD OF THE EXPERIMENT #2

### 5.1. INTRODUCTION

Given the results found in the previous chapter, it was decided to extend the investigation of the SCWG process. In this chapter, an attempt to recreate the results of a lab-scale turbulent flow experiment was held. This new numerical experimentation uses the same model than the previous experiment on Chapter 4, these common characteristics are: thermo-physical properties for the species, chemical reactions and kinetic parameters. The differences with the previous experiment are reactor geometry (smaller diameter and longer length), operating condition (same pressure but lower temperature), and simulation in the transient state.

Just like the previous numerical experimentation, the same set of equations (mass, momentum, energy and species transport) needs to be solved, in addition to the ones involving turbulence. There are several turbulence models available out there, a literature review (of the already small amount of publications about numerical modeling of the SCWG) indicates that  $k$ - $\epsilon$  models have been used lately to describe the physics involved [29, 30] accurately.

Specifically, the realizable  $k$ - $\epsilon$  model over the standard one, because this model satisfies certain mathematical constraints on the Reynolds stresses which are consistent with the physics of turbulent flow. A benefit of this model has proven superior performance for flows involving boundary layers under high adverse pressure gradients [44]. The modeled transport equations for the turbulence kinetic energy  $k$  and turbulence dissipation rate  $\epsilon$  are shown in the Appendix 2.

### 5.2. EXPERIMENT

The study of the SCWG process in turbulent flow regime was done through a numerical simulation of the work of Promdej and Matsumura [14]. The tubular reactor has an internal diameter of 1 mm, an external diameter of 1.59 mm and with a length of 20 m. The reactor material is also stainless steel. The experimental setup is shown in the Figure 28 below:

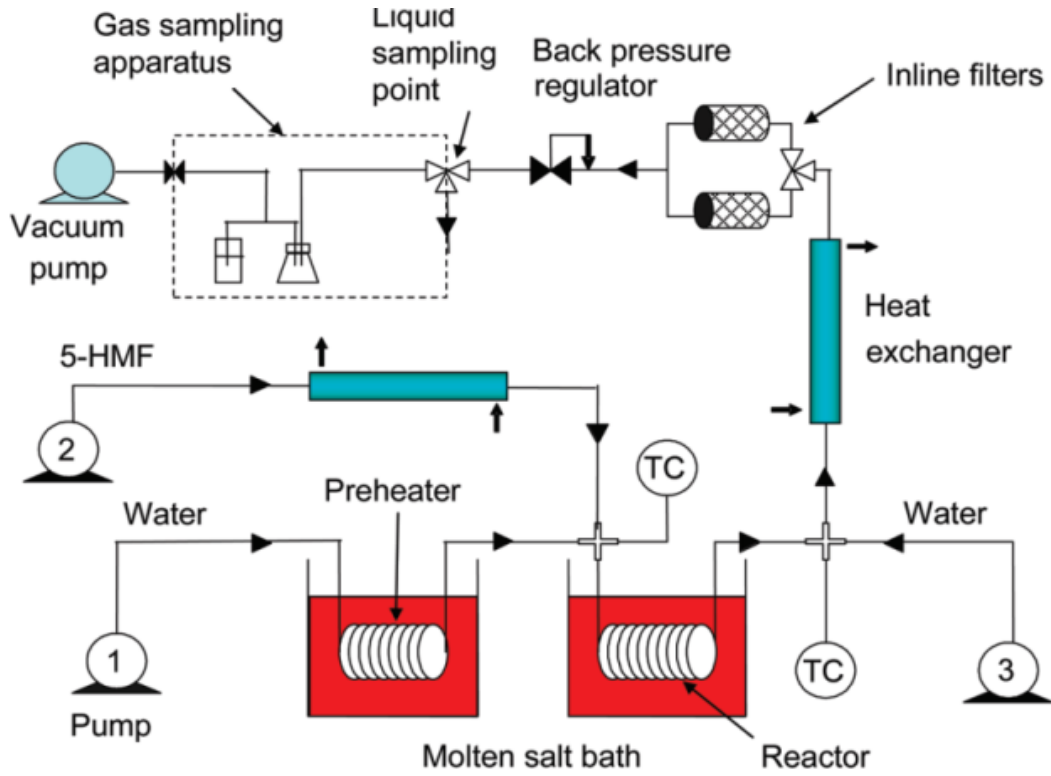


Figure 28: Turbulent flow experimental setup [20]

According to the experimental procedure, an aqueous solution of glucose in a 1:4 ratio by volume is fed in the reactor. Water inside the reactor is pressurized up to 25 MPa and heated at a temperature of 573 K. The residence time was adjusted by changing the flow rate applied, in order to achieve up to 60 seconds.

Taking into account the operating conditions of the experiment, the Reynolds number is calculated (considering only water) with the Equation X to confirm the use of the right viscous physical model. This calculation is shown below:

$$Re = \frac{\rho V_{axial} D_H}{\mu} = \frac{743.3 \text{ kg/m}^3 * 0.3 \text{ m/s} * 0.001 \text{ m}}{9.17 * 10^{-5} \text{ Pa/s}} \cong 2,431$$

Equation X: Reynolds number calculation for the turbulent flow case

Where  $\rho$  and  $\mu$  are the density and viscosity at the operating pressure and temperature respectively,  $V_{axial}$  is the mean velocity of the fluid and  $D_H$  the hydraulic diameter which in this case is the reactor diameter. In this experiment the considered residence time is 60 s, this is directly accomplished by changing the mass flow rate across the reactor. A residence time of 60 s correspond to an axial velocity of 0.3 m/s which results into a Reynolds number of 2,431. Residence time of 30 and 10 s for example results into Reynolds numbers of 5,350 and 16,211 respectively. Therefore, a turbulent viscous model was used in the simulations.

The numerical model validation is achieved by comparing three main parameters: yield of glucose decomposition, yield of char formation and yield of produced output gas which are shown in the Figure 29 below:

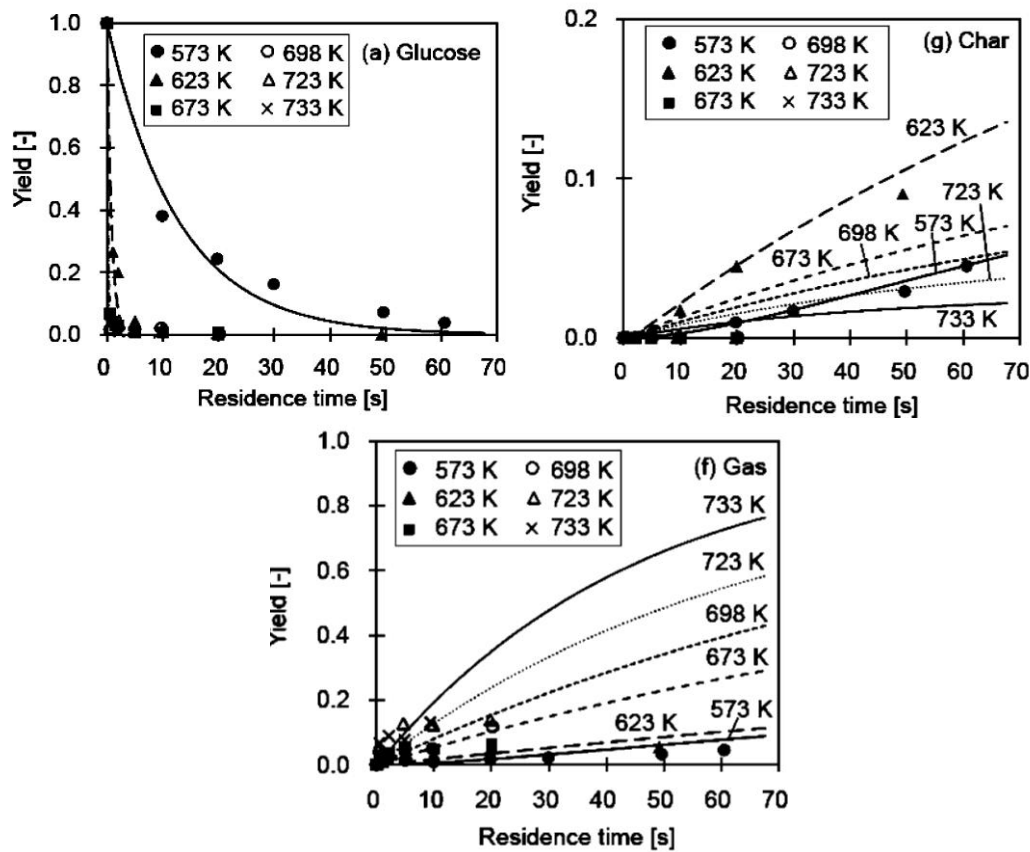


Figure 29: Product distribution of hydrothermal decomposition of glucose [14]

The glucose decomposition, char formation and output gas production yields were calculated on the basis of the carbon content in the feed, according to the Equation XI shown below. The procedure for this validation goes as follow: convergence of the simulation first is reached in steady state, and then the simulation is run again in transient state.

$$(\text{product yield}) = \frac{(\text{carbon content in product}) \left[ \frac{\text{mol C}}{\text{dm}^3} \right]}{(\text{inlet carbon content}) \left[ \frac{\text{mol}}{\text{dm}^3} \right] * 6 \left[ \frac{\text{mol C}}{\text{mol}} \right]}$$

Equation XI: Product yields

While is running in transient state, data collection monitors for the variables of interest (molar concentrations of the substances, temperature, etc.) are activated. This monitors record the information generated at each time step. Afterward, this data logging is processed for the whole duration of the simulation and the yields are calculated.

The numerical model validation is achieved by comparing the yields mentioned before. Given the difficulty to read accurately the graphs in the publication, only the results at 573 K were considered. Validation is assured by replicating results at two operating conditions of interest: at 60 and 30 seconds of residence time at this temperature.

### 5.3. NUMERICAL MODEL

Given the extensive length of this reactor, it was decided to have also a 2D representation of the domain. A scheme can be seen in the Figure 30. A different meshing strategy was applied in this case. First, it is a known fact that after a certain point, flow is fully developed and maintains a steady velocity and temperature profile no matter where is measured anymore. Regarding velocity for most practical engineering applications ten times the diameter is enough [45], but some authors suggest 40 up to 150 diameters (for high Reynolds number) [45, 46].

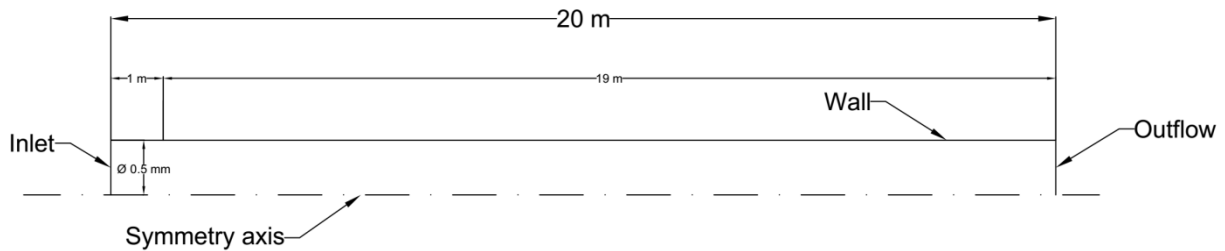


Figure 30: Turbulent flow domain scheme

Considering temperature, in order to have a stable profile is necessary to surpass the "thermal entrance length" which for turbulent flow is about ten times the pipe diameter [47]. In the case of our reactor, this means 10 millimeters considering common engineering practices for velocity and temperature. However, just to be sure a security factor of 10 was applied to ensure stability in the profiles.

Taking into account the previous consideration, our domain was divided into two zones: in the first meter a very fine mesh was applied (1 mm element size in the axial direction), and for the nineteen remaining meters a coarse mesh was used (2-5 mm element size). This was done to decrease the amount of cell in the final mesh, therefore reducing computation time and resources. In the radial direction, it was considered to have a fixed number of elements of 50 (which means an element size 0.02 mm).

### 5.4. MESH INDEPENDENCE STUDY

Three meshes were obtained varying the element size of the second part of the reactor length, which resulted in 168,000 up to 546,000 rectangular elements. To decide which mesh to use, a grid independence study was conducted. This study consists of simulating fluid flow at room conditions under the influence of the heated walls at the operating temperature of the lab scale experiment. The general objective of this study is to produce velocity and temperature profiles to compare the accuracy of the obtained solutions by the different meshes. These profiles were obtained evaluating the solution at various planes at two location of interest: at the end of the first part of the reactor (slightly ahead 1 m) and half of it (10 m).

Evaluating the velocity profiles in the first plane of interest, it was found that the differences are quite small and hard to notice only in a graphical comparison (see Figure 31). In the maximum

value of velocity (top of the dome) at the position equal to 0, the "168k" and the "546k" meshes show a difference, while the "250k" is almost overlapping the "546k". Numerically speaking considering the "546k" as comparison base, the difference percentage against the "250k" and "168k" is 0.03% and 3.78% respectively. From the results up to this point, it can be seen that there is no need to use the "546k" mesh because the "250k" with half of the number of elements already obtain good results.

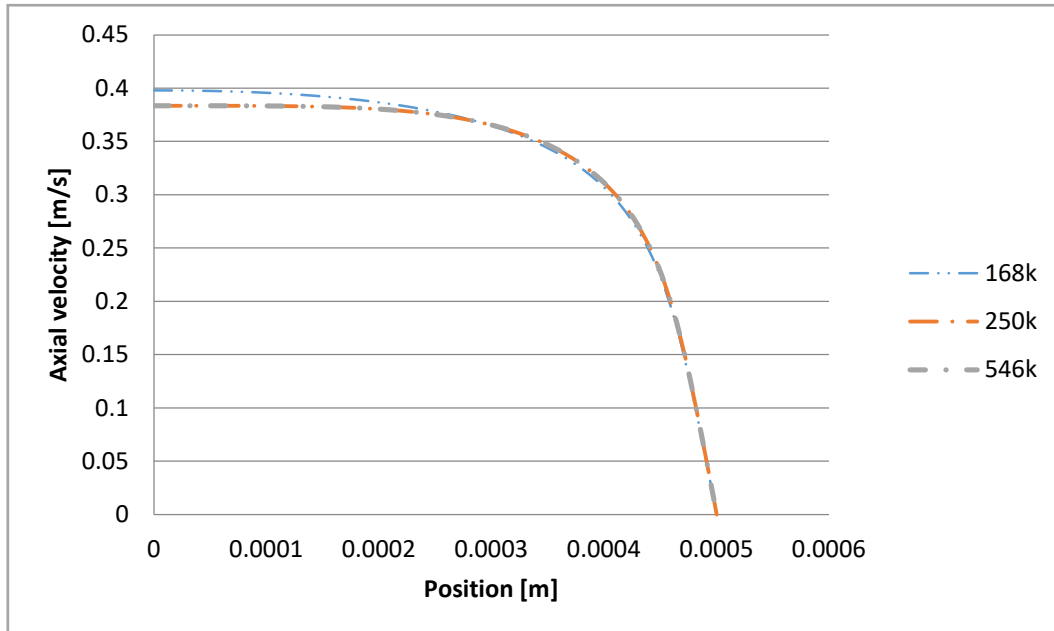


Figure 31: Velocity profiles comparison

To be sure, the comparison was also made at the second plane of interest (half of the reactor). Given the fact that the velocity profile is already developed, there were no differences between the meshes. Therefore, the result does not contribute significantly to what has already been found.

Following the same procedure, the temperature values were also evaluated. However the diameter is so small and the element size (in the radial direction) is the same for all the meshes, which resulted in practically no numerical difference.

To choose between the "168k" and "250k" meshes, a full simulation was done. It was found that with the "168k" mesh, right convergence level in the energy equation residuals was not possible to obtain. It must be remembered that in this mesh, the second part of the reactor has an element size of 8 mm in the axial direction. Therefore, for the rest of the simulations, it was considered to use the "250k" mesh.

The applied solution method considers SIMPLE pressure-velocity coupling, first order upwind scheme for the turbulent kinetic energy and dissipation rate and second order upwind scheme for the solution of energy and all the species transport equations. The convergence criteria of the simulations aim for residuals in the  $10^{-3}$  order for all the equations except for the energy residual which aims for  $10^{-6}$ . Also, the mass and energy net imbalance was monitored and is preferred to keep it below 0.5% and 5% respectively. First, the simulations were converged using steady-state solver. Then, it was changed to transient solver with a step size of 0.1 s during the desired residence time according to the operating condition needed.

To obtain good convergence, the equations were also solved in a ladder: first the flow and turbulence, then the energy, then the glucose inlet and finally the remaining species. The simulations were finished when the desired residence time was achieved.

## 5.5. RESULTS

For this round of simulations, it was only considered the empirical stoichiometry for time reasons. The parameters that were varied were: operating temperature and residence time (by indirectly through changing the mass flow). A summary of the parameter settings and applied operating conditions is shown in the Table 6 below:

*Table 6: Parameter settings and operating conditions for turbulent flow simulations*

Parameters	Value
<b>Geometry</b>	
Diameter (m)	0.001
Length (m)	20 m
Grid size (mm)	axial 1-5, radial 0.01
<b>Boundary conditions</b>	
<b>Inlet</b>	
Water and feed inlet pressure (MPa)	25
Feed and water inlet temperature (K)	573 K
<b>Wall</b>	
Wall temperature (K)	573 K
Characteristics	Stationary, no slip, material: steel
<b>Outlet</b>	
Average pressure specification (MPa)	25
Average temperature specification (K)	573 K
Residence time	30 and 60 s
<b>Methods</b>	
Scheme	Second order upwind
Algorithm	SIMPLE
Time step	0.1
No. of iterations	100 max per step size
Relaxation factors	0.25-0.75
Convergence criteria	0.001-0.000001

The experimental glucose decomposition yield for the 573 K operating temperature is reproduced in the Figure 32. The calculation procedure is as follows. Two numerical simulations were run at 30 and 60 s residence time (which mean applying different mass flows in each simulation). The data obtained from both simulations, only contribute with two specific points of the graph. Glucose decomposition yield at 30 and 60 s residence time. This two points are shown and contrasted against the experimental data curve in the aforementioned figure. It can be noted that the point at 30 s residence time is almost in the curve while the 60 s residence time is slightly above the curve.

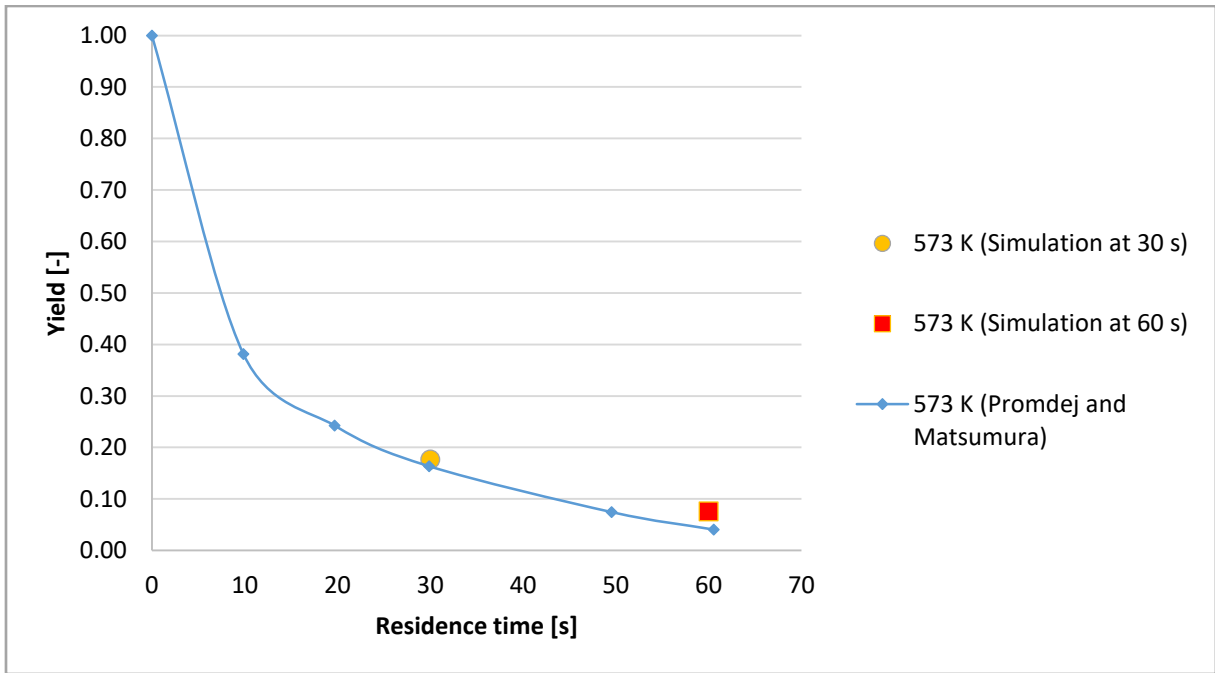


Figure 32: Glucose decomposition results

Following the calculation procedure described before. The experimental char formation yield is shown in the Figure 33 below. Again, the data points were calculated at 30 and 60 s residence time and plotted against the experimental results. It can be seen how the numerical results are in good agreement with the experimental ones.

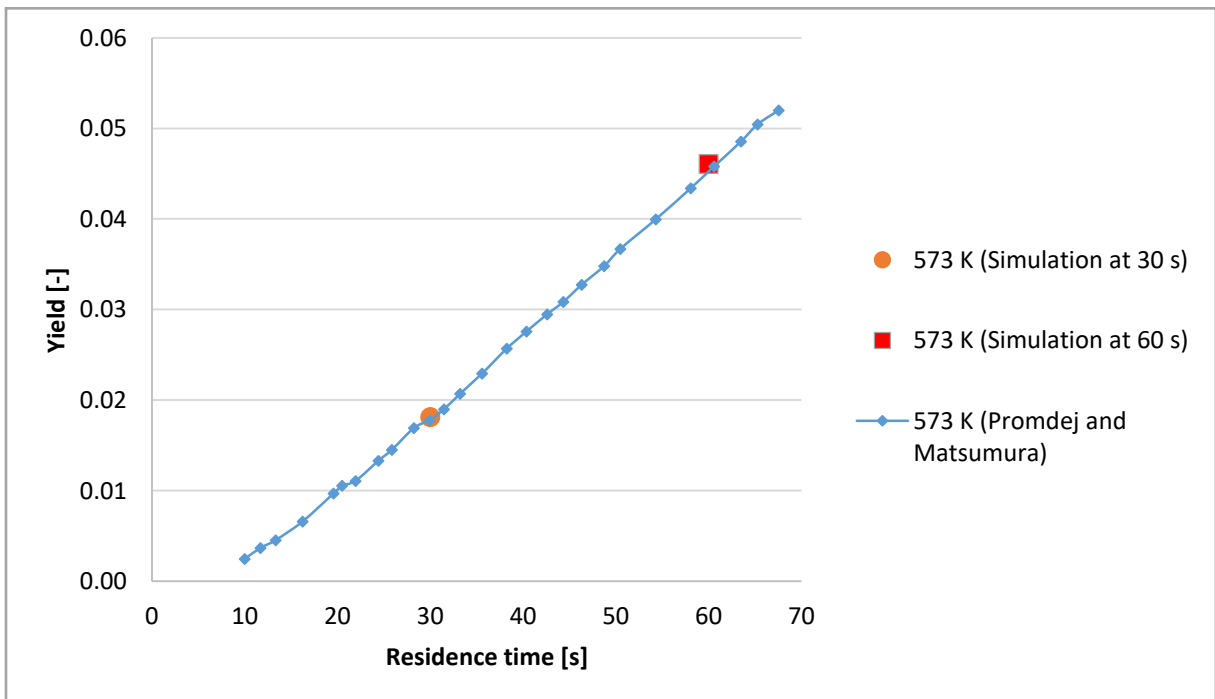


Figure 33: Char formation results

Finally, the output gas yield is shown in the Figure 34 below. It should be emphasized that, only the following species were considered (given the fact that the yield calculation only takes into account carbon content): carbon monoxide, carbon dioxide and methane.

Here the results are slightly off the general trend. At 30 s residence time, the output gas formation is slightly over predicted while at 60 s residence time is a bit under predicted. This difference is justified by the following arguments:

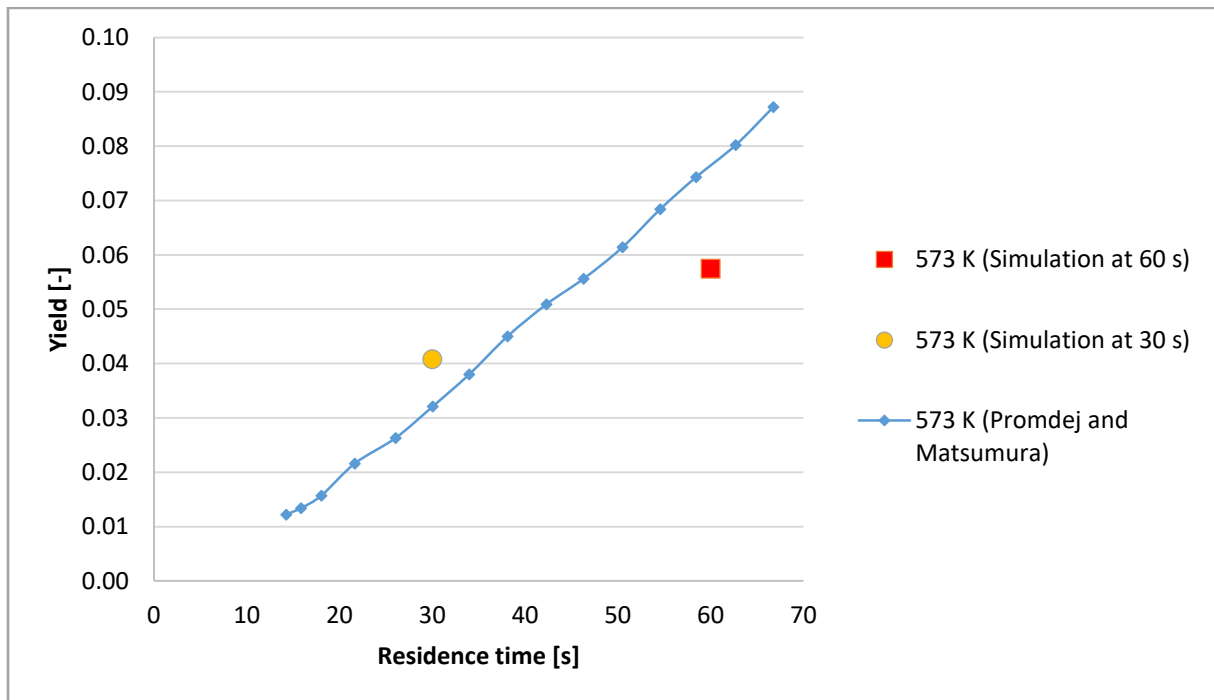


Figure 34: Output gas formation results

The reproduction of the experimental data curve is done by extracting points from the paper (where the resolution is not the best) with a digital tool. This operation induce error in the data retrieving and therefore in the comparison against the numerical simulation result. Also, it should be noted that the paper does not report any measurement error during the experimental procedure, which can be "human" errors or because poor instrument calibration, etc.

In the Figure 35 the mass fraction contours of char in transient state are shown. At initial time 0.1 s the char formation shows a local maximum at order of magnitude of  $10^{-4}$ , which increases in time as can be seen in the successive figures up to  $10^{-1}$  at 60 s. However, it must be remembered that the global values are different because the entire char produced is dispersed in the water contained in the reactor.

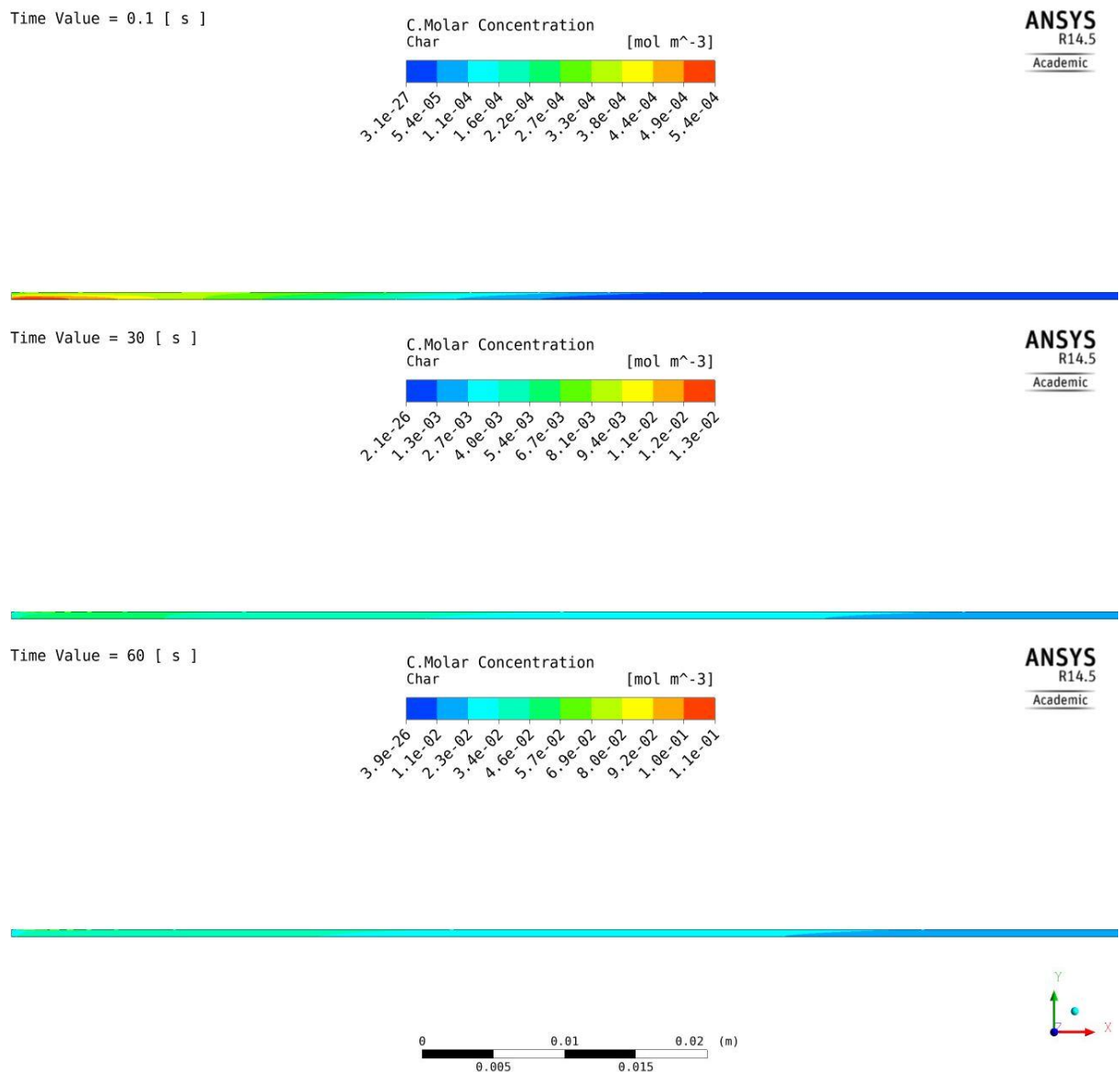


Figure 35: Char mass fraction transient contours

Additionally in the Figure 36, Figure 37, Figure 38 and Figure 39 mass fractions contours for the hydrogen, carbon monoxide, carbon dioxide and methane in the transient state are shown respectively. These gaseous show a similar "formation" behavior along the reactor as the char, increasing its concentration progressively in time.

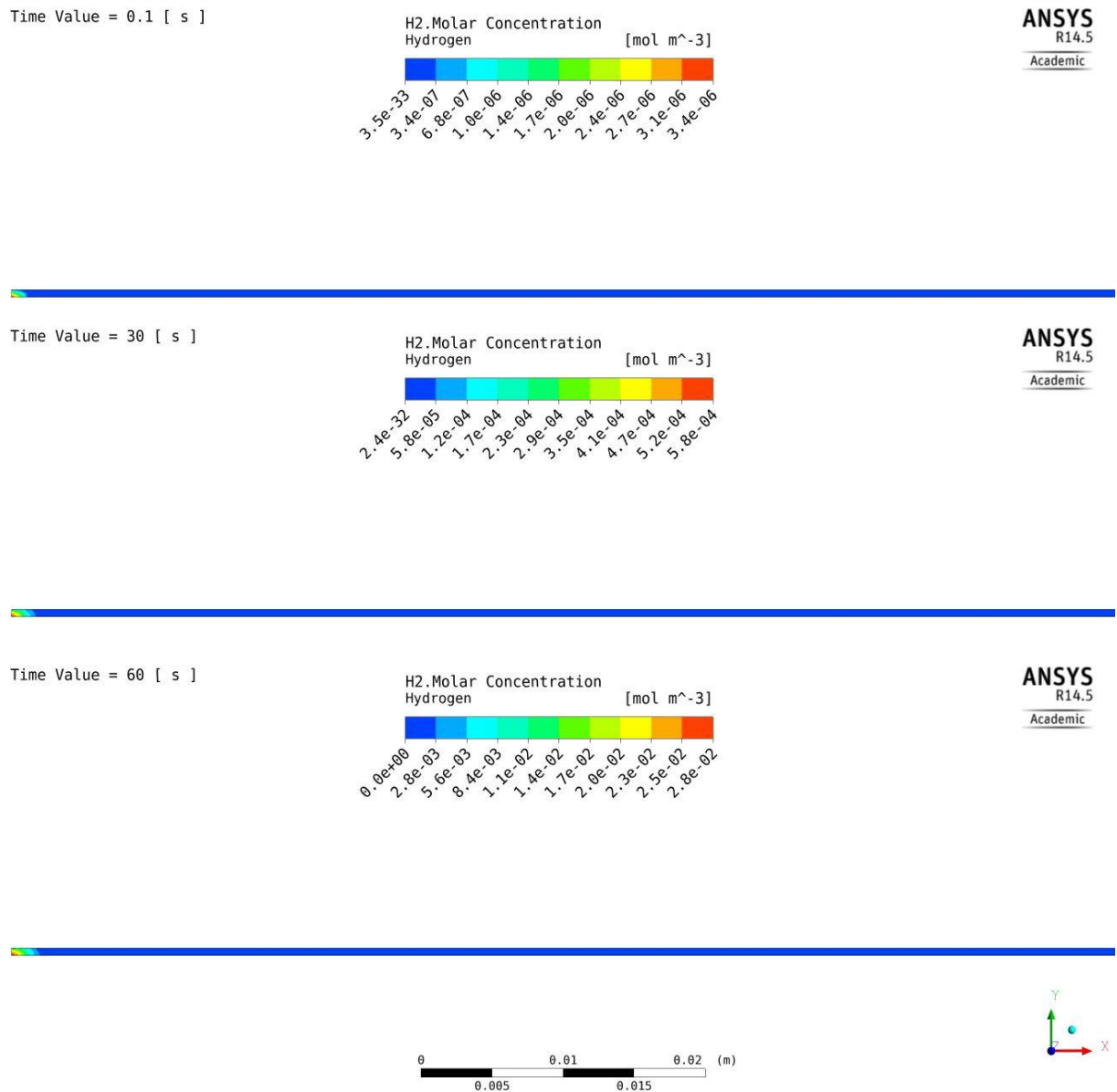
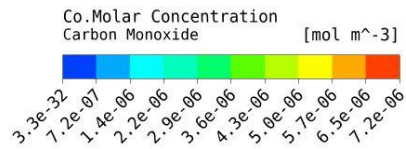
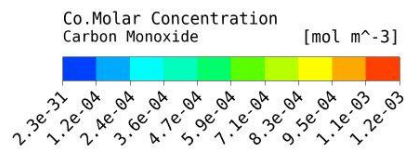


Figure 36: Hydrogen mass fraction transient contours

Time Value = 0.1 [ s ]



Time Value = 30 [ s ]



Time Value = 60 [ s ]

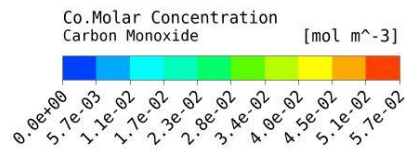
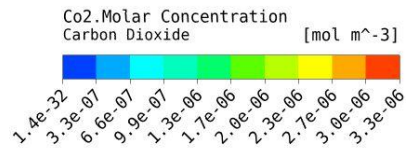
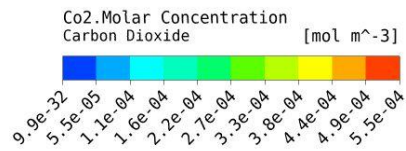


Figure 37: Carbon monoxide mass fraction transient contours

Time Value = 0.1 [ s ]



Time Value = 30 [ s ]



Time Value = 60 [ s ]

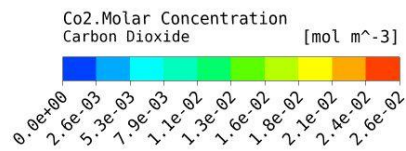
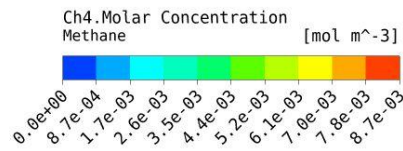
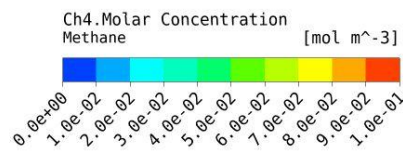


Figure 38: Carbon dioxide mass fraction transient contours

Time Value = 0.1 [ s ]



Time Value = 30 [ s ]



Time Value = 60 [ s ]

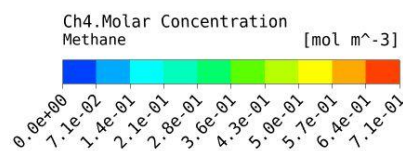


Figure 39: Methane mass fraction transient contours

To conclude, the validation of the numerical model also allows further investigation on the influence of changing operating parameters on the variables of interest (output gas and char formation). Additional results and analysis about: influence of variation of residence time and inlet feed temperature can be found in the Appendix 5.

## 5.6. DISCUSSION

From the numerical model results shown above, it can be noted that regarding glucose decomposition and char formation, the results for turbulent flow are in good agreement with the experimental results. Output gas formation results, however, are slightly offset from the experimental results trend. The possible cause of this error is the poor resolution of the experimental data graphs and the human error in the process of retrieving the information.

It must be remembered also that the numerical model includes certain assumptions which make impossible to fully reproduce the SCWG process like in reality. As for the physics of the model: modeling the mixture as just one fluid oversimplifies the heat transfer between gases and particles (glucose and char), also the heat transfer between the wall and the fluid does not take into account the thickness of the material. Fluid-particle interactions such as: drag, lift, collision effects, heat and mass exchange are not taken into account by the one fluid assumption too.

As for the chemistry of the model, it must be remembered that the kinetic used was derived from experimental data which assumed for all the reactions a reaction order of unity. Which means that the concentration of the glucose is not affecting the kinetic and therefore the production of more or less char and gaseous products.

Regardless of the assumptions and simplifications of the model, the results are very positive taking into account the ones obtained from the laminar flow experiment and allow further investigation. It must also be remembered, that the primary goal of this work is the development of a numerical model which can reproduce accordingly the char formation during the SCWG process. It can be said that under the investigated conditions, the numerical model replicated the experimental data results. Which proves that the used kinetics for the char formation and gaseous species production is the right one.

The mass fraction transient contours in overall terms show the progressive formation of char and the gaseous products according the kinetics and chemical reactions. However, the model does not show the correct motion of the gas in the water inside the reactor. This disadvantage comes from representing the mixture as just one fluid.

Examining more closely the influence of temperature on kinetic rates, the model was able to predict the char kinetic rate behavior correctly with changing temperature. When compared to the gas kinetic rate, the char proved to be predominant within its "preferred" temperature range of influence. Afterward, the gas kinetic rate formation dominates the species production.

The difference between the results of both experiments is explained by several factors. First, convergence is easier to obtain in the second experiment because the turbulent physical model in ANSYS Fluent is more "robust" and further described than the laminar one used in the first experiment. Second, the velocity in the second experiment (0.3333 m/s) is almost 145 times bigger than the first experiment (0.0023 m/s). It must be remembered that the slow velocity in the first experiment highly increased the global carbon efficiency (GCE) which did not agree with the experimental value however in the second experiment a more "logic" velocity allow a calculation of the right yield of char formation and glucose decomposition.

## 6. IMPACT OF SCWG UTILIZATION FOR AGRICULTURAL LIFE

### 6.1. INTRODUCTION

According to the latest report by the Food and Agriculture Organization of the United Nations (FAO), one-third of food produced for human consumption from agricultural activities is lost or wasted globally (approximately 1.3 billion tons per year). Organic waste is wasted along the supply chain, starting with agricultural activities to final human consumption [48].

Organic waste itself is not the only negative situation; there is also the problem of its disposal. Agricultural waste and food is usually disposed of in landfills or in open dumps which result in undesirable odor, proliferation of pest and contribution to GHG emissions. Another way to dispose this organic waste is incineration, but this produces pollutants such as dioxins, furans, and particulates creating environmental concern and health risks [49].

Even if appropriate waste management policies are applied to land filling, the emission problem is not avoided. The decomposition of organic waste by bacteria produces biogas, which its central component is methane ( $\text{CH}_4$ ), a greenhouse gas that is 25 times more potent than carbon dioxide ( $\text{CO}_2$ ) in a period of 100 years.

Despite the fact that agricultural practices and recycling technologies for collection, separation and further reuse have improved over the years, they are still case-limited. And being even more precise, reuse of agricultural and food waste for the production of interesting products such as biofuels, biomaterials and green chemicals is still very niche focused and not common.

In general, agricultural and food residues are used as animal feed first, fertilizers for new crops or as a very inefficient fuel (combustion to obtain heat mostly). However this “recycling” processes are not economically attractive because of their low product value in the market. This situation can change with the use of novel technologies as anaerobic digestion for the production of biogas, composting, fermentation to alcohols or thermo chemical conversion routes such as gasification and pyrolysis.

These organic waste typically consist of carbohydrates (sugars, cellulose and starch), lignin, protein, oils, fats, and water. Moreover, this aqueous component depending on the specific type of residue can be up to 95 wt. % (e.g., sludge, wastewater), which can be a problem because it means that the process may need a pre-treatment step to decrease this water content, decreasing the energy efficiency and the profitability of the process itself.

For this reason, supercritical technologies have gained attention during the past decades especially for very wet biomass waste ( $> 50$  wt. %). Moreover, the use of this technology is compatible with the in-situ “biorefinery” concept and can be fully integrated to current

agricultural processes to obtain novel high-value products such as phytochemicals, green fuels, and energy from waste streams.

**6.2. ENERGY SITUATION IN THE NETHERLANDS**

The Netherlands is the tenth most populated country in Europe, with approximately 17 million inhabitants in around 34,000 km<sup>2</sup> of land. Besides it concentrates 90.2% of its population in urban centers where also can be found large industrial and business areas [50]. The electricity generation is distributed as following: 42% gas, 39% coal, 1% oil, 4% nuclear, and 14% renewables (6% biofuels & waste, 1% solar and 7% wind) as seen in Figure 40. The Netherlands plays a very important role in Europe as the second largest natural gas producer and its open market and integrated supply chain.

Despite its commitment to decarbonisation and climate change mitigation initiatives and policies, the Netherlands remains as one of the most fossil-fuel and CO<sub>2</sub>-intensive economies among International Energy Agency (IEA) member countries [51]. For example in 2014, energy from biomass (includes municipal & industrial waste, solid & liquid biofuels and biogas) for electricity and heat production accounted for 6.42% and 13.01% of the total energy generated respectively [52].

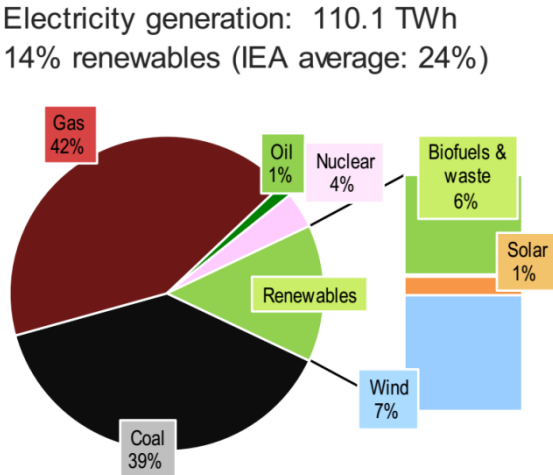


Figure 40: Dutch energy matrix [51]

Besides natural gas, coal also has a strong presence in the Netherlands. In 2013, three new coal power plants started their operations with a total capacity of 3,500 MW due to a scenario where natural gas has high prices (therefore is more attractive to sell it) and low coal prices (to satisfy the country energy needs). However, to alleviate the GHG emissions five coal power plants will be shut down in 2017 (with a total capacity of 2,700 MW).

Efforts to further change this situation has been made, for example between 1990 and 2012, the Netherlands carried away a successful decoupling program of GHG emission from economic growth, and after 2013, an agreement was reach with key stakeholders on specifics action to support this economic growth and sustainable initiative towards 2020. And recently committed to a specific set of actions [53] in the 2015 Paris Agreement, such as:

- ...that 100% of electricity generation has to come from renewable sources at the latest by 2025. This includes a complete phase-out of coal latest by 2020;
- ...that the demand for gas for heating in residential and commercial buildings must be reduced from its current levels of more than 90% of demand to zero between 2025 and 2035, shifting the supply towards district heating and/or air and ground heat pumps, while maintaining a high renovation rate for buildings to ensure high insulation and energy efficiency standards;
- ...that CO<sub>2</sub> emissions from agriculture, in particular from the greenhouse sector, should be reduced to zero between 2025 and 2035, by shifting to renewable sources (as per the energy demand target mentioned above) or by radical shrinking of the greenhouse sector;
- ...in the longer term, that measures need to be introduced to reduce the non-CO<sub>2</sub> emissions from agriculture (methane and nitrous oxide) to zero by 2080-2085.

These goals are very ambitious; in fact, the Netherlands faces a very steep road toward their accomplishment. It is known that in certain sectors the country is lagging behind its other European counterparts, such as energy supply diversification where the share of renewables is too low. Therefore, it is necessary to develop further and implement renewable energy technologies including biomass sourced ones.

Biomass in the Netherlands is mostly used as animal feed or for the production of heat and electricity. Mainly by direct/indirect co-firing in conventional coal-fired or traditional combustion power plants. It is known that the product of this "traditional" way of recycling biomass is not economically attractive because the current prices for electricity and heat (from other sources such as fossil fuels) are low. In order to produce high-value products from this biomass is necessary to change to novel technologies in different sectors of the Dutch economy [54].

Biorefineries can be a solution for both problems, in this high-efficiency facility a biomass conversion process and equipment are combined to produce not only fuels and power (as traditional petroleum refineries) but also extra fuel or chemical from the "waste" or intermediate products of the process itself. As shown in Figure 41, the majority of the streams are efficiently used. Every product helps increasing the profitability of the project and helps meet GHG emission reduction goals.

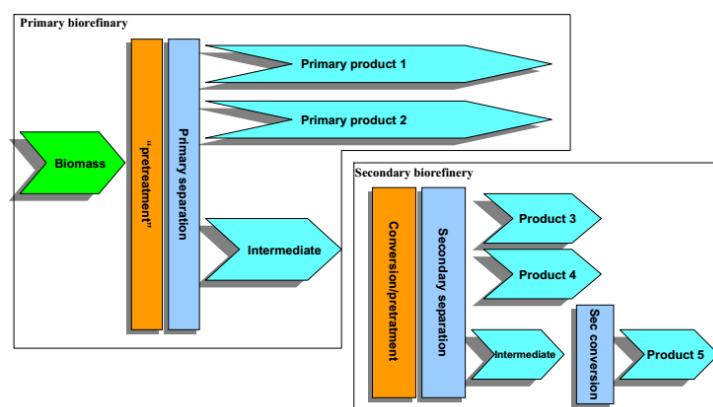


Figure 41: Schematic overview general integrated biorefinery process [54]

Aiming to achieve this goal, the Netherlands government in 2007 implemented a bio-based economy roadmap (updated recently in 2012). The objective is to use biomass as a "green" raw material in the chemical industry and for non-food applications in to produce materials like

plastics, adhesives, paints and to generate traditional fuels and energy. This will strengthen the Dutch position in the green business sector, mitigate the climate change problem, reduce waste (and save resources in its disposal), and reduce dependency on fossil fuels [55].

This is a joint effort between the following stakeholders, governmental agencies such as the Ministry of Economic Affairs, the Ministry of Housing, Spatial Planning and the Environment, the Ministry of Agriculture and Nature Conservation, the business and research sector. Within this roadmap, several routes were outlined and managed by “platforms,” formed by the representatives of the relevant stakeholders.

Within this context, the Dutch biorefinery route [56] established some short and midterm actions and planning towards long-term goals, the following biorefineries directions were identified:

- Based on domestic crops, focusing on a collaboration between the agro (including the plant-breeding sector) and chemical sector.
- Based on aquatic biomass (e.g. algae) using microbiology, plant breeding, and new research.
- Based on imported biomass using the advantageous Dutch logistic and petrochemical infrastructure.
- Based on residues, based on cooperation and gathered by a new network (production chains and businesses) in reasonable distances. a new network (production chains and businesses) in reasonable distances.

### 6.3. ESTIMATION OF POTENTIAL

The targeted biomass resource in the Netherlands is found as "waste" in the national accounts. This resource is divided into: chemical, recyclable, discarded materials, animal and vegetable, mixed, sludge and mineral waste. Which is also subdivided by the destination this waste: recycling, incineration, dumping and disposal on land and for exporting purposes.

For the interest of this work, the focus will remain in the waste which has a high content of water (or moisture) and is usually dumped or disposed in landfills. The animal/vegetable and sludge waste resource can be found in the Table 7 below:

*Table 7: Biomass-based waste for SCWG [57]*

Subjects	Animal and vegetable waste			Sludge		
	2008	2010	2012	2008	2010	2012
Periods						
Origin-destination	1,000 ton					
Dumping and disposal on land	36	59	56	40	43	37

From the collected data, it can be inferred the average amount of biomass-based waste available in 50,300 and 40,000 tons per year or 5.74 and 4.57 ton per hour of animal/vegetable and sludge waste respectively. For the purposes of the economic assessment shown further ahead, for practical reasons a feedstock of 1 ton per hour was chosen, which represents less than 20% of

what is available. This decision was taken in order to support the realistic assumption that not all the biomass available can be hoarded and used just by one "client".

However, it should not be forgotten that the considered biomass is only the one disposed or discarded, there is still more biomass used in recycling and incineration applications which may not be as financially and environmentally attractive as supercritical gasification, as shown in Table 8 below:

*Table 8: Total waste available [58]*

Subjects	Animal and vegetable waste			Sludge		
	2008	2010	2012	2008	2010	2012
Periods						
Origin-destination	1,000 ton					
Total processing of producers	15,175	16,323	18,174	645	619	609
Recycling	14,332	15,209	17,098	221	248	225
Incineration	807	1,054	1,020	384	328	347
Total to abroad	5,368	5,708	5,553	65	44	38
Total destination	20,543	22,031	23,727	710	663	647

#### 6.4. TECHNO-ECONOMIC ASSESSMENT OF SCWG

In any project is important to perform a techno-economic assessment, in overall profitability is the decisive criterion for the construction of a facility. This evaluation also allows for example investigation of cash flow over the project lifetime; evaluate the impact of different scales of production and comparison of the economic performance of other technologies for the same purpose.

The traditional procedure is intended to calculate and optimize the production cost, where the goal is to minimize it by identifying opportunities for savings/improvement in the process or obtaining extra revenue from the sale of intermediate products (if applicable).

The yield of hydrogen and syngas were selected, based on the best results from the different modeling approaches available (kinetic, stoichiometric and process design models) for sewage sludge and real life results in the available literature. According to Castello and Fiori [35], the maximum yield of hydrogen is 232.6 kg/ton feedstock using the stoichiometric model. Taking into account the whole process design Fiori et al. [59] obtained 8.56 kg/ton feedstock of hydrogen and 200 kg/ton feedstock of syngas (which means 20% GCE). While for the real life "VERENA" [60] pilot plant (although using different feedstock) the hydrogen yield is only 0.63 kg/ton feedstock. Clarifying that the above data are taken as a guide, since the production of hydrogen depends on the operating temperature used.

The significant difference in these values makes especially difficult the evaluation of a realistic techno-economic assessment. Therefore, due to the lack of real experimental data at "pilot" scale specifically with sewage sludge. The yields from Fiori et al. [59] were considered for this study.

Regarding the process design, after some literature review and careful examination of pilot plan schemes. It was decided to apply a general configuration based on the work of [61], in such a way that the techno-economic analysis can be used as a representative of any SCWG process design.

Of course, the process can be more complex or integrated with other technologies (e.g.: cogeneration, solar PV, energy storage, hydrogen fuel cells, etc.) but that is outside the scope of this work. The flowchart of the selected process design is shown in the Figure 42 below:

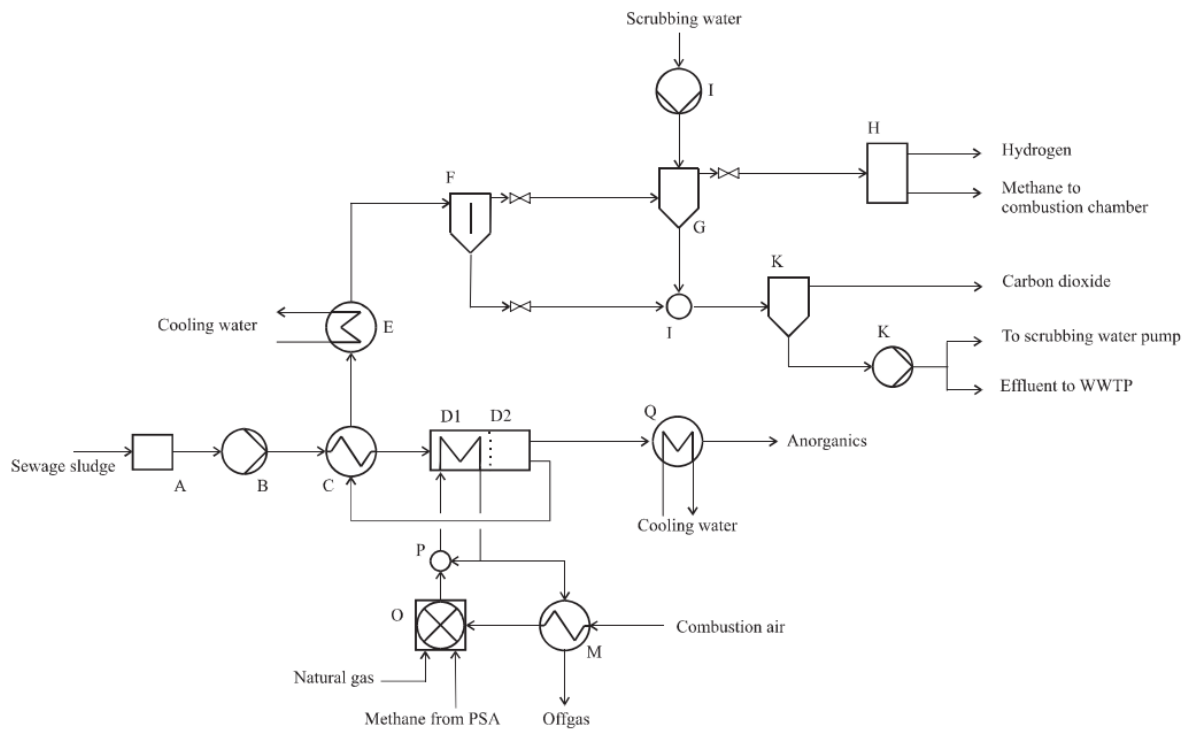


Figure 42: Flowchart of SCWG process:

*A, conditioning unit; B, high-pressure pump; C, HEX; D1, HEX; D2, reactor; E, HEX; F, gas-liquid separator; G, scrubber; H, pressure-swing adsorption (PSA); I, high-pressure pump; J, mixing unit; K, expansion unit; L, sewage water pump; M, HEX; O, combustion chamber; P, mixing unit; Q, HEX. [61]*

The process starts in the conditioning unit (A) where the necessary tasks (e.g.: crushing, dispersion, mixing, etc.) to ensure a homogenous mixture with a solid content of 20 wt%, then the mixture is pressurized up to 250 MPa by the high-pressure pump (B) and then pre-heated using the heat exchanger (C) with leftover heat from the reactor (D2). The 600 °C reaction temperature is achieved in the heat exchanger (D1), this heat comes from the combustion chamber (O) which is fed with combustion air, natural gas and methane recirculation from the process itself.

The output gas leaves the reactor and is cooled down by the heat exchanger (E) before entering to the gas-liquid separator (F). Afterward, the output gas is cleaned in the scrubber (G), where the CO<sub>2</sub> is washed away, and the water is re-circulated into the system. Finally, the clean gas is separated into pure hydrogen, and methane (or syngas) in the PSA unit (H), the high-pressure flow of combustible gas is redirected towards the combustion chamber (O) to decrease the external fuel consumption of the process. Additionally, the remaining solid fraction (possible char and ash) from the reactor (D2) is cooled down by the heat exchanger (Q) and further disposed of.

The production cost of this SCWG process example is analyzed using the total annual revenue requirement approach (TRR). The TRR is defined as the money needed to construct, operate and maintain a facility which sells one or more products and by-products during a year to be

economically feasible. This significant revenue is divided into two broad categories: carrying charges and expenses. Carrying charges are usually subdivided in capital recovery and return on debt ( $TCR$ ), they represent obligations related for example to depreciation, taxes, insurance, interest, etc. In this case, expenses are subdivided into fuel/energy ( $FC$ ) and operating and maintenance costs ( $O\&M$ ). The  $TRR$  is calculated using the Equation XII shown below:

$$TRR = TCR - FC - O\&M$$

*Equation XII: Total revenue requirement*

The procedure for the calculation of the costs of the process is:

- 1) Estimation of the capital (major equipment) and associated (direct and indirect) costs using information from the literature review of similar processes and the application of ratio factors.
- 2) Estimation of the energy/fuel and O&M costs needed to run the process.
- 3) Levelization of all the variable costs in time (facility lifetime).

#### 6.4.1. ESTIMATION OF THE TOTAL CAPITAL INVESTMENT (TCI)

Some references about the major equipment involved in the SCWG process can be found in the literature. In 2008 Gasafi et al. [61] evaluated SCWG of sewage sludge with a throughput of 5 ton per hour and 20%wt dry matter content. Lu and Guo in 2011 [62], estimated a similar concept than Gasafi but including a solar receiver (as source of heat for the reactor) into the process, but is quite optimistic and has big differences against other references.

Based on this literature review and in comparison with earlier data gathered by [61], it was decided to use Gasafi data as the main reference. But adjusted to the intended capacity of this study (1 ton per hour of feedstock) through the "six-tenths rule" widely used in industry as quick estimation [63]. This rule of thumb has a 20-30% margin of error, and it should be followed only as a guideline for costing, the Equation XIII is shown below:

$$c_1 = c_2 \left( \frac{x_1}{x_2} \right)^{0.6-0.7}$$

*Equation XIII: Six-tenths rule for capacity estimation*

Where  $c_1$  is the unknown cost at the required  $x_1$  capacity, and  $c_2$  and  $x_2$  are respectively the known capacity and costs of the used reference. The Table 9 list the major equipment considered scaled to a throughput of 1 ton per hour, these values were also corrected with inflation to the 2017 euro value.

Table 9: Major equipment costs based on [61] and corrected to 2017

Major equipment	Costs in 1,000 €
Feeding	44
High-pressure pump	35
Pre-heater	334
Reactor pre-heater	128
Burner	255
Air pre-heater	9
Product cooler	64
Cooling unit for ashes	118
Reactor pre-heater	21
Gas-liquid separator	28
Scrubber	35
PSA	154
Effluent pump	4
Scrubbing water pump	13
Total	1,243

#### 6.4.2. DIRECT AND INDIRECT COSTS

For the estimation of the direct and indirect costs of the total major equipment cost, the factor method was applied. Used also as a rough guide, it has a 20-30% margin of error. The direct costs account for the installation and erection of major equipment, construction, and installation of the auxiliary systems needed (pipe system, instrumentation and control devices, electrical connection and associated grid, support structures, civil works, land, and buildings). The indirect costs take into account the contractor fees, engineering and design, contingency and the working capital needed to start up the facility. Table 10 shows the factors used for this estimations.

Table 10: Direct and indirect costs estimation based on [61] and corrected to 2017

<b>Direct costs</b>	<b>Ratio factor</b>	<b>Subtotal in 1,000 €</b>
Purchased	39%	485
Equipment installation		
Piping	31%	385
Instrumentation and controls	13%	162
Electrical systems	10%	124
Land	6%	75
Buildings	39%	485
Service facilities	55%	684
<b>Total direct costs</b>		<b>2,399</b>
<b>Indirect costs</b>		
Engineering and supervision	32%	398
Construction	34%	423
Expenses (of above costs)		
Contingency	15%	843
<b>Total indirect costs</b>		<b>1,663</b>
<b>Other outlays</b>		
Startup costs	7%	371
Working capital	10%	531
<b>Total other outlays</b>		<b>902</b>

### 6.4.3. OPERATING COSTS

The necessary costs to run the facility are operation and maintenance (O&M) and fuel/energy needed for the process. The operation costs account for the salaries of the facility workers and the maintenance labor required to ensure continued operation. For this estimation, it was considered a capacity factor of 91% (around 8,000 hours per year) and is calculated applying an 8% factor to the direct costs value.

Because the SCWG process is endothermic, is necessary to provide energy for it. This energy is provided in the form of heat obtained through the combustion of natural gas and later by the combustion of the produced methane fraction of the output gas. The natural gas price of 3.167 ct €/kWh was taken from 2017 data [64] with a low heating value (LHV) of 38.05 MJ/kg from Groningen as a reference [65].

### 6.4.4. COST LEVELIZATION

To calculate all the components of the total revenue requirement accurately, the components that change in time must be leveled across the lifetime of the facility. These costs are

for example fuel/energy and O&M. Fuel, supplies, electricity prices are subjected to inflation and market volatility that is why they change in time. Operation and maintenance cost usually increase because in time a facility needs more work and repairs to keep functioning as it was new.

The leveled or present value  $P$  of the  $TRR$  is the result of an annuity  $A$  calculated from the Equation XIV. The  $CRF$  is calculated considering a constant rate of interest  $i$  is assumed of 10% spread among 20 years of the facility's lifetime  $n$ , using the Equation XV. The cost escalation of value is calculated using with the Equation XVI relating the current value  $P_o$  and the respective annuity using an inflation rate  $r_n$  of 1.6% [66].

$$A = CRF * P$$

*Equation XIV: Present value*

$$CRF = \frac{i(1+i)^n}{(1+i)^n - 1}$$

*Equation XV: Capital recovery factor*

$$CELf = \frac{A}{P_o} = \frac{k(1-k^n)}{(1-k)} CRF$$

*Equation XVI: Cost escalation levelization factor*

$$k = \frac{1+r_n}{1+i}$$

The calculation results of all the leveled costs are shown in Table 11. For 20 year facility lifetime, is necessary to cover approximately 1.14 million euro per year. The majority of this monetary load comes from the equipment/installation itself with a 64% contribution, while fuel and O&M costs account for a contribution of 16% and 20% respectively. However, in this calculation is not included yet the fuel savings obtained by burning the produced syngas.

*Table 11: Levelized annual costs*

<b>Levelized annual costs</b>	<b>mil €</b>	<b>Contribution</b>
Carrying charges	729	64%
Fuel cost	185	16%
O&M costs	224	20%
Annual revenue requirement	1,138	

#### 6.4.5. RESULTS

After the calculation of all the associated costs, the production cost of the target product can be calculated. In this exercise, the final product is the pure hydrogen. However, there are interesting by-products and "benefits" which are taken into account to help the profitability of the project. The primary product unit costs  $MPUC$  is calculated with the annual revenue

requirement, the by-products revenues  $BPR$  and the main product quantity  $MPQ$ , which are all related through the Equation XVII shown below:

$$MPUC = \frac{TRR - BPR}{MPQ}$$

*Equation XVII: Main-product unit costs*

The extra revenues considered in the BPR calculation are the saved fuel and the incentive for the sludge disposal. Due to the lack of "upgrading" step after the separation of the syngas from the output gas, it was considered that the low-heating value is half of the natural gas considered here as a fuel. In Europe, the sludge disposal cost fluctuates between 40-160 euro per ton. Therefore it was considered as an average of 100 euro per ton. The yields and their corresponding selling price are shown in the Table 12 below:

*Table 12: Product and by-products output*

	Unit	Value	Selling price
Hydrogen output	kg/h	8.56	-
Syngas output	kg/h	200	3.167 € ct/kWh
Sludge dry matter recycling	t/h	0.2	102 €/t

Replacing these values in the Equation XVII, the calculated production cost of hydrogen for this particular process design is 86.51 €/GJ. In overall terms, these production costs can be compared with other hydrogen production technologies to have an idea of the feasibility of the project. Lemus and Duart [67] in 2010, published a review of the current and foreseen production costs of hydrogen.

Hydrogen market price from centralized biomass gasification facilities is in the range of 44-82 €/GJ. From hydropower sources, the range is between 45-66 €/GJ. From geothermal and tidal technologies is predicted to be 75.7 and 53.4 €/GJ respectively. From grid-connected windmills is 34 €/GJ (75.2 from isolated systems). From grid-connected solar photovoltaic is 41.7 €/GJ (51-166 from autonomous systems) and finally from distributed electrolysis is between 25-98 €/GJ.

#### 6.4.6. DISCUSSION

From the comparison of the hydrogen production cost obtained in this techno-economic assessment against other hydrogen production technologies. It can be seen that the SCWG option (although is not the cheapest one) is feasible and already placing itself, in between more conventional and established technologies such as standard gasification and electrolysis. However, competing with these technologies (for hydrogen and syngas production) should not be the objective. SCWG technology can aim for a particular niche which is not covered by any other technology so far.

Treating highly humid biomass is a problem for other technologies (e.g.: incineration, standard gasification, pyrolysis, etc.) because energy needs to be put in a pre-treatment step which is drying the biomass down to permissible levels of water content. In this context, the competing technology to SCWG is the anaerobic digestion (AD).

Unlike SCWG, AD needs large volumes (which translate into high expenditure on land and storage tanks) and residence time (15-30 days, while SCWG only needs minutes) to process the feedstock. Another important disadvantage of AD is the unwanted production of a liquid fraction which has a high organic load and therefore cannot be discharged or disposed easily. The preceding constitutes a competitive advantage for the SCWG technology, and furthermore, the high-pressure output gas is ideal for further biofuel generation integrating it with other technologies such as Fischer-Tropsch synthesis, methanol, synthetic natural gas upgrading, etc. Also according to GHG emissions comparative studies [68], SCWG can capture up to 2 times more CO<sub>2</sub> than AD.

In the Dutch context, there is a fascinating niche which SCWG technology can prove its worth and, at the same time solve a delicate problem for the livestock farmer industry. In recent years there is an oversupply of manure coming from the livestock sector. In 2000, the animal density in the Netherlands was 3.9 animal units per hectare (in Belgium is 3.1 and 1.6 in Denmark as a comparison) [69]. Also, to have an idea how big is this industry; Europe represents 71.2% of Dutch dairy exports. The problem relies on the excessive accumulation of nitrates and phosphates in groundwater due to the use of this manure as "natural" fertilizer. The Dutch government has concrete rules on the amount of nitrate from fertilizer that is allowed to seep into the soil, therefore is need a way to get rid of this manure while still meeting environmental regulations.

AD for this purpose started to being used from the late 70's, however many projects (at individual farmers level) faced technological problems, limited economic feasibility, weak governmental support and a sudden decrease of energy prices. Therefore, the interested shifted to building larger and larger plants (over 200,000 tons per year) however the produced residues couldn't compete with artificial fertilizer because they had to contain precise amounts of nutrients or minerals and have a low production cost. This and other reasons caused AD to fail as a solution to this problem [70].

Given the rising wave of subsidies in policy on climate change plus the thread of closing coal-fired plants, organic waste found a waste to be disposed through co-combustion. Besides legal resistance from neighboring people and environmental groups, this technology has a significant constraint for its application at large scale: complying strict and sometimes confusing or overlapping emission standards (like BEES and BLA standards). Fortunately for the SCWG technology, these problems can be avoided and face less resistant for its application at large scale. Manure and organic waste can be mixed in the right proportion with water and then converted into syngas. This represents a tailor-made solution for a real waste management problem. And this is an example of the niches where SCWG can be applicable and justify its development.

## 7. CONCLUSIONS AND RECOMMENDATIONS

### 7.1. CONCLUSIONS

In this work, a numerical model built in ANSYS Fluent is used to investigate and predict the char formation inside the reactor of an SCWG process. Also, a techno-economic assessment is presented in order to estimate the feasibility of this technology. The model includes complete thermo-physical properties at supercritical conditions, chemical reactions and kinetic data from lab-scale experimental results for the formation of char and gaseous products.

First, the model is intended to be validated against experimental data from a laminar flow experiment. However, in this numerical investigation, the produced char and the gasification conversion efficiency (GCE) results showed great differences with the experimental values. The fluid velocity is very low and therefore, allows the glucose to experience a long residence time. This results in a high GCE and char production. These indications lead to the conclusion that there are uncertainties in the reported experimental data. Therefore, the model could not be validated because it is considered that the experimental data is not reliable.

Due to the above, it was decided to test the model under a different regime. The second investigation was made implementing the chemical reactions and kinetic data in a turbulent flow numerical model, also with the intention of being validated with experimental data. Unlike the previous investigation, this time the compared parameters were: glucose decomposition, char formation and output gas production yields in time (transient simulations). Under the investigated operating condition, the simulations results show good agreement with the experimental data. The model not only followed the right trend but also it predicts right yields of glucose decomposition into char and gaseous products. Therefore the model is replicated, however it must be acknowledged the redundancy of the results because the second experiment used the reactor and operating conditions from the source that gave the kinetic for the numerical model.

Concerning the first research question, the developed model can predict the char formation in the SCWG process and that it was validated against experimental data. Therefore, is reasonable to conclude that it works and is valid for others operating conditions as well.

Regarding the second research question, the developed model confirms the insights given by the literature review. Char formation is highly influenced by the changing temperature. When the "hot" water flow suddenly interacts with the incoming "cold" biomass, the production of char happens instantly and at very fast rate until a peak is reached. Then, the whole mixture increases its temperature and the formation of gaseous products is preferred.

Finally, SCWG technology was assessed from a techno-economic point a view. Considering the availability of organic waste and, current energy scenario in the Netherlands. It was proved that it may be feasible and that it also has opportunities to compete in specific niches where other technologies are partly or wholly inapplicable. Specifically, where anaerobic digestion shows weaknesses and disadvantages, supercritical gasification emerges as the clear winner and obvious alternative as tailor-made waste management solution.

## **7.2. RECOMMENDATIONS**

Improvements can be made to this work for future investigations. The resolution of discrepancies between results in various fluid regimes must be solved. Experimental data for turbulent flow real life experiments are needed to further adjust the model. This could reconcile the model and make it valid for all operating conditions of interest.

A one-fluid model neglects the influence of one phase over the other, and this phase interaction could predict more accurately effects such as buoyancy, mass, and heat exchange and drag over particles (of particular interest for char), etc. This is a complex task, which can start with a parametric study for each multiphase flow model available. Even further, with the thermo-physical properties of char, the dynamics can be more thoroughly investigated.

A parametric study of the turbulence model constants can be made; in order to evaluate which set of parameters can predict even more accurately the SCWG process. Also, this may give valuable insights which can be used for reactor optimization and further ahead a whole process design.

As far into the techno-economic analysis, it might be interesting to perform a sensitivity analysis taking into account: possible incentives or subsidies (through waste management policy for example), increase in the price of natural gas, etc. Digging deeper into the social aspect, it might be interesting to start positioning SCWG technology in a particular niche, and therefore create the necessary infrastructure to support it: promotion and awareness, community and stakeholders engagement, networking, specific policy, etc.

## BIBLIOGRAPHY

1. Pachauri, R.K., et al., *Climate change 2014: synthesis report. Contribution of Working Groups I, II and III to the fifth assessment report of the Intergovernmental Panel on Climate Change*. 2014, IPCC.
2. Institute, W.R., *Cumulative CO2 Emissions 1850-2011*.
3. Agency, I.E. *Bioenergy*. [cited 2017 June]; Available from: <https://www.iea.org/topics/renewables/subtopics/bioenergy/>.
4. Agency, E.E., *Scheme of Biomass Conversion Routes*.
5. Amin, S., R. Reid, and M. Modell, *Reforming and decomposition of glucose in an aqueous phase*. 1975.
6. Müller, J.B. and F. Vogel, *Tar and coke formation during hydrothermal processing of glycerol and glucose. Influence of temperature, residence time and feed concentration*. *The Journal of Supercritical Fluids*, 2012. 70: p. 126-136.
7. Supercritiques, I.F. *Supercritical fluids: Applications*. [cited 2017 June]; Available from: <http://www.supercriticalfluid.org/Applications.149.0.html>.
8. Eckert, C.A., B.L. Knutson, and P.G. Debenedetti, *Supercritical fluids as solvents for chemical and materials processing*. *Nature*, 1996. 383(6598): p. 313.
9. Commons, W., *Phase diagram of water*.
10. Piore, I. and S. Mokry, *Thermophysical properties at critical and supercritical conditions*. *Heat Transfer: Theoretical Analysis, Experimental Investigations and Industrial Systems*, A. Belmiloudi, ed., INTECH, Rijeka, Croatia, 2011: p. 573-592.
11. Chakinala, A.G., *Supercritical water gasification of biomass: an experimental study of model compounds and potential biomass feeds*. 2013: Universiteit Twente.
12. Yakaboylu, O., et al., *Supercritical water gasification of biomass: A literature and technology overview*. *Energies*, 2015. 8(2): p. 859-894.
13. Molino, A., et al., *Glucose gasification in super-critical water conditions for both syngas production and green chemicals with a continuous process*. *Renewable Energy*, 2016. 91: p. 451-455.
14. Promdej, C. and Y. Matsumura, *Temperature effect on hydrothermal decomposition of glucose in sub- and supercritical water*. *Industrial & Engineering Chemistry Research*, 2011. 50(14): p. 8492-8497.
15. Castello, D., A. Kruse, and L. Fiori, *Low temperature supercritical water gasification of biomass constituents: glucose/phenol mixtures*. *Biomass and bioenergy*, 2015. 73: p. 84-94.
16. Susanti, R.F., et al., *High-yield hydrogen production from glucose by supercritical water gasification without added catalyst*. *international journal of hydrogen energy*, 2012. 37(16): p. 11677-11690.
17. Hendry, D., et al., *Exploration of the effect of process variables on the production of high-value fuel gas from glucose via supercritical water gasification*. *Bioresource technology*, 2011. 102(3): p. 3480-3487.
18. Zhang, L., P. Champagne, and C.C. Xu, *Screening of supported transition metal catalysts for hydrogen production from glucose via catalytic supercritical water gasification*. *international journal of hydrogen energy*, 2011. 36(16): p. 9591-9601.
19. Chuntanapum, A. and Y. Matsumura, *Char formation mechanism in supercritical water gasification process: a study of model compounds*. *Industrial & Engineering Chemistry Research*, 2010. 49(9): p. 4055-4062.

20. Chuntanapum, A. and Y. Matsumura, *Formation of tarry material from 5-HMF in subcritical and supercritical water*. Industrial & engineering chemistry research, 2009. 48(22): p. 9837-9846.
21. Hao, X., et al., *Hydrogen production from glucose used as a model compound of biomass gasified in supercritical water*. International journal of hydrogen energy, 2003. 28(1): p. 55-64.
22. Lee, I.-G., M.-S. Kim, and S.-K. Ihm, *Gasification of glucose in supercritical water*. Industrial & Engineering Chemistry Research, 2002. 41(5): p. 1182-1188.
23. Karayıldırım, T., A. Sınağ, and A. Kruse, *Char and coke formation as unwanted side reaction of the hydrothermal biomass gasification*. Chemical engineering & technology, 2008. 31(11): p. 1561-1568.
24. Williams, P.T. and J. Onwudili, *Composition of products from the supercritical water gasification of glucose: a model biomass compound*. Industrial & engineering chemistry research, 2005. 44(23): p. 8739-8749.
25. Matsumura, Y., S. Yanachi, and T. Yoshida, *Glucose decomposition kinetics in water at 25 MPa in the temperature range of 448– 673 K*. Industrial & engineering chemistry research, 2006. 45(6): p. 1875-1879.
26. Yoshida, T., S. Yanachi, and Y. Matsumura, *Glucose decomposition in water under supercritical pressure at 448-498 K*. Journal of the Japan Institute of Energy, 2007. 86(9): p. 700-706.
27. Jin, H., et al., *A mathematical model and numerical investigation for glycerol gasification in supercritical water with a tubular reactor*. The Journal of Supercritical Fluids, 2016. 107: p. 526-533.
28. Su, X., et al., *Numerical study on biomass model compound gasification in a supercritical water fluidized bed reactor*. Chemical Engineering Science, 2015. 134: p. 737-745.
29. Caputo, G., et al., *Experimental and fluid dynamic study of continuous supercritical water gasification of glucose*. The Journal of Supercritical Fluids, 2016. 107: p. 450-461.
30. Yoshida, T. and Y. Matsumura, *Reactor development for supercritical water gasification of 4.9 wt% glucose solution at 673 K by using computational fluid dynamics*. Industrial & Engineering Chemistry Research, 2009. 48(18): p. 8381-8386.
31. Tang, H. and K. Kitagawa, *Supercritical water gasification of biomass: thermodynamic analysis with direct Gibbs free energy minimization*. Chemical Engineering Journal, 2005. 106(3): p. 261-267.
32. Lu, Y., et al., *Thermodynamic modeling and analysis of biomass gasification for hydrogen production in supercritical water*. Chemical Engineering Journal, 2007. 131(1): p. 233-244.
33. Castello, D. and L. Fiori, *Supercritical water gasification of biomass: thermodynamic constraints*. Bioresource technology, 2011. 102(16): p. 7574-7582.
34. Louw, J., et al., *Thermodynamic modelling of supercritical water gasification: Investigating the effect of biomass composition to aid in the selection of appropriate feedstock material*. Bioresource technology, 2014. 174: p. 11-23.
35. Castello, D. and L. Fiori, *Supercritical water gasification of biomass: a stoichiometric thermodynamic model*. International Journal of Hydrogen Energy, 2015. 40(21): p. 6771-6781.
36. Wagner, W. and A. Pruß, *The IAPWS formulation 1995 for the thermodynamic properties of ordinary water substance for general and scientific use*. Journal of physical and chemical reference data, 2002. 31(2): p. 387-535.
37. Wagner, W. and H.-J. Kretzschmar, *IAPWS industrial formulation 1997 for the thermodynamic properties of water and steam*. International Steam Tables: Properties of Water and Steam Based on the Industrial Formulation IAPWS-IF97, 2008: p. 7-150.
38. Yaws, C. and P. Narasimhan, *Critical properties and acentric factor-organic compounds*. Thermophysical properties of chemicals and hydrocarbons, 2009. 2.
39. Zehe, M.J., S. Gordon, and B.J. McBride, *CAP: A computer code for generating tabular thermodynamic functions from NASA Lewis coefficients*. 2001.
40. Chung, T.H., L.L. Lee, and K.E. Starling, *Applications of kinetic gas theories and multiparameter correlation for prediction of dilute gas viscosity and thermal conductivity*. Industrial & engineering chemistry fundamentals, 1984. 23(1): p. 8-13.

41. Liu, H., C.M. Silva, and E.A. Macedo, *Unified approach to the self-diffusion coefficients of dense fluids over wide ranges of temperature and pressure—hard-sphere, square-well, Lennard–Jones and real substances*. *Chemical engineering science*, 1998. 53(13): p. 2403-2422.
42. Bühler, W., et al., *Ionic reactions and pyrolysis of glycerol as competing reaction pathways in near-and supercritical water*. *The Journal of Supercritical Fluids*, 2002. 22(1): p. 37-53.
43. Kruse, A. and A. Gawlik, *Biomass conversion in water at 330– 410 C and 30– 50 MPa. Identification of key compounds for indicating different chemical reaction pathways*. *Industrial & Engineering Chemistry Research*, 2003. 42(2): p. 267-279.
44. Fluent, A. *Realizable k-epsilon Model*. [cited 2017 June]; Available from: <https://www.sharcnet.ca/Software/Fluent6/html/ug/node480.htm>.
45. Yunus, A.C. and J.M. Cimbala, *Fluid mechanics fundamentals and applications*. International Edition, McGraw Hill Publication, 2006. 185201.
46. Nikuradse, G., *Laws of Turbulent Flow in Smooth Pipes*. 1966.
47. Bergman, T.L. and F.P. Incropera, *Fundamentals of heat and mass transfer*. 2011: John Wiley & Sons.
48. Gustavsson, J., et al., *Global food losses and food waste*. Food and Agriculture Organization of the United Nations, Rom, 2011.
49. Nanda, S., et al., *Gasification of fruit wastes and agro-food residues in supercritical water*. *Energy Conversion and Management*, 2016. 110: p. 296-306.
50. Worldometers.info. *European Countries by population (2017)*. 2017 [cited 2017 May]; Available from: <http://www.worldometers.info/population/countries-in-europe-by-population/>.
51. Agency, I.E. *Netherlands: In-depth country review*. 2015 [cited 2017 May]; Available from: <http://www.iea.org/countries/membercountries/thenetherlands/>.
52. Agency, I.E. *Netherlands: Renewables and Waste for 2014*. 2014 [cited 2017 May]; Statistic Report]. Available from: <http://www.iea.org/statistics/statisticssearch/report/?year=2014&country=NETHLAND&product=RenewablesandWaste>.
53. Sterl, S., N. Höhne, and T. Kuramochi, *What does the Paris Agreement mean for climate policy in the Netherlands?* 2016.
54. Elbersen, W., *Biorefineries for the chemical industry—A Dutch point of view*.
55. Kees Kwant, S., *Biomass in the Netherlands*. 2009.
56. van Ree, R. and E. Annevelink, *Country Report The Netherlands 2010: IEA Bioenergy Task 42*. 2010.
57. Netherlands, S., *Waste balance, kind of waste per sector; national accounts, 2008-2012*.
58. Netherland, S., *Waste balance, kind of waste per sector; national accounts, 2008-2012*.
59. Fiori, L., M. Valbusa, and D. Castello, *Supercritical water gasification of biomass for H<sub>2</sub> production: process design*. *Bioresource technology*, 2012. 121: p. 139-147.
60. Boukis, N., et al. *Gasification of wet biomass in supercritical water. Results of pilot plant experiments. in 14th European Biomass Conference, Paris, France*. 2005.
61. Gasafi, E., et al., *Economic analysis of sewage sludge gasification in supercritical water for hydrogen production*. *Biomass and Bioenergy*, 2008. 32(12): p. 1085-1096.
62. Lu, Y., L. Zhao, and L. Guo, *Technical and economic evaluation of solar hydrogen production by supercritical water gasification of biomass in China*. *international journal of hydrogen energy*, 2011. 36(22): p. 14349-14359.
63. Sweeting, J., *Project Cost Estimating: Principles and Practice*. 1997: IChemE.
64. Eurostat. *Natural gas price*. 2017; Available from: [http://ec.europa.eu/eurostat/statistics-explained/index.php/Natural\\_gas\\_price\\_statistics#Natural\\_gas\\_prices\\_for\\_industrial\\_consumers](http://ec.europa.eu/eurostat/statistics-explained/index.php/Natural_gas_price_statistics#Natural_gas_prices_for_industrial_consumers).
65. Phyllis2, E. *Groningen natural gas (#929)*. [cited 2017 June]; Available from: <https://www.ecn.nl/phyllis2/Biomass/View/929>.

66. Data, W.I. *Historic inflation The Netherlands - CPI inflation*. [cited 2017 June]; Available from: <http://www.inflation.eu/inflation-rates/the-netherlands/historic-inflation/cpi-inflation-the-netherlands.aspx>.
67. Lemus, R.G. and J.M.M. Duart, *Updated hydrogen production costs and parities for conventional and renewable technologies*. *International Journal of Hydrogen Energy*, 2010. 35(9): p. 3929-3936.
68. Molino, A., et al., *Process Innovation Via Supercritical Water Gasification to Improve the Conventional Plants Performance in Treating Highly Humid Biomass*. *Waste and Biomass Valorization*, 2016. 7(5): p. 1289-1295.
69. Henkens, P. and H. Van Keulen, *Mineral policy in the Netherlands and nitrate policy within the European Community*. *NJAS-Wageningen Journal of Life Sciences*, 2001. 49(2-3): p. 117-134.
70. Raven, R., *Implementation of manure digestion and co-combustion in the Dutch electricity regime: a multi-level analysis of market implementation in the Netherlands*. *Energy policy*, 2004. 32(1): p. 29-39.
71. Elke Goos, A.B.a.B.R. *New NASA Thermodynamic Polynomials Database With Active Thermochemical Tables updates. Report ANL 05/20 TAE 960*. [cited 2017 February]; Available from: <http://burcat.technion.ac.il/dir>.

# APPENDIX 1

## WATER PROPERTIES IN THE SUPERCRITICAL REGION

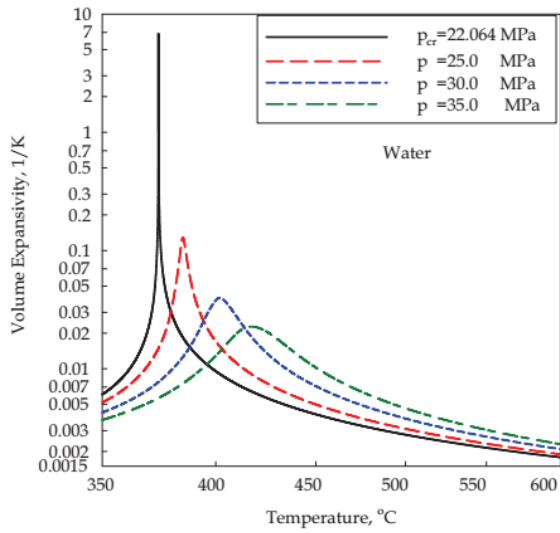


Figure 43: Volume expansivity vs. Temperature [10]

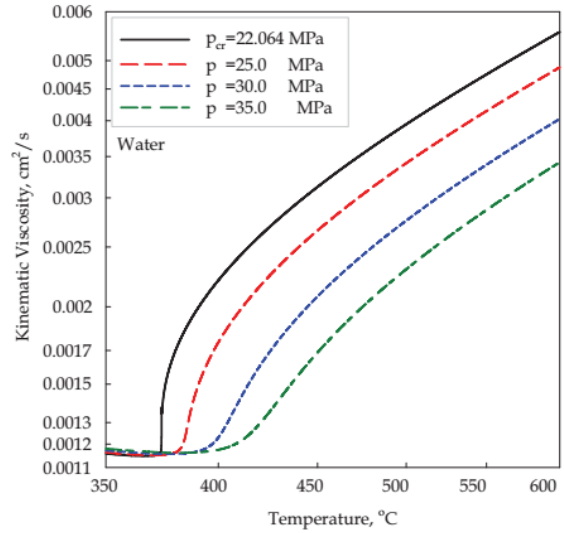


Figure 44: Kinematic viscosity vs. Temperature [10]

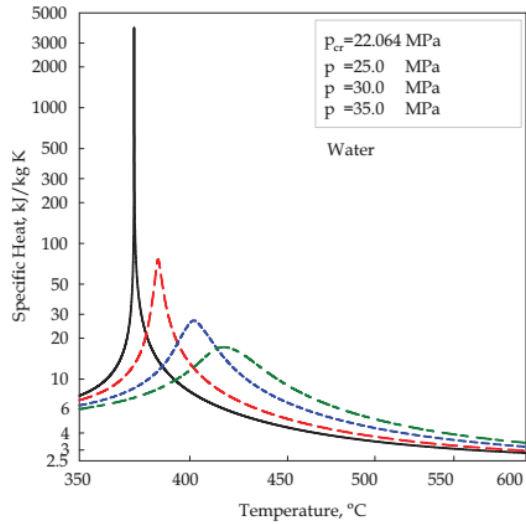


Figure 45: Specific heat vs. Temperature [10]

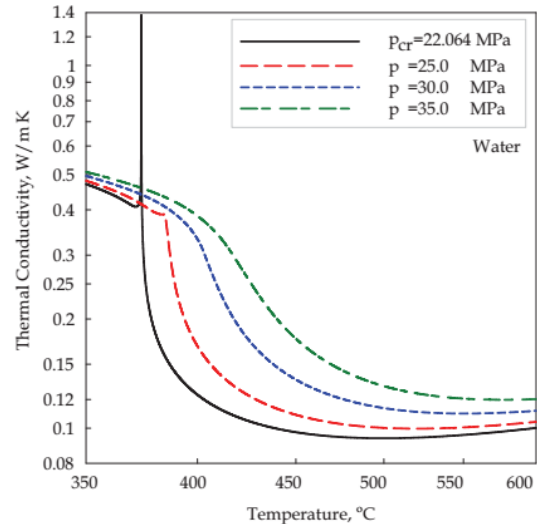


Figure 46: Thermal conductivity vs. Temperature [10]

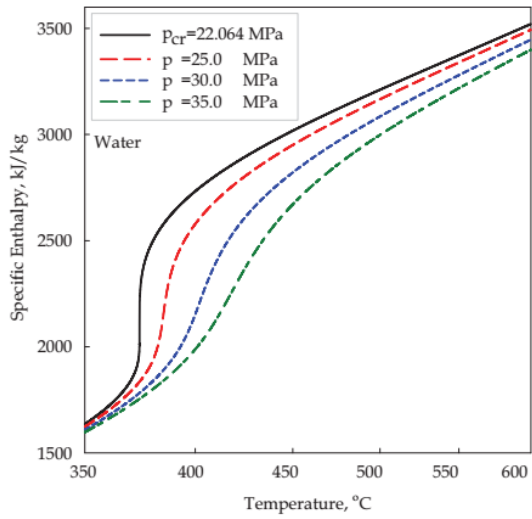


Figure 47: Specific enthalpy vs. Temperature [10]

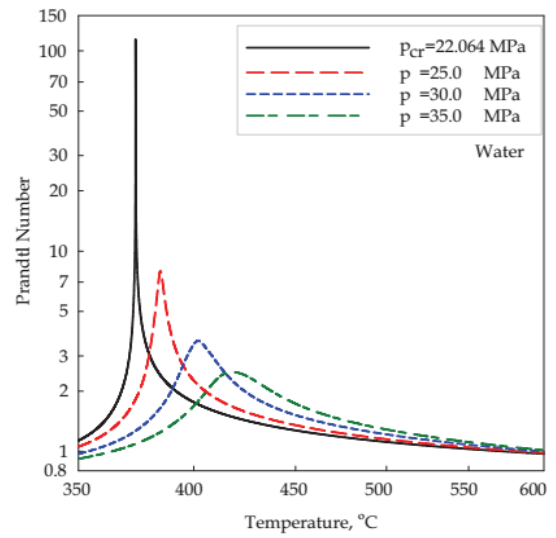


Figure 48: Prandtl number vs. Temperature [10]

## APPENDIX 2

### LAMINAR AND TURBULENT FLOW EQUATIONS

**Mass conservation:**

$$\frac{\partial \rho}{\partial t} + \nabla * (\rho \vec{v}) = 0$$

*Equation XVIII: Mass conservation*

where  $\rho$  is the fluid density and  $\vec{v}$  is the velocity vector.

**Momentum conservation:**

$$\frac{\partial}{\partial t} (\rho \vec{v}) + \nabla * (\rho \vec{v} \vec{v}) = -\nabla p + \nabla \vec{\tau} + \rho \vec{f}$$

*Equation XIX: Momentum conservation*

where  $\vec{\tau}$  is the viscous stress tensor and  $\vec{f}$  the mass force vector.

**Energy conservation:**

$$\frac{\partial(\rho h)}{\partial t} + \nabla * (\rho \vec{v} h) = \nabla * \left( \lambda \nabla T - \sum_i h_i J_i \right) + \frac{Dp}{Dt} + \vec{\tau} : \nabla \vec{v}$$

*Equation XX: Energy conservation*

where

$$h = \sum_j Y_j h_j$$
$$h_i = h_i^0(T_{ref,i}) + \int_{T_{ref,j}}^T c_p dT$$

$\lambda$  is the thermal conductivity and  $h_i^0(T_{ref,i})$  is the standard mole enthalpy of the formation species  $i$ .

**Species conservation:**

$$\frac{\partial}{\partial t} (\rho Y_i) + \nabla * (\rho \vec{v} Y_i) = -\nabla * \vec{J}_i + R_i$$

*Equation XXI: Species conservation*

where  $Y_i$  is the mass fraction of  $i$ ,  $\vec{j}_i$  is the diffusion flux of species  $i$ ,  $R_i$  is the total chemical reaction rate, and

$$R_i = M_{w,i} \sum_{r=1}^N v_i Q_r$$

where  $Q_r$  is the reaction rate of reaction  $r$ ,  $v_i$  is the stoichiometric coefficient of species  $i$  in the reaction  $r$ , and  $M_{w,i}$  is the molecular weight of species  $i$ .

**Turbulence:**

$$\frac{\partial}{\partial t}(\rho k) + \frac{\partial}{\partial x_j}(\rho u_j k) = \frac{\partial}{\partial x_j} \left[ \left( \mu + \frac{\mu_t}{\sigma_k} \right) \frac{\partial k}{\partial x_j} \right] + G_k + G_b - \rho \epsilon - Y_M + S_k$$

*Equation XXII: Turbulence kinetic energy conservation*

$$\frac{\partial}{\partial t}(\rho \epsilon) + \frac{\partial}{\partial x_j}(\rho u_j \epsilon) = \frac{\partial}{\partial x_j} \left[ \left( \mu + \frac{\mu_t}{\sigma_\epsilon} \right) \frac{\partial \epsilon}{\partial x_j} \right] + C_1 \frac{\epsilon}{k} \rho S_\epsilon - C_2 \rho \frac{\epsilon^2}{k + \sqrt{\nu \epsilon}} + C_{1\epsilon} \frac{\epsilon}{k} C_{3\epsilon} \epsilon G_b + S_\epsilon$$

*Equation XXIII: Turbulence dissipation conservation*

where

$$C_1 = \max \left[ 0.43, \frac{\eta}{\eta+5} \right], \eta = S \frac{k}{\epsilon}, S = \sqrt{2S_{ij}S_{ij}}$$

In these equations,  $G_k$  represents the generation of turbulence kinetic energy due to the mean velocity gradients.  $G_b$  is the generation of turbulence kinetic energy due to buoyancy.  $Y_M$  represents the contribution of the fluctuating dilatation in compressible turbulence to the overall dissipation rate.  $C_2$  and  $C_{1\epsilon}$  are constants.  $\sigma_k$  and  $\sigma_\epsilon$  are the turbulent Prandtl numbers for  $k$  and  $\epsilon$ , respectively.  $S_k$  and  $S_\epsilon$  are user-defined source terms.

# APPENDIX 3

## NEW NASA THERMODYNAMIC POLYNOMIALS DATABASE WITH ACTIVE THERMOCHEMICAL TABLES UPDATES [71]

C6H12O6 D-Mannose HF298=-1032.02 kJ Chemo 9/15 Joback Method  
 3 T 9/15 C 6.00H 12.000 6.00 0.00 0.00 0 180.1558800 -1032020.000  
 50.000 200.000 7 -2.0 -1.0 0.0 1.0 2.0 3.0 4.0 0.0 33506.961  
 -1.997008482D+04 1.486105629D+03-3.758818490D+01 5.009218890D-01-2.070292432D-03  
 4.787163570D-06-4.375408870D-09 0.000000000D+00-1.328194583D+05 1.862506827D+02  
 200.000 1000.000 7 -2.0 -1.0 0.0 1.0 2.0 3.0 4.0 0.0 33506.961  
 -5.780649280D+05 9.134037020D+03-5.477648680D+01 2.628540968D-01-3.123675859D-04  
 1.969144652D-07-5.067543360D-11 0.000000000D+00-1.710605669D+05 3.315490650D+02  
 1000.000 6000.000 7 -2.0 -1.0 0.0 1.0 2.0 3.0 4.0 0.0 33506.961  
 9.041899630D+06-4.021735850D+04 8.593749920D+01-4.913778670D-03 7.067762570D-07  
 -5.141328060D-11 1.403000950D-15 0.000000000D+00 1.073846940D+05-5.207933500D+02

H2- HF298=311.68+/-2.94 KJ REF=ATCT C 2011

2 T 6/11 H 2.00E 1.00 0.00 0.00 0.00 0 2.0164286 311680.000  
 298.150 1000.000 7 -2.0 -1.0 0.0 1.0 2.0 3.0 4.0 0.0 8620.592  
 -9.753406510D+04 1.221146654D+03-2.264491580D+00 1.237177358D-02-1.127065635D-05  
 5.366996730D-09-1.049351408D-12 0.000000000D+00 3.041627828D+04 3.050501137D+01  
 1000.000 6000.000 7 -2.0 -1.0 0.0 1.0 2.0 3.0 4.0 0.0 8620.592  
 9.598668370D+04-9.144525080D+02 5.149403040D+00-1.016481356D-04 5.446716690D-08  
 -6.154911190D-12 2.822317100D-16 0.000000000D+00 4.154313170D+04-1.440769502D+01

CD4 METHANE-D4 ANHARMONIC HF298=-89.01 KJ BURCAT 1980 FROM GURVICH'S CH4  
 3 T11/09 C 1.00D 4.00 0.00 0.00 0.00 0 20.0671080 -89010.000  
 50.000 200.000 7 -2.0 -1.0 0.0 1.0 2.0 3.0 4.0 0.0 10342.516  
 -5.750294670D+02 4.158388450D+01 2.803135821D+00 1.730055951D-02-1.286764614D-04  
 4.341241730D-07-3.824994810D-10 0.000000000D+00-1.208147578D+04 5.613030190D+00  
 200.000 1000.000 7 -2.0 -1.0 0.0 1.0 2.0 3.0 4.0 0.0 10342.516  
 -3.974009420D+04 1.162371596D+03-6.288389560D+00 3.384695040D-02-3.156562879D-05  
 1.764742235D-08-4.489503280D-12 0.000000000D+00-1.684477700D+04 5.460509810D+01  
 1000.000 6000.000 7 -2.0 -1.0 0.0 1.0 2.0 3.0 4.0 0.0 10342.516  
 1.492108617D+06-8.616961450D+03 1.867281643D+01-1.721680888D-03 4.902039880D-07  
 -4.511640620D-11 2.112337227D-15 0.000000000D+00 3.790295480D+04-1.025188891D+02

CO- CARBON MONOXIDE ANION RUSCIC ATCT D 2013 HF298=36.2+/-3.1 KJ  
 2 T 3/16 C 1.000 1.00E 1.00 0.00 0.00 0 28.0106486 36200.000  
 298.150 1000.000 7 -2.0 -1.0 0.0 1.0 2.0 3.0 4.0 0.0 8678.563  
 -9.923103340D+04 1.218103901D+03-2.129570898D+00 1.171500617D-02-1.046490875D-05  
 4.786349790D-09-8.897247230D-13 0.000000000D+00-2.721598545D+03 3.724917840D+01  
 1000.000 6000.000 7 -2.0 -1.0 0.0 1.0 2.0 3.0 4.0 0.0 8678.563  
 9.554574680D+04-9.173499890D+02 5.158633320D+00-2.505846559D-04 5.581385460D-08  
 -6.324386500D-12 2.905705055D-16 0.000000000D+00 8.432220260D+03-7.053734500D+00

CO2 TRIPLET RUSCIC ATCT D 2013 HF298=49.6+/-2.4 KJ  
 3 T 7/15 C 1.000 2.00 0.00 0.00 0.00 0 44.0095000 49600.000  
 50.000 200.000 7 -2.0 -1.0 0.0 1.0 2.0 3.0 4.0 0.0 9365.469  
 1.601544414D+03-1.024433955D+02 5.992378520D+00-2.813100791D-02 1.379250084D-04  
 -1.736474241D-07-8.072160340D-11 0.000000000D+00 5.176759990D+03-3.729633690D+00  
 200.000 1000.000 7 -2.0 -1.0 0.0 1.0 2.0 3.0 4.0 0.0 9365.469  
 4.521640180D+04-5.643329200D+02 4.949821680D+00 3.494032910D-03-1.681903893D-06  
 3.289740270D-10-4.024410520D-14 0.000000000D+00 7.715613050D+03-3.999178090D+00  
 1000.000 6000.000 7 -2.0 -1.0 0.0 1.0 2.0 3.0 4.0 0.0 9365.469  
 3.372054190D+05-2.431420648D+03 9.006795370D+00-4.721730320D-04 1.023852229D-07  
 -1.196398770D-11 7.357581800D-16 0.000000000D+00 1.831339195D+04-3.056739031D+01

# APPENDIX 4

## GLUCOSE DECOMPOSITION COMPLETE KINETIC DATA [14]

kinetic parameters	reaction	k [s <sup>-1</sup> ]					
		573 K <sup>o</sup>	623 K <sup>o</sup>	673 K <sup>o</sup>	698 K	723 K	733 K
gf	isomerization	$2.09 \times 10^{-2}$	$2.21 \times 10^{-1}$	$2.86 \times 10^{-1}$	$1.62 \times 10^{-1}$	$1.30 \times 10^{-1}$	$1.42 \times 10^{-1}$
gfu	dehydration	0	0	$1.60 \times 10^{-1}$	$2.20 \times 10^{-1}$	$7.18 \times 10^{-2}$	$9.35 \times 10^{-2}$
gt	decomposition	$5.13 \times 10^{-2}$	$9.30 \times 10^{-1}$	3.60	6.26	5.74	6.49
g5	dehydration	$6.00 \times 10^{-3}$	$3.27 \times 10^{-2}$	$2.15 \times 10^{-1}$	$2.76 \times 10^{-1}$	$5.23 \times 10^{-2}$	$7.51 \times 10^{-2}$
f5	dehydration	$1.62 \times 10^{-1}$	$3.30 \times 10^{-1}$	$3.82 \times 10^{-1}$	$3.00 \times 10^{-1}$	$1.32 \times 10^{-1}$	$1.50 \times 10^{-1}$
ffu	dehydration	$5.94 \times 10^{-2}$	$2.74 \times 10^{-1}$	$1.91 \times 10^{-1}$	$1.18 \times 10^{-1}$	$9.32 \times 10^{-2}$	$8.70 \times 10^{-2}$
ft	decomposition	0	0	0	0	0	0
5t	decomposition	0	$2.45 \times 10^{-5}$	0	$3.03 \times 10^{-2}$	$4.07 \times 10^{-2}$	$3.98 \times 10^{-2}$
5c	polymerization	$1.59 \times 10^{-3}$	$1.28 \times 10^{-2}$	0	0	0	0
fut	decomposition	0	$9.94 \times 10^{-3}$	0	$1.44 \times 10^{-2}$	$1.23 \times 10^{-2}$	$5.80 \times 10^{-2}$
fuc	polymerization	0	0	0	0	0	0
tc	polymerization	$9.35 \times 10^{-4}$	$1.29 \times 10^{-3}$	$1.60 \times 10^{-3}$	$1.16 \times 10^{-3}$	$9.30 \times 10^{-4}$	$6.44 \times 10^{-4}$
tg	gasification	$2.69 \times 10^{-3}$	$2.35 \times 10^{-3}$	$6.64 \times 10^{-3}$	$9.27 \times 10^{-3}$	$1.46 \times 10^{-2}$	$2.27 \times 10^{-2}$
g	total reaction	$7.81 \times 10^{-2}$	1.18	4.26	6.92	6.00	6.80

## APPENDIX 5

### LAMINAR FLOW EXPERIMENT MESH INDEPENDENCE STUDY

The domain in this reactor is shown in the Figure 49 below. The inlet boundary condition is divided into two zones: water and biomass inlet. The domain is defined by the parameters "a", "b" and "c"; which represent the distance of the water inlet, the biomass inlet and the reactor length respectively.

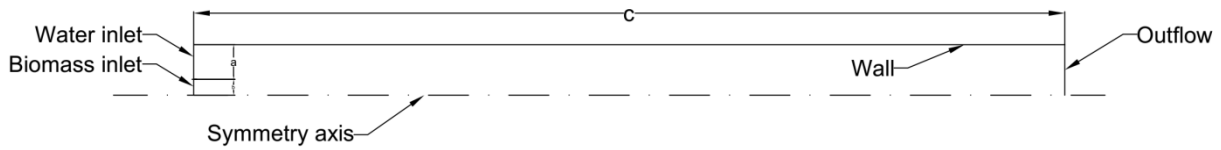


Figure 49: Laminar flow domain definition

The mesh is obtained by defining the number of elements for each domain parameter. In general, the procedure consisted of doubling each parameter at a time and generating the corresponding mesh. The values for each parameter and the total number of generated cells for the domain can be seen in the Table 12 below:

Table 13: Domain parameters

a	b	c	N° cells
50	10	400	23,600
100	20	800	95,200
200	40	1600	382,400

It is a known fact that after a certain point, flow is fully developed and maintains a steady velocity and temperature profile no matter where is measured anymore. For laminar flows, the hydrodynamic entry length is a function of the Reynolds number [45], and is calculated using the Equation XXIV below:

$$L_{h,laminar} = 0.05 * Re * D = 0.05 * 1.03 * 25 = 1.29 \text{ mm}$$

Equation XXIV: Hydrodynamic length entrance

Considering temperature, in order to have a stable profile is necessary to surpass the "thermal entrance length" which for laminar flow is also a function of the Reynolds number and the Prandtl number, and is calculated at the operating condition of the experiment using the Equation XXV below:

$$\begin{aligned} x_{fd,t} &\approx 0.05 * Re * Pr * D = 0.05 * Re * \left( \frac{\mu * c_p}{k} \right) * D \\ &= 0.05 * 1.03 * \left( \frac{4.12 * 1000 * 0.00085}{0.62} \right) * 25 = 7.27 \text{ mm} \end{aligned}$$

Equation XXV: Thermal entrance length

In the case of our reactor, this means 7.3 millimeters considering the bigger distance between the velocity and temperature criteria. However, just to be sure a security factor of 10 was applied to ensure stability in the profiles.

To decide which mesh to use, a grid independence study was conducted. This study consists of simulating fluid flow at room conditions under the influence of the heated walls at the operating temperature of the lab scale experiment. The general objective of this study, is to produce velocity and temperature profiles to compare the accuracy of the obtained solutions by the different meshes. These profiles were obtained evaluating the solution at a location of interest: after the thermal entrance length (which also ensures fully developed velocity).

Evaluating the velocity profiles in the plane of interest, it was found that the differences are quite small and hard to notice in the graphical comparison (see Figure 50). In the maximum value of velocity (top of the dome) at the position equal to 0, the "95.2k" and the "23.6k" meshes (which have the least number of cells) show nearly no difference and the graphs are almost overlapping.

The solution of the "382.4k" mesh took too much time, and considering that in this study only continuity and energy equations are solver, therefore it was already discarded. Numerically speaking considering the "95.2k" as comparison base, the difference percentage against the "23.6k" and "382.4k" is only 0.3%. From the results up to this point, it can be seen that there is no need to use the "382.4k" mesh because the "23.6k" already gives good results.

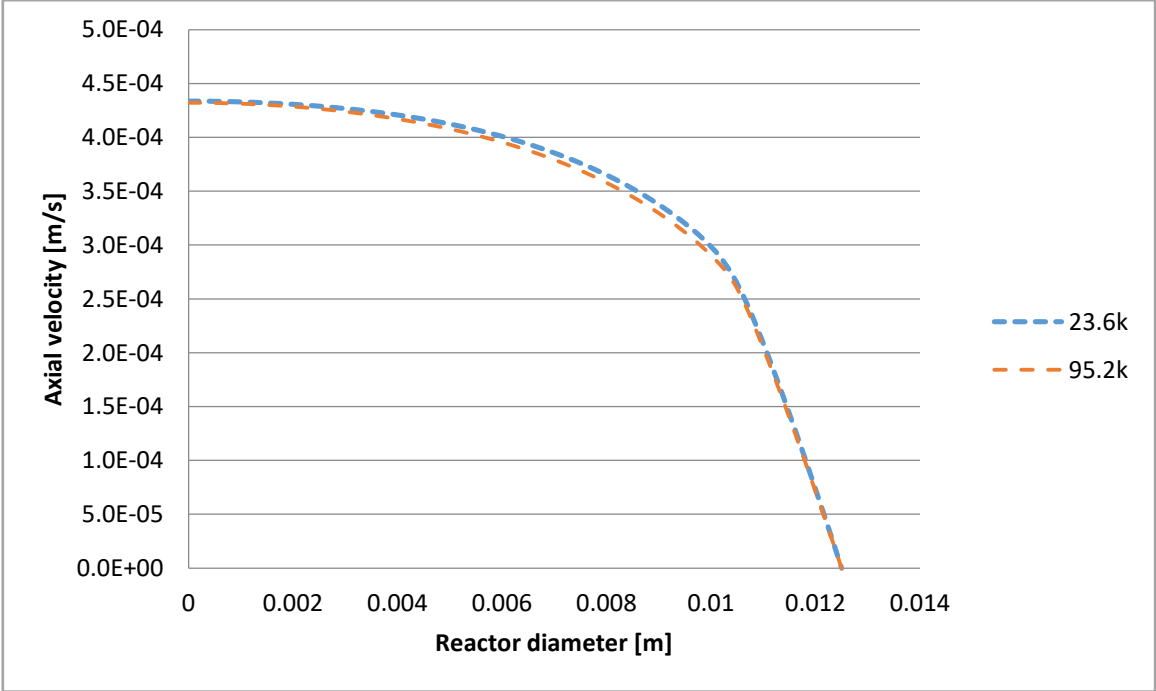


Figure 50: Velocity profiles comparison

To be sure, the comparison was also made for the temperature profiles. Given the fact that the diameter is so small and the element size (in the radial direction) is one order of magnitude smaller than the axial direction. The graphs are almost overlapping (see Figure 51) and there is practically no numerical difference between the temperature profiles. Therefore, the "23.6k" mesh was the selected one for the laminar flow numerical simulations execution.

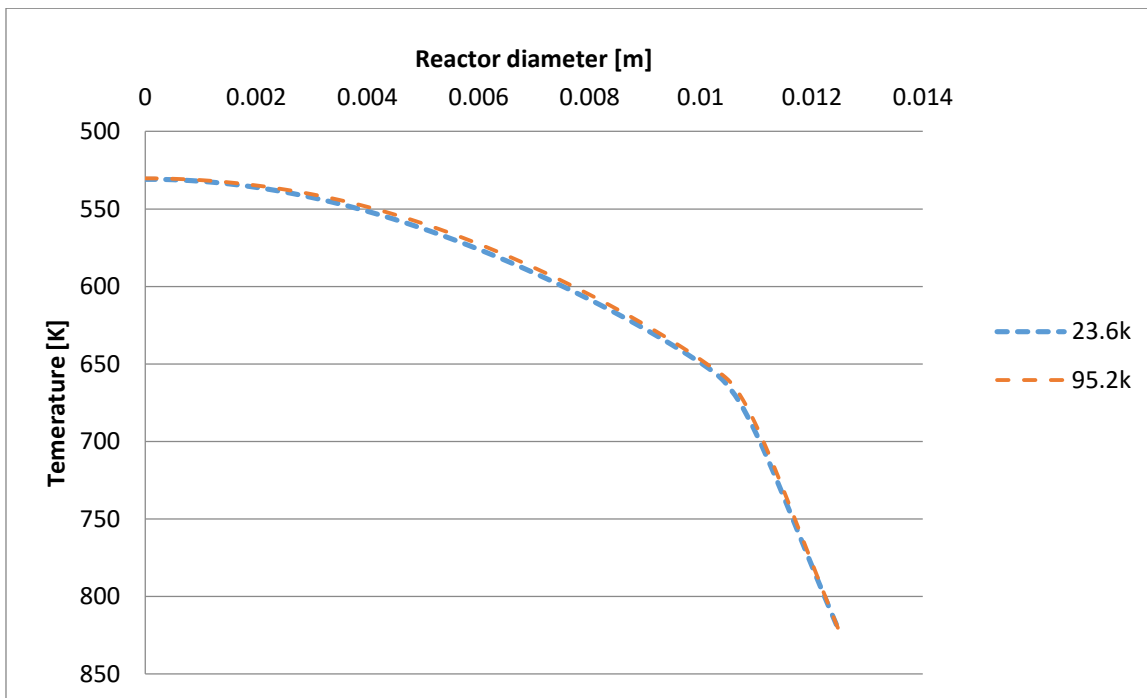


Figure 51: Temperature profile comparison

## TURBULENT FLOW NUMERICAL SIMULATION COMPLEMENTARY RESULTS

### Residence time influence

Varying the residence time (by directly changing the mass flow rate) has a significant impact in terms of the axial velocity and turbulence intensity experienced by the fluid. Considering the change in residence time from 60 to 30 s, this parameters were increased by a factor of 2. This insight is given as a side note, the progressive increase in turbulence intensity, makes convergence difficult to achieve when the residence time drop below 30 s (for certain temperature levels, the needed residence times are even below 10 s). Axial velocity and turbulence intensity contours are shown in the Figure 52 below. This parameter greatly influences the development of the numerical simulations in turbulent flow as is explained in the following paragraphs.

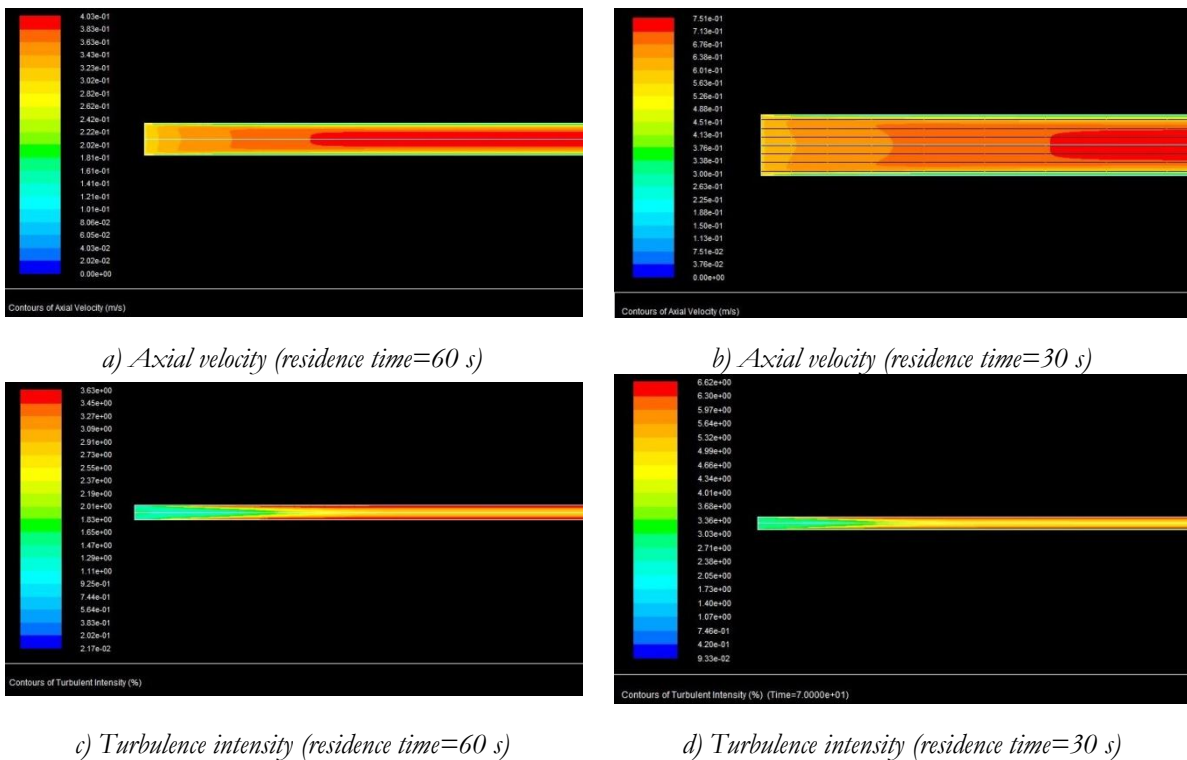


Figure 52: Velocity and turbulence intensity contours

### Temperature influence

In order to investigate the influence of the temperature in char formation rates a parametric study was done. In these simulations the feed inlet temperature was set at 450 K,

while the wall temperature was set at the desired operating temperature. In the Figure 53, can be seen how different operating temperatures values produced different bulk fluid temperature profiles. For all the cases the temperature stabilized more or less around the first meter of the reactor length (negligible variations after that).

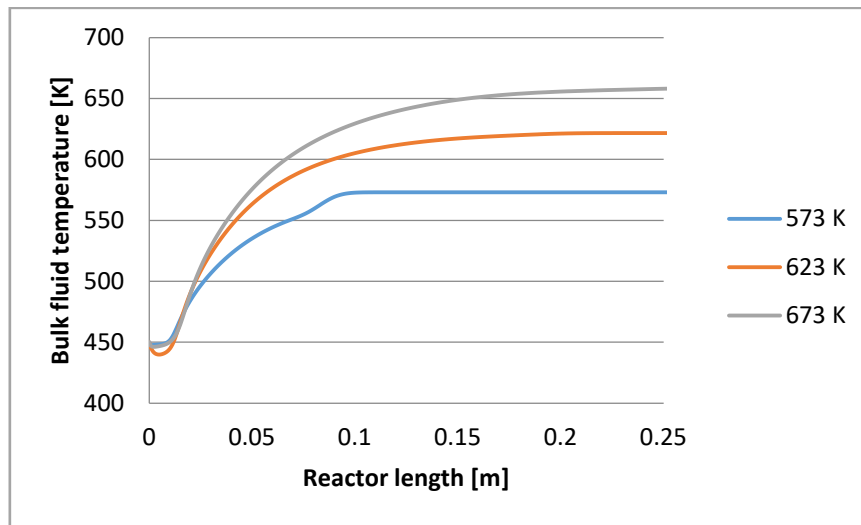


Figure 53: Bulk fluid temperature profiles

The temperature changes have a direct impact in the char kinetic rates, which are temperature dependent as the Arrhenius equation describes. In the Figure 54, the impact of the previous temperature profiles in the char formation kinetic rates is shown. Note immediately that after certain reactor length, the kinetic rates stabilized more or less in the same order of magnitude (which matches the temperature profile stabilization of the previous figure).

During the "clash" of the cold feed inlet with the hot wall temperature, the kinetic rates experience a sudden peak and then drops. It was previously known (by literature review research) the smaller the temperature difference, the smaller is the production of char. And this graph is the proof of that, it can be seen how with increasing temperature (from 573 to 623 K) the kinetic rate reaches its peak and then decreases when the bulk fluid temperature is higher (from 623 to 673 K).

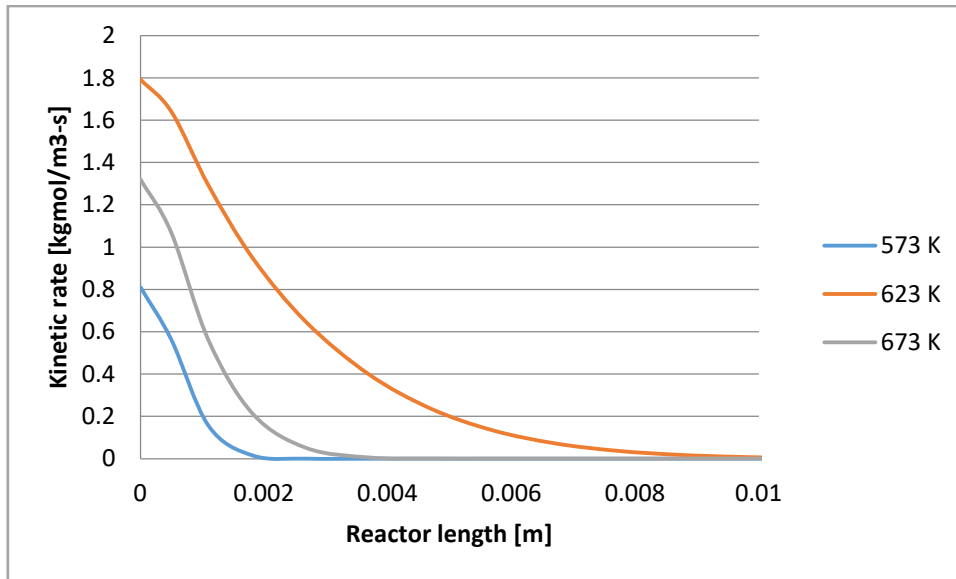


Figure 54: Char kinetic profiles at different operating temperatures

Looking closer to the kinetic rates at 623 K operating temperature as shown in Figure 55, it can be noted how different the peaks for the gas and char kinetic rates are. The char kinetic rate is 60 times bigger than the gas one. As the mixture flows through the reactor and is heated, these formation rates decrease and stabilize.

Eventually the gas overcomes the char kinetic rate of  $1.47 \times 10^{-29}$  and stabilize at value of  $4.02 \times 10^{-27}$  which is 273 times more, this behavior confirms that at the beginning the chemical reactions are "dominated" by the char formation but eventually the gas one predominates because they have different temperature ranges where are more active. At this specific operating condition, this turning points occurred approximately at 25 mm from the reactor inlet where the bulk fluid temperature is around 508 K.

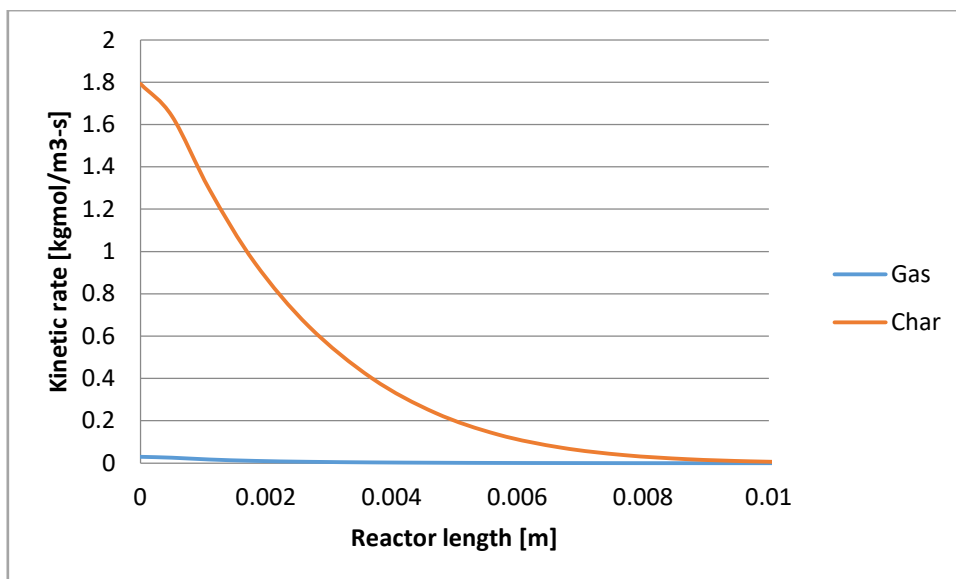


Figure 55: Kinetic rates at 623 K

